TARGETING MICROGLIAL DIVALENT METAL TRANSPORTER 1 IN NEUROINFLAMMATION AND ALZHEIMER'S DISEASE

By

Katrina Volk Robertson

Dissertation

Submitted to the Faculty of the

Graduate School of Vanderbilt University

in partial fulfillment of the requirements

for the degree of

DOCTOR OF PHILOSOPHY

in

Molecular Physiology and Biophysics

May 10, 2024

Nashville, Tennessee

Approved:

Julio E. Ayala, Ph.D.

Fiona E. Harrison, Ph.D.

Nancy Carrasco, M.D.

Richard B. Simerly, Ph.D.

Alyssa H. Hasty, Ph.D.

To God, the giver of life and maker of science,

and

To my grandfather – whose strong and steady mind was overtaken by the evils of this yet-incurable disease…

ACKNOWLEDGMENTS

First, I would like to immensely thank my mentor, Dr. Alyssa Hasty. She graciously embraced the challenge of working with me to initiate a new neuroscience project in her lab, which had historically not studied the brain. Through five years of working together, Alyssa trusted and empowered me to ask bold scientific questions, experiment with innovative techniques, and independently drive my project. She taught me a great deal about how to conduct research thoroughly, responsibly, and critically. Most of all, I am deeply grateful for Alyssa's humility, kindness, and compassion as a mentor. The eventful, and oftentimes unpredictable, years of graduate school brought numerous ups and downs (including a global pandemic), and I am ever grateful for Alyssa's gracious, steady, and faithful mentorship throughout. She leads her lab with wisdom and integrity, and her mentorship was one of the biggest blessings of my graduate career. I also thank my co-mentor, Dr. Fiona Harrison, and her lab members. I met Fiona during a first-year neuroscience course and was drawn to her compassionate, humorous, honest, and thoughtful nature. As the resident Alzheimer's expert in my corner, Fiona was indispensable in counseling me on almost all aspects of my study designs, behavioral data analyses, and scientific and life pursuits. I am so grateful for our office pop-in meetings about proper statistical analyses that morphed into critical conversations about career paths and life. Her capacity to lighten the heart of a tired graduate student is something I deeply admire and will miss.

My lab mates over the years have all helped my projects progress in some manner. Nathan Winn was instrumental in assisting with mouse gavages and injections. I am deeply indebted to Alec Rodriguez for his assistance with mouse husbandry and extensive behavioral studies. Matt Cottam, Heather Caslin, Elysa Wolf, Jamie Garcia, Mike Schleh, and Magdalena Ameka helped with tissue collection days and contributed thoughtful insight as I developed my project. They each encouraged and challenged me in ways that empowered me to be a stronger scientist and peer. Our Hasty lab gatherings were some of my favorite moments in graduate school and it has been an honor to work alongside and know each of them as colleagues and friends. Marnie Gruen was essential in supporting my work, from ordering reagents to implementing protocols. Outside of science, Marnie's warm, gentle, and humble spirit was often a salve to my heart on hard days. I will deeply miss our Monday morning chats and lab barbeques hosted at the Gruen family farm.

My committee members, Dr. Julio Ayala, Dr. Fiona Harrison, Dr. Nancy Carrasco, and Dr. Rich Simerly were a critical component during my graduate school career. Each member contributed an insightful and diverse perspective, which helped drive my project forward and into novel directions. Their depth of knowledge and years of experience were instrumental in bringing this dissertation to completion and it was a tremendous privilege to receive personal advice from them. I am grateful Dr. Julio Ayala agreed to serve as chair of my committee, as I cannot imagine my graduate experience without his approachable, thoughtful, and generous guidance. I acknowledge my funding sources (*see Appendix*), which were paramount to allow me to conduct this research. Core personnel in the Murine Neurobehavior Lab, Dr. John Allison and Krista Paffenroth, assisted with behavioral study setup and analyses. The undergraduate students who worked with me, Skylar Pile, Kyle Schroeder, and Arianna Valenti brought a more vibrant energy into my lab experience. They helped troubleshoot difficult cell culture experiments and showcased a remarkable work ethic. It was an immense joy mentoring and watching them grow in science and life. My fellow graduate school friends were a constancy during my six years, and I am thankful for our coffee chats and laughing fits. I am also thankful for non-PhD friends near and far who helped ground me in the reality of a world outside of the pressures of graduate school.

Lastly, I could not have made it through graduate school without the tremendous support of my family. My brothers and sister who visited me in Nashville made graduate school more exciting and cheered me on enormously from afar. I owe a great deal to my parents, John and Ann Volk, who recognized and encouraged a passion for learning in their daughter from a young age. They have modeled and taught me a stubborn perseverance that in no doubt fueled my capacity to finish this dissertation. Despite physical distance and time differences, they served as a consistent and ever-present source of support, motivation, and affirmation. They often received the brunt of many disheartened thoughts and frustrations in teary phone calls, and their immense pride in and love for me strengthened my determination to finish my graduate work. I aspire to love my family one day as deeply as they do. Gaining a second family of support has been an incredible joy. My Robertson family and parents-in-law, Lynne and Ken, provided a soft place to land for me in Nashville, especially during my initial transition to the city. Their welcoming, warm, and consistently hospitable disposition towards me is something I am extremely grateful for. Finally, I thank and acknowledge my husband and best friend, John Robertson. His unending support and love for me carried me through the hard seasons graduate school inevitably brought. His extraordinary capacity to know the needs of my heart and to provide steady encouragement, instill confidence in me, and uplift my weary soul is one of the greatest gifts I have ever received. He is my greatest daily cheerleader, encourager, advocate, and safe haven and makes life remarkably more fun. I am so excited to continue to grow with him and co-explore this life together.

Contents

LIST OF TABLES

Table Page

LIST OF FIGURES

LIST OF ABBREVIATIONS/SYMBOLS

Aβ – Amyloid-beta

AD – Alzheimer's disease

Apoe – Apolipoprotein E

APP – Amyloid precursor protein

BDNF – Brain-derived neurotrophic factor

CCL – C-C motif chemokine ligand

CD – Cluster of differentiation

CNS – Central nervous system

Cp – Ceruloplasmin

Cre – P1 bacteriophage cyclization recombination recombinase

Cx3cr1 – CX3C motif chemokine receptor 1

DAM – Disease-associated microglia

DMSO – Dimethyl sulfoxide

DMT1 – Divalent metal transporter 1

ELISA – Enzyme-linked immunosorbent assay

EOAD – Early-onset Alzheimer's disease

ER – Estrogen receptor

EZ maze – Elevated zero maze

FAC – Ferric ammonium citrate

FAD – Familial Alzheimer's disease

Fe^{2+} – Ferrous iron

Fe^{3+} – Ferric iron

Fth – Ferritin heavy chain

Ftl – Ferritin light chain

Fpn – Ferroportin

Hamp – Hepcidin

Hb-Hp – Hemoglobin-haptoglobin

Hfe – Homeostatic iron regulator

HO1 – Heme oxygenase 1

ICP-MS – Inductively coupled plasma mass spectrometry

IFNγ – Interferon γ

IL – Interleukin

IMG – Immortalized mouse microglial cell line

iNos – Inducible nitric oxide synthase

i.p. – Intraperitoneal

IRE/IRP – Iron-responsive element/Iron regulatory protein

LRP1/CD91 – LDL-related receptor 1, cluster of differentiation 91

LOAD – Late-onset Alzheimer's disease

LPS – Lipopolysaccharide

MCP-1 – Monocyte chemoattractant protein 1

MWM – Morris water maze

NFκB – Nuclear factor kappa-light-chain-enhancer of activated B cells

NLRP3 – NOD-like receptor family pyrin domain containing 3

NSAID – Non-steroidal anti-inflammatory drug

NTBI – Non-transferrin-bound iron

p.o. – Oral administration

P2ry12 – Purinergic receptor P2Y12

ROS – Reactive oxygen species

Slc11a2 – Solute carrier family 11 member 2 (gene, DMT1)

Slc40a1 – Solute carrier family 40 member 1 (gene, ferroportin)

STEAP3 – Six-transmembrane epithelial antigen of the prostate 3

Tf – Transferrin

Trem2 – Triggering receptor expressed on myeloid cells 2

Tfrc – Transferrin receptor, gene

TfR1 – Transferrin receptor, protein

T*gfβ1* – Transforming growth factor β 1

TLR – Toll-like receptor

Tmem119 – Transmembrane protein 119

TNFα – Tumor necrosis factor α

CHAPTER 1

Introduction

1.1 Alzheimer's disease: prevalence and clinical manifestation

Alzheimer's disease (AD) – first described by physician Alois Alzheimer in 1906 – is one of the most common neurodegenerative disorders and is the most frequent cause of dementia, affecting over 6.7 million people in the United States of America [5] and 32 million worldwide [6]. This disease most commonly affects individuals aged 65 years and older, where about 1 in 9 individuals in the U.S. over the age of 65 develop AD-related dementia [7]. As the age of the general population increases, it is predicted that the total number of individuals in the U.S. with AD will rise to 14 million by 2050 unless preventative measures are developed, representing a significant burden on the country's healthcare system, economy, and individual caregivers [7]. The disease is clinically characterized by a progressive and significant loss of memory, problem-solving ability, language, executive function, and overall cognitive capacity. Eventually, individuals with AD become entirely dependent on a caregiver to help them with daily tasks of living as the disease progresses into its most severe stages, leading ultimately to death [8].

1.2 Neuropathology of Alzheimer's disease

At the neuropathological level, AD is characterized by the hallmark accumulation of extracellular protein aggregates known as amyloid beta (Aβ) plaques and the presence of neurofibrillary tangles composed of a hyperphosphorylated microtubule-stabilizing protein, tau, in neuronal cell bodies [9]. Aβ aggregation and deposition in the brain is typically observed first, decades before the onset of clinical cognitive decline, peaking early during the course of symptomatic disease [10]. The

deposition of these aggregated proteins in the brain is thought to be a primary initiating event for the disease, eventually leading to widespread synaptic dysfunction, neuronal death, hippocampal atrophy, and significant cognitive deficits [11]. This well-known hypothesis, known as the amyloid cascade hypothesis, is predicated in part on the fact that patients with early-onset familial Alzheimer's disease (FAD) – those who develop symptoms before the age of 65 and represent only <5% of all AD cases – exhibit familial mutations in the genes encoding for amyloid precursor protein (APP) and presenilin 1 and 2. These mutations result in the preferential cleavage of APP by proteolytic enzymes β-secretase and γ-secretase into abnormal aggregation-prone Aβ species [12]. In FAD patients, overproduction of Aβ is thought to be the primary causative factor in the onset of this aggressive form of AD. However, in 95% of AD cases, patients present with a form of disease known as "sporadic AD" or late-onset Alzheimer's disease (LOAD). In these patients, disease etiology is complex and multifactorial, with age being the most significant risk factor for development of LOAD [13]. While Aβ plaque deposition in critical brain regions is a defining feature of LOAD patient brains as well, there has been immense debate on the centrality of Aβ in the pathogenic process [14]. Reports have shown significant Aβ deposition in cognitively-normal aged individuals [15, 16] and many studies suggest a lack of correlation between amyloid load and degree of cognitive decline, especially in aged populations [17-19]. Additionally, clinical trials targeting amyloid have brought further into question the role of amyloid in AD pathology, as many of the developed pharmaceuticals have failed to significantly improve cognitive function despite their efficacy in clearing plaques [20]. Thus, there is a lack of consensus on the role of amyloid in driving AD pathogenesis [21, 22]. Greater attention has begun to be placed on other hallmark pathologies of AD, which are often found in conjunction with amyloid, including the presence of significant neuroinflammation, metabolic dysfunction, brain hypoperfusion and decreased brain

glucose consumption, calcium imbalance, oxidative stress, and metal (e.g., iron) dyshomeostasis [13] (Fig. 1.1).

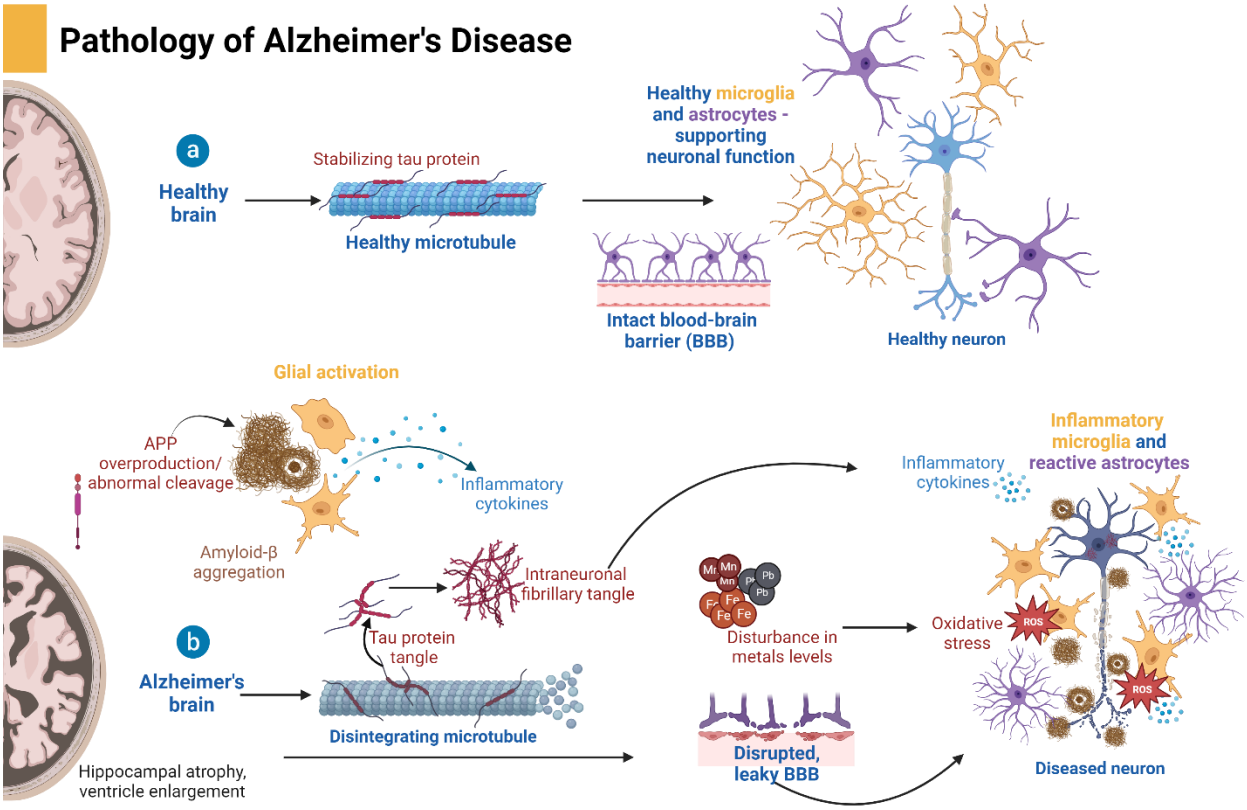

Figure 1.1. Basic neuropathology of Alzheimer's disease.
In the early stages of AD development (b), aberrant amyloid-β protein production and subsequent plaque aggregation is a defining feature of disease. Microglial cells are thought to be activated early in response to Aβ aggregation and appear chronically activated throughout the course of disease. Later in disease progression, aberrant hyperphosphorylation of tau protein in neurons results in the toxic accumulation of neurofibrillary tau tangles, which contribute to inflammatory signaling from glial cells and consequent neuronal damage. In addition to these two primary protein abnormalities in AD brains, AD etiology involves complex and multifactorial processes. Blood brain barrier (BBB) disruption and leakage (likely leading to hypoperfusion and entrance of foreign and/or toxic materials into the brain), an imbalance in brain heavy metals, oxidative stress, as well as chronic microglia and astrocyte activity are several of the other key pathologies associated with AD development.
Figure modified from a BioRender.com template, with permission.

1.3 Cell types in Alzheimer's disease

In addition to the overall gross changes that occur in the AD brain, much research has focused on the cellular pathologies observed during disease progression. Neuronal cell dysfunction, damage,

and death is the eventual cause of cognitive decline; thus, the only approved treatment for AD for several decades (prior to the recent approval of amyloid-targeting drugs) were acetylcholinesterase inhibitors, which act to increase neuron-derived acetylcholine levels in the brain – the primary neurotransmitter thought to be deficient in AD brains [23]. However, there are a plethora of changes that occur prior to the onset of dementia and are thought to underlie the widespread neurodegeneration typical of late-stage AD. For example, neurons are the primary producers of APP and associated Aβ peptide, and neuronal cell bodies accumulate hyperphosphorylated tau fibrillary tangles. Detected even earlier than these changes, however, hyperexcitability of neurons has been observed as an early marker of disease [24]. Pre-clinical AD models demonstrate more frequent neuronal action potential firing [24, 25] and work has found a higher incidence of seizure activity in individuals with AD [26]. At the molecular level, increases in calcium signaling [27] and enhanced glutamatergic release [28] are significantly associated with this hyperexcitable phenotype. Additionally, defects in the endosomal-lysosomal system in neurons is a significant early disturbance during the course of AD development [29-31]. Outside of neuronal pathology, it has been widely accepted that glia – predominantly astrocytes and microglia – play a significant role during AD pathogenesis as well. Indeed, neuronal changes may occur in response to pathological glial activity [32, 33]. While greater attention in recent decades has been placed on determining the function of these non-neuronal cells in AD, their role in disease progression has not been fully understood. Astrocytes represent the most abundant type of glial cell in the brain and are responsible for processes such as maintenance of blood-brain barrier integrity and function, neurotransmitter re-uptake and clearance, regulation of synaptic activity, maintenance of ion homeostasis, and regulation of inflammation. During AD, astrocytes appear as highly reactive, pro-inflammatory cells [34, 35]. In addition to their role in propagating inflammation in the AD

brain, astrocytes also actively participate in Aβ generation and contribute to the dysfunctional glutamatergic signaling mentioned earlier [36]. Other significant changes to cell types in the brain during AD include changes in oligodendrocytes [37], cells associated with vasculature [38], and microglia. The role of microglia in AD will be discussed in detail below in section **1.8.**

1.4 Mouse models of Alzheimer's disease

Much of what is known about AD at the genetic and pathological level has driven the generation of appropriate animal models to study the disease's pathogenesis. Mouse models have served a critical role in aiding our understanding of disease progression and in allowing pre-clinical testing of different therapeutics. While the field lacks a model that recapitulates all the features of human AD, there have been numerous genetically-modified mouse models generated to study aspects of the disease [39]. Aβ-driven models include the widely used APPswe/PS1dE9 (*APP/PS1*) and 5xFAD mouse lines, which both harbor a humanized *APP* transgene containing inserted mutations known to cause FAD. In the *APP/PS1* mouse line, the "Swe" (from a family of Swedish descent) mutation in *APP* increases APP proteolytic processing through the pathogenic β-secretase pathway, resulting in elevated Aβ production in the brain [40] (Fig. 1.2). Additionally, the *APP/PS1* model includes a human *PSEN* (gene for presenilin 1) with exon 9 deleted. This mutation in presenilin 1 – the proteolytic subunit of the γ-secretase enzyme – is also strongly associated with FAD and results in increased production of Aβ due to preferential cleavage of APP by γ-secretase into aggregation-prone Aβ fragments [41, 42].

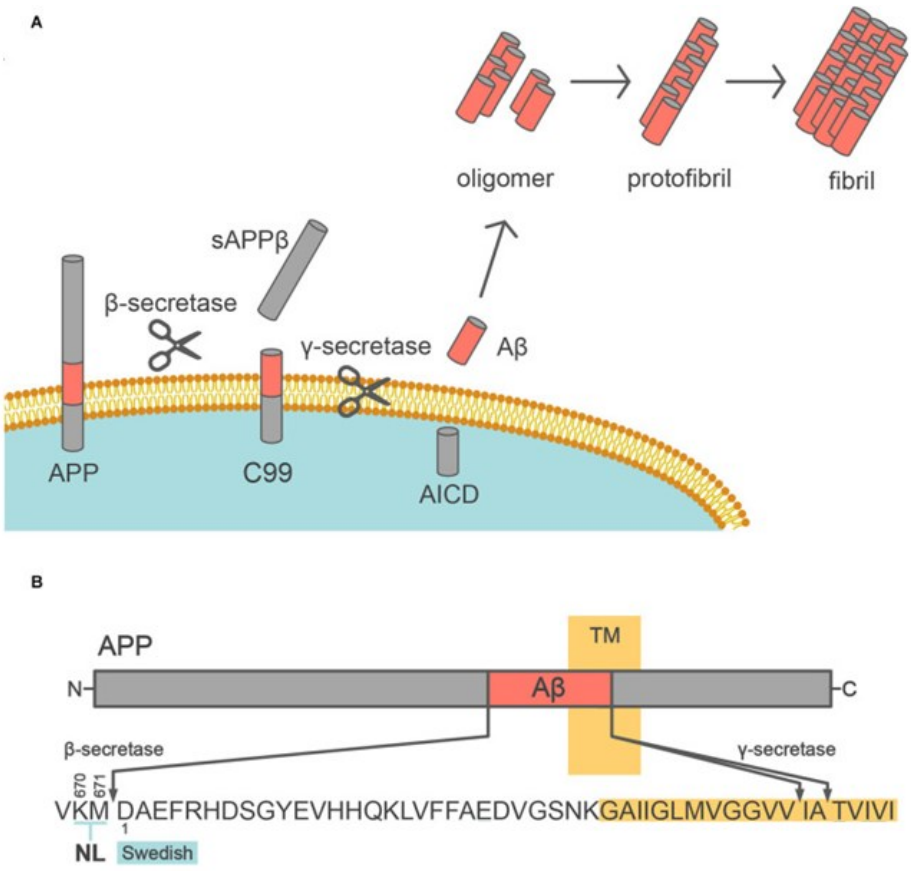

Figure 1.2. Mutations involved in processing of APP into aggregation-prone Aβ fragments.
a) In the Aβ production pathway, amyloid precursor protein (APP) is cleaved first by the enzyme β-secretase (resulting in a soluble APPβ fragment), followed by sequential proteolysis by γ-secretase. This sequential cleavage produces a cytoplasmic C-terminal domain (AICD) and critically releases extracellular Aβ monomer, which is prone to form oligomers, protofibrils, and fibrils which eventually aggregate into plaques. **b)** Diagram of mutations in the sequence of *APP* associated with FAD development and utilized in the *APP/PS1* mouse model of AD. The Swedish mutation is a double missense mutation found at codon positions 670 and 671 of human *APP* near the N-terminal cleavage site of Aβ, where two amino acid substitutions are thought to result in pathogenic cleavage of Aβ by β-secretase. The highlighted portion represents the transmembrane (TM) segment of Aβ, where γ-secretase acts to cleave APP and release extracellular Aβ.
Figure modified from Yokoyama, Kobayashi, Tatsumi, and Tomita, 2022, Figure 1, with permission [3].

The *APP/PS1* model has been widely used for decades of AD research focused on Aβ deposition and associated pathologies [43, 44]. The 5xFAD model was generated in 2006 and has become another widely used model for the study of AD pathogenesis related to Aβ plaque pathology. This model contains five mutations in *APP* and *PSEN1* known to cause FAD, resulting in a more rapid

and significant accumulation of Aβ compared to the *APP/PS1* model [45]. Although both these mouse lines have been two of the most commonly used models in AD research, there are now over 200 models in use for studying AD pathology including mice with *APOE* and/or *TREM2* mutations (known genetic risk factors for the development of LOAD), mutations in *SORL1* (endosomal trafficking receptor thought to be important for Aβ degradation), and models driven by mutant tau (resulting in tau tangle-related pathology) [46].

In my work, I utilized the *APP/PS1* mouse model of AD, which is the topic of Chapter IV of this dissertation. This model was chosen for several reasons: 1) it has been extensively characterized in regards to its neuropathological features and behavioral phenotype in both sexes [47-49], 2) it holds relevance to aging-associated AD development as these mice develop AD hallmarks in a more gradual and progressive manner than models such as the 5xFAD mouse, 3) and others have previously demonstrated significant iron deposition and microglial activation in this model [50, 51]. Microglial function and iron load are two significant directions of my research and will be discussed in sections **1.6** and **1.8** of this chapter; thus, this well-established animal model serves as an appropriate choice to assess the effects of an intervention targeting an aspect of microglial iron-handling machinery. Furthermore, related to my interest in iron-associated AD pathology, an Aβ-driven model was chosen based on demonstrated associations between iron and Aβ aggregation in AD brains [52], which will be discussed in more detail in section **1.5**.

In addition to genetic models of AD, other models have been generated to study particular pathologies associated with AD development. Specifically, models of neuroinflammation have garnered wide attention in recent years, as chronic neuroinflammation is a significant component of AD pathology. These models include those driven by injection of compounds such as lipopolysaccharide (LPS, a component of Gram-negative bacteria), PolyI:C (a viral stimulus), or

inflammatory molecule interleukin (IL)-1β [53]. Injection of LPS particularly represents one of the most widely used neuroinflammatory models in AD-related research, as it has been shown in rodents to induce cognitive impairment and a plethora of clinically-relevant behaviors that mimic those observed in patients with neurodegenerative disease (i.e., weight loss, anorexia, decreased movement, decreased exploratory behavior, and depressive-like behavior) [54]. LPS is a component of the cell wall of gram-negative bacteria and activates cellular inflammatory pathways via engagement of Toll-like receptor 4 (TLR4). Relevant to AD, TLR4 is expressed on microglial cells and is also activated by Aβ, resulting in the production of inflammatory cytokines and other signaling molecules, which are key to the neuroinflammatory process [55]. Furthermore, neuronal damage occurs in response to microglial activation by LPS [56, 57] and LPS itself has been found in AD patient brains [58]. Thus, LPS-induced models serve as a significant tool for the focused study of how neuroinflammatory processes – in particular, those mediated by microglia – contribute to neurodegenerative disease pathology [59]. Use of an LPS-induced animal model of neuroinflammation to study the effects of a decreased microglial iron import gene on the inflammatory response is the topic of Chapter III of this dissertation.

1.5 Iron homeostasis

In addition to the known pathologies mentioned in section **1.2**, iron dyshomeostasis has been recognized as a critical feature during the pathogenesis of AD and several other neurodegenerative diseases [60-62]. The most abundant transition metal in the brain, iron serves essential roles in mitochondrial metabolism and cellular energy production, enzyme catalysis, neurotransmitter synthesis, and myelination. The ability of iron to redox-cycle – readily switch back and forth between ferrous (Fe^{2+}) and ferric (Fe^{3+}) states by accepting or donating electrons – is essential for

its role in mediating cellular reactions and processes. However, due to its transitionary state, excess iron levels also catalyze the formation of reactive oxygen species (ROS) such as superoxide anion and hydroxyl radical, which can act to induce severe oxidative stress, DNA and protein damage, and eventually cellular death [63, 64]. Indeed, the critical importance of maintaining appropriate iron homeostasis is evidenced by a variety of diseases of both iron deficiency and overload such as anemia, hemochromatosis, obesity, cancer, and neurodegeneration [65].

Thus, iron levels must be tightly regulated in both the body and brain to avoid the toxic accumulation of iron. In humans, only about 1-2 mg of iron is absorbed via dietary intake per day through regulated enterocyte iron uptake [63]. Instead, much of the biochemically available iron in the body is recycled internally through elaborate systemic and cellular mechanisms that serve to supply iron to cells and tissues as needed (Fig. 1.3). Systemically, iron primarily exists in the circulation in the ferric state bound to soluble transferrin (Tf) protein, which is taken up by erythroid precursors to aid in erythropoiesis [66]. These systemic iron levels are maintained predominantly through the action of the peptide hormone hepcidin, produced principally by the liver [67]. Hepcidin binds to and induces the internalization of the mammalian cellular iron exporter, ferroportin (gene, *Slc40a1*), to decrease circulating iron concentrations in conditions such as iron overload.

At the tissue-level, the majority of surplus iron found in healthy mammalian systems is stored in a non-toxic form in hepatocytes in the liver and in tissue-resident macrophages, which are equipped with the necessary machinery to import, store, and export iron in accordance with tissue demands [1] (Fig. 1.4). In healthy states, most iron handling in macrophages is primarily performed by specialized splenic red pulp macrophages and liver Kupffer cells, which phagocytose senescent erythrocytes and release iron via hemoglobin degradation in the cell [68]. This iron is

then recycled for Tf-receptor 1 (TfR1)-mediated import in maturing erythropoietic cells, which use it for hemoglobin synthesis and proliferation [69]. Other tissue-resident resident macrophages typically process smaller amounts of iron than splenic red pulp macrophages and Kupffer cells in homeostatic conditions and can take up iron via multiple other mechanisms of import. These mechanisms include the import of Tf-bound iron via TfR1, iron contained in heme-hemopexin via LDL-related receptor 1 (LRP1 or CD91), iron contained in hemoglobin-haptoglobin via scavenger receptor CD163, and non-transferrin-bound Fe^{2+} iron (NTBI) via membrane-bound divalent metal transporter 1 (DMT1). It is thought that tissue-resident macrophages are less involved in red blood cell phagocytosis (which involves heme-iron handling via CD163 and/or CD91) and predominantly utilize TfR1 to mediate cellular iron uptake [69, 70]. In this case, holo-Tf binds to TfR1 found at the plasma membrane, which is then internalized and trafficked to the endosome. Once Tf-TfR is in the endosome, iron is released from the complex, reduced to Fe^{2+} (via metalloreductase six-transmembrane epithelial antigen of the prostate 3, or STEAP3), and transported into the cytosol through an endosomal membrane-bound form of DMT1. Once in the cytoplasmic 'labile iron pool', this iron can then be readily used for reactions in the cytosol, trafficked to the mitochondria for assistance with cellular respiration, recycled and exported via ferroportin, or safely stored intracellularly in a non-toxic iron storage protein, ferritin [containing both heavy (H) and light (L) chains involved in Fe^{2+} oxidation and long-term iron storage, respectively] (Fig. 1.4). Expression levels of these importers and storage molecules are regulated by an exquisite system at both the transcriptional and post-transcriptional levels. In cases of iron deficiency, mRNA gene expression of iron importers *DMT1* (gene, *Slc11a2*) and *TfR1* increases significantly [71, 72]. At the post-transcriptional level, the genes for TfR1, some isoforms of DMT1, and ferritin-H and L contain "iron-responsive elements" (IREs) in their untranslated

regions which are regions where iron regulatory proteins (IRPs) bind [73]. These IRPs remain bound to IREs or dissociate from IREs upon sensing iron levels in the cell and can either stabilize or inhibit translation of the mRNA [74, 75]. While TfR-mediated cellular iron uptake is thought to be the typical mechanism of importing iron in cells in healthy states, the importer DMT1 can also mediate the import of extracellular non-transferrin bound Fe^{2+}. Particularly in conditions of iron overload and Tf saturation, the resultant accumulation of NTBI has been associated with the development of a variety of pathological conditions, and DMT1-mediated iron uptake may become more relevant in these aberrant states, which will be discussed further in section **1.6** below [65, 76].

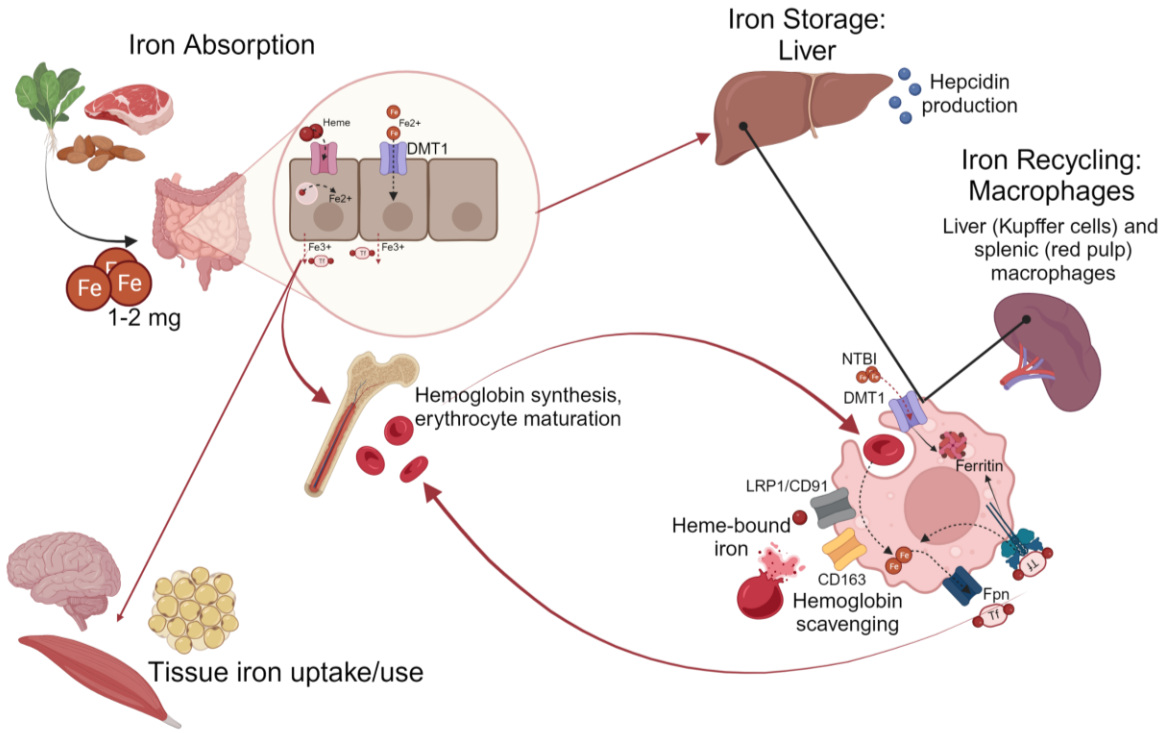

Figure 1.3. Systemic iron lifecycle and recycling by macrophages.
Dietary iron absorption in the gut accounts for only 1-2 mg of iron handled in the body each day. In enterocytes, this iron is up-taken by a heme-iron importer and/or via DMT1, bringing Fe^{2+} into the cell from the intestinal lumen. From there, the absorbed iron is oxidized at the plasma membrane before export and transported into the bloodstream bound to transferrin for uptake and use by various tissues. The remaining iron handled in the body is recycled primarily by macrophages of the liver and spleen. These cells phagocytose dying and/or dead red blood cells (RBCs) and scavenge iron associated with heme and hemoglobin via receptors CD163 and LRP1. Heme and hemoglobin-associated iron is then metabolized in the cell and exported as Tf-Fe^{3+} for the maturation of new RBCs in the bone marrow. In conditions of systemic iron overload, excess iron is stored in hepatocytes and macrophages of the liver, which is also the organ site for hepcidin production (molecule that acts systemically to inhibit tissue iron release during iron overload). Additionally, excess iron in these conditions can be imported as Fe^{2+} via DMT1 into macrophages of various tissues.
Figure made with BioRender.com, with permission.

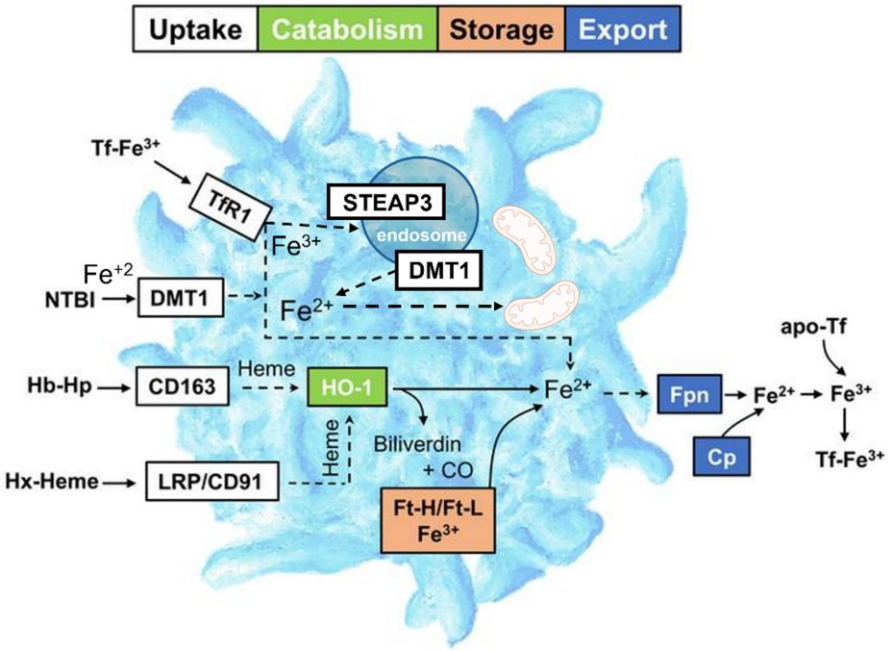

Figure 1.4. Macrophage iron-handling overview.
Importers TfR1, DMT1, CD163, and LRP1/CD91 are responsible for cellular import of iron at the plasma membrane. TfR1 mediates the import of transferrin-bound Fe^{3+}, which is then reduced in the endosome by metalloreductase enzyme STEAP3, and the resultant Fe^{2+} is transported out of the endosome into the cytosol via endosomal-bound DMT1. At the plasma membrane, DMT1 mediates the import of NTBI Fe^{2+} directly. CD163 and LRP1, also known as CD91, mediate the import of hemoglobin-haptoglobin (Hb-Hp) and hemopexin-heme (Hp-Heme), respectively. Heme-iron extracted from these sources is then metabolized by enzyme heme-oxygenase 1 (HO-1). Iron from all four importers can be trafficked to the mitochondria for use in energy production, oxidized and stored in ferritin (Ft-H and Ft-L complex), or oxidized and exported out of the cell via ceruloplasmin (Cp) and ferroportin (Fpn), respectively.
Figure modified using BioRender.com from Winn, Volk, Hasty, 2020, Figure 1, [1], with permission.

1.6 Divalent metal transporter 1 in health and disease

DMT1 (originally known as natural resistance associated macrophage protein 2, Nramp2) is a twelve-transmembrane domain proton (H^+)-dependent transporter responsible for the cellular uptake of a variety of divalent metals [77, 78]. The first mammalian transmembrane iron transporter to be identified, DMT1 (gene name, *Slc11a2*) can also transport metals Zn^{2+}, Mn^{2+}, Cu^{2+}, Co^{2+}, Cd^{2+}, and Pb^{2+}, although iron – in the form of Fe^{2+} – appears to be its most prominent physiological substrate [79, 80]. DMT1 also exists in an endosomal-bound form inside the cell, where it is critically important for transporting Fe^{2+} (the usable form of iron in the cell) into the

cytosol following cellular endocytosis of Tf-TfR and trafficking of Tf-bound Fe^{3+} to the endosome. Thus, although a role for DMT1 in uptake of extracellular NTBI Fe^{2+} may not emerge until conditions of iron overload occur, endosomal DMT1 is essential in ensuring imported Tf-bound iron can be used by the cell during homeostatic conditions. Consequently, mutations in *Slc11a2* and complete ablation of DMT1 in rodents result in significant anemia and early mortality [81-83] and polymorphisms of *Slc11a2* in humans are associated with significant risk of anemia [84-86]. These studies demonstrate the essential role DMT1 plays in transporting bioavailable iron, which other transporters fail to compensate for.

As mentioned in section **1.5**, DMT1 may play a pivotal role in mediating the pathologic accumulation of iron in disease. An increase in DMT1 expression was found to be the primary driver of osteoarthritis in a mouse model of iron overload-induced joint cartilage damage [87] and increased DMT1 transport activity of NTBI has been implicated in cardiomyopathy associated with elevated heart iron levels [88, 89]. Additionally, it has been suggested that upregulations in intestinal DMT1 significantly contribute to the iron overload observed in hemochromatosis (one of the most common iron overload disorders), which leads to multi-organ dysfunction and is associated with diseases such as diabetes and liver cirrhosis [90, 91]. Although widely studied in the context of iron absorption in the gut and disruptions in systemic iron levels [81, 92-94], the role of DMT1 in the brain has been less extensively studied. *In vivo* mouse studies have shown that DMT1 is essential for proper neuronal development and memory capacity [95]. In oligodendrocytes, DMT1 is critical for cellular maturation and myelinating function [96]. DMT1 expression has also been shown in astrocytes [97] and microglia [98], although the function of DMT1 in these cell types is not well understood. Overall alterations in brain levels and function of DMT1 have been implicated in a variety of neurodegenerative disorders [99-102]. However,

the specific mechanisms by which DMT1 is involved in neurodegenerative disease pathology, as well as how DMT1 functions in specific cell types during the disease process are still widely unknown.

1.7 Iron load in neurodegeneration and Alzheimer's disease

Excess iron has been found in AD patient brains [103, 104] as well as mouse models of the disease [105, 106]. In particular, focal iron deposits have been found in and near Aβ plaques [107] and iron has been directly shown to increase the production of Aβ and exacerbate its toxicity [108-110]. While iron gradually increases in the brain throughout aging, it is thought that an excessive and specific accumulation of iron in brain regions relevant to AD development (i.e., hippocampus, entorhinal cortex, frontal cortex) is a significant contributor to the onset of disease [111]. Indeed, iron plays a central role in the group of diseases known as Neurodegeneration with Brain Iron Accumulation (NBIA), which are a category of genetic disorders caused by mutations in genes such as the gene encoding for ferritin light chain or ceruloplasmin (Cp, ferroxidase important for cellular iron export). In these disorders, iron accumulates significantly and specifically in the basal ganglia of the brain, which leads to significant deficits in motor control and often in intellectual ability [112]. Considering the central role of iron in NBIA and the hallmark accumulation of this metal found in AD brains, a key role for iron in AD pathology has become to be appreciated [52, 60, 62].

Much of the research in the past few decades has focused on how iron exacerbates amyloid-related toxicity and pathology. *APP* contains an IRE and is responsive to changes in iron levels [113, 114], and iron binds to and increases the cytotoxicity of Aβ plaques [108, 115]. However, more recent publications suggest a central role for iron in propagating AD pathological decline,

even outside of its role in worsening amyloid production and toxicity. Studies have shown significant correlations between increased iron levels and cognitive decline [116, 117], which is not mirrored in correlations between Aβ burden and cognition [118]. In fact, there is a negative association between iron levels and cognitive ability even at pre-clinical stages of disease, suggesting iron plays a significant role during the initial stages of disease onset [119, 120]. In mouse models of AD, iron chelation significantly improves markers of disease and cognitive performance [121, 122], further suggesting iron homeostasis as a potential therapeutic target for the treatment of AD.

1.8 Microglial cells

1.8.1 Background

Microglia are the primary innate immune cells of the central nervous system (CNS), acting as resident macrophages of the brain to provide surveillance of neural tissue and to protect against infection and CNS injury. While similar to other tissue-resident macrophages in many roles they play in the brain, microglia represent a distinct and highly specialized population of myeloid-derived cells. Microglial precursors arise from the yolk sac during embryonic development and migrate to colonize the embryonic brain, where specific brain-derived cues lead to their unique differentiation. Following initial brain colonization, microglia repopulate and maintain cell numbers exclusively via self-renewal in homeostatic conditions [123]. These cells have been known to play active and essential roles in the pruning of synapses during neural circuit development, phagocytosing debris and dying cells in response to foreign material or damage in the CNS, and maintaining overall neural homeostasis [124, 125]. Highly branched processes, which extend from the cell body, allow microglia to survey the brain parenchyma and respond

rapidly to changes in brain homeostasis to perform these functions and govern healthy neural function. Indeed, in response to alterations in the brain parenchyma, microglia can exist on a broad and dynamic continuum of activation states, rapidly modifying their morphology and motility, cytokine and chemokine secretion profiles, intracellular metabolism, and cellular functions according to the needs of the surrounding tissue [126] (Fig. 1.5).

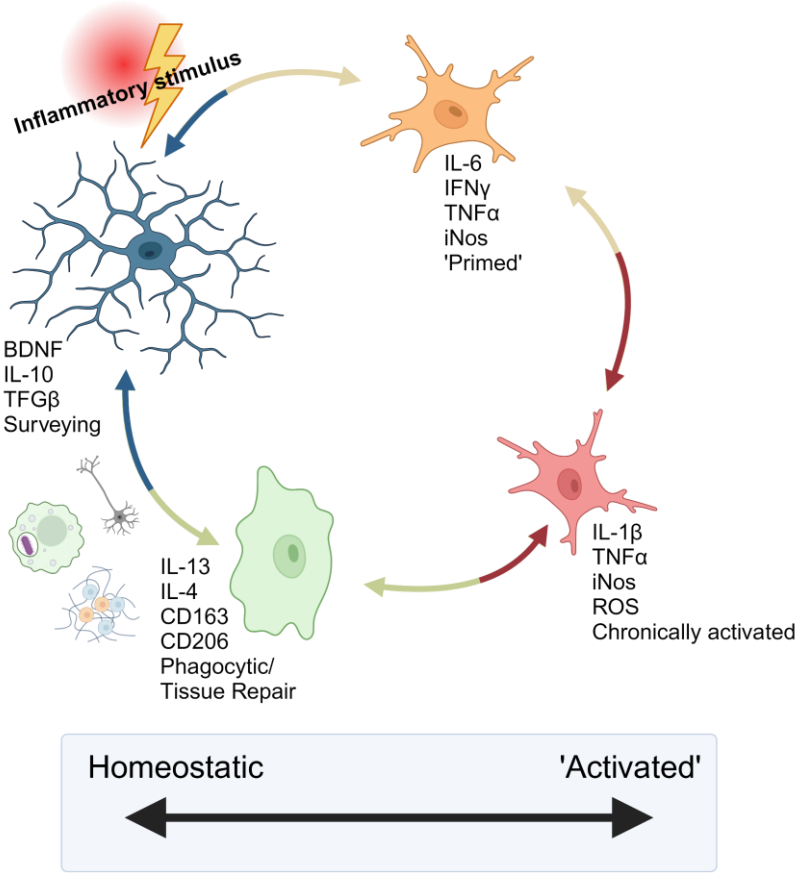

Figure 1.5. Microglia adopt a wide spectrum of dynamic activation states.
During homeostatic conditions, surveying microglia patrol brain tissue and maintain homeostasis via secretion of growth factors and anti-inflammatory cytokines. In response to an acute stimulus, microglia rapidly adapt their inflammatory profile and secrete pro-inflammatory cytokines and chemokines. If inflammatory settings remain, microglia can become chronically activated, secreting high amounts of pro-inflammatory cytokines and ROS. To repair tissue following acute inflammation or damage, microglia become phagocytic and release anti-inflammatory and pro-resolving molecules to return tissue to homeostasis.
Figure made in BioRender.com, with permission.

1.8.2 Microglia in neuroinflammation and Alzheimer's disease

Over the past several decades, microglial cells have emerged as significant players in AD pathology and in the pathology of several other neurodegenerative diseases [127-129]. The presence of significant neuroinflammation [i.e., robust production of pro-inflammatory cytokines including interleukin (IL)-1β, IL-6, and tumor necrosis factor α (TNFα), chemokines like C-C motif chemokine ligand (CCL) 1, CCL-2, and ROS] is a key feature of AD patient brains, and this chronic inflammation is thought to be a driver of disease pathology [130]. While several cell types in the brain are known to contribute to the widespread neuroinflammation seen in the diseased brain, microglia are considered to be one of the predominant cell types involved in mediating the inflammatory cascade. Genome-wide association studies of patients with LOAD have revealed that variants in genes exclusively and/or preferentially expressed in microglia significantly increase an individual's risk of developing AD, positioning microglia as central players in disease pathogenesis [126]. Indeed, astrocytes – the other glial cell known to mediate inflammation in the AD brain – have been shown to respond to early microglia activation [131, 132]. Furthermore, microglial-mediated inflammation is a key feature of many of the known risk factors associated with an individual's increased propensity to develop AD (i.e., aging, obesity, traumatic brain injury, stroke, gut dysbiosis, and sleep deficits) [4].

However, the complex and dynamic roles microglia play during the development and progression of AD have not been fully elucidated. Transcriptomic studies have demonstrated a gradual shift in microglial phenotype from a homeostatic state to a disease-associated state over the course of AD in mouse models and human brains [133, 134]. These 'disease-associated' microglia ("DAMs") upregulate signature markers such as apolipoprotein E (*Apoe*) and triggering receptor expressed on myeloid cells 2 (*Trem2*) and downregulate classic microglial homeostatic

genes such as *Cx3cr1, Tgfbr1, P2ry12,* and *Tmem119* [135]. Conflicting results indicate that this transcriptional cell state is related to an anti-inflammatory and phagocytic response which offers neuroprotection [136], while others suggest this pathway is involved in an exaggerated inflammatory response which promotes cellular dysfunction and neurotoxicity [137]. It is likely that transcriptional changes in microglia exert effects on disease progression that are time-, context-, and pathway-specific. The work in this dissertation aimed to target a particular transcriptional pathway in microglia at a specific time during disease to further parse out the disparate roles that microglia have been shown to play in propagating or protecting against disease.

Activated microglia surrounding Aβ plaques have also been isolated and profiled as a distinct disease-related subset of microglia in AD, with DAM-like upregulations in genes associated with complement signaling, lysosomal degradation, immune response, and redox reactions [138, 139]. Microglia express a variety of receptors that bind Aβ, such as TLR2, TLR4, and CD36 [126] and Aβ directly stimulates microglial activation and inflammatory signaling [140], which may be beneficial to initiate plaque clearance mechanisms [141, 142]. If prolonged, however, it is thought that excessive Aβ-induced microglial activation contributes to neuronal degradation and disease progression [143, 144] (Fig. 1.6). Thus, the specific role these disease-associated microglia play in protecting against or promoting disease during each step of pathology is still a matter of intense debate. This again suggests that assessing a specific aspect of microglial function at distinct time points during disease is essential to fill the gap in our understanding of the role these cells play in disease. The work in this dissertation thus sought to explore the effects of altering a distinct function of microglia early in disease and is discussed in Chapter IV.

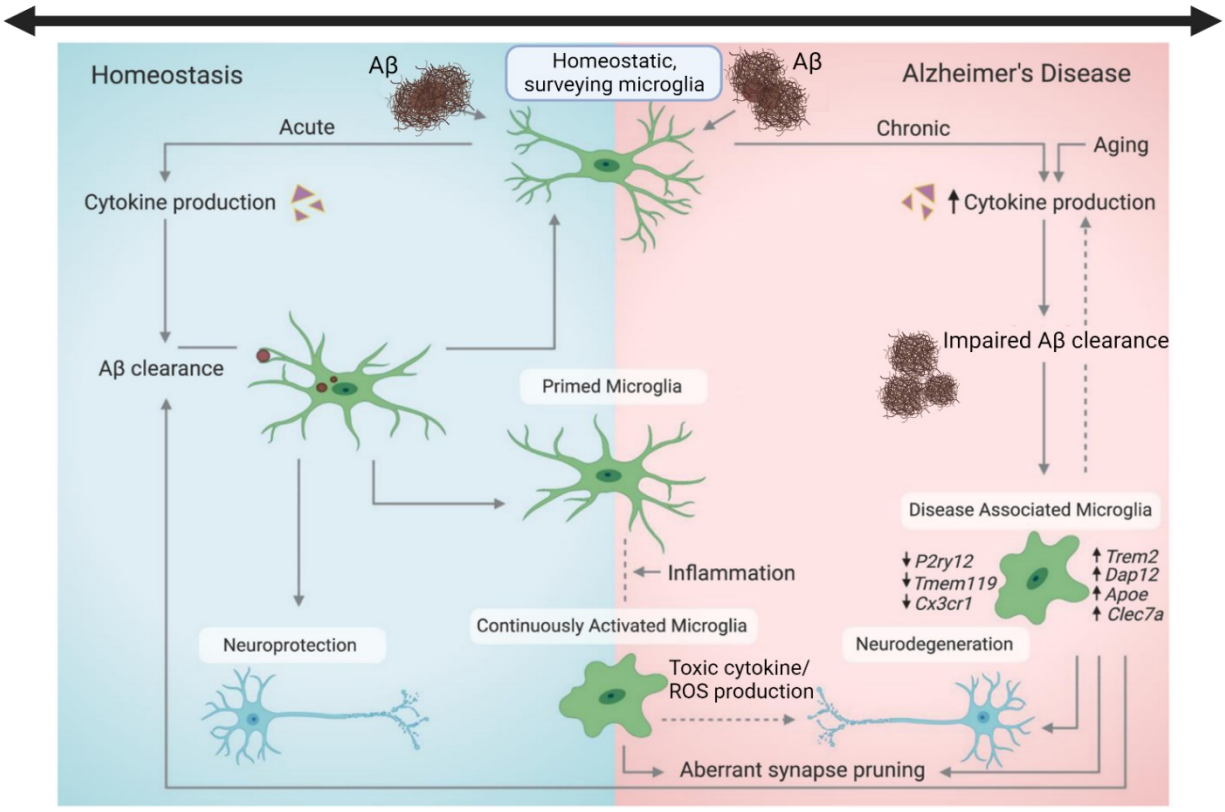

Figure 1.6. Divergent, 'double-edged sword' roles of microglia during AD progression.
During homeostatic conditions in a healthy brain (blue background), microglia survey the brain parenchyma for foreign material and/or damage. Upon identification of amyloid-β deposits, microglia respond with an acute release of cytokines, effectively clear (i.e., phagocytose) Aβ from the brain, and typically return to homeostasis. This is neuroprotective and is thought to occur initially in response to early amyloid deposition in the pre-clinical AD brain. However, prolonged exposure to inflammation (systemic or other brain inflammation via stroke, infection, or other brain injury), or prolonged exposure to Aβ can cause these primed microglia to continuously secrete toxic amounts of pro-inflammatory cytokines and ROS (pink background). This pro-inflammatory phenotype worsens with age and cellular senescence and is associated with defects in cellular ability to phagocytose Aβ. It is thought that cells exist on a spectrum of activation states during AD development, eventually transitioning into "DAM"s – a phenotype characterized by downregulation of homeostatic genes and upregulation in inflammatory markers. Although the beneficial versus detrimental roles for DAM subsets are still debated, the transition to the "DAM" phenotype is a significant hallmark of AD progression associated with neurodegeneration.
Figure modified from Ennerfelt and Lukens, 2020, with permission [4].

1.8.3 Microglial iron handling

Single cell RNA sequencing studies suggest the disparate roles of microglia during AD development may be in part due to the heterogeneity of cell subpopulations found in diseased brains and the various activation states these cells assume over the course of disease progression

[127, 145]. In particular, recent studies have revealed a specific disease-associated microglial subpopulation in AD patient brains and mouse models characterized by the significant accumulation of iron [50, 51, 146]. As tissue-resident macrophages of the brain, microglia are equipped with the necessary machinery to import, store, and recycle (i.e., export) iron [1]. Studies have demonstrated that iron transport occurs preferentially in microglia compared with other cells in the brain [147, 148] and microglia are thought to store iron more efficiently as well [149]. Additionally, neurons and oligodendrocytes respond significantly to changes in microglial iron content [150-152], suggesting microglia play a similar central role in maintaining local iron homeostasis as other tissue-resident macrophages mentioned in **1.4.** Indeed, work over the past decade has elucidated a critical role for microglia in regulating brain iron homeostasis [153]. Microglia loaded with iron have been described in AD patient brains [146, 154, 155], models of Parkinson's disease [156, 157], amyotrophic lateral sclerosis [158], and multiple sclerosis [159]. This iron-loaded microglial phenotype has been closely linked with significant neuroinflammation, oxidative stress, and neurodegeneration [156, 160]. In fact, recent pioneering work done by Ryan et al. in a disease-related tri-culture cell system demonstrated the centrality of microglia in mediating iron-induced neuronal death [161]. In this study, microglial iron overload led to an iron-dependent form of cell death known as ferroptosis [162], which was shown to mediate nearby neuronal toxicity. Indeed, work *in vivo* has also suggested that a subset of microglia defined by significant iron load – senescent, or dystrophic, microglia – are the chief drivers of neuroinflammatory and neurodegenerative pathology [163-165]. Dystrophic, iron-loaded microglia secrete high amounts of pro-inflammatory cytokines (i.e., TNFα, IL-1β, IL-6, Type I IFN) and ROS, leading to significant neurotoxicity [166, 167]. Additionally, it has been posited that senescent, iron-loaded microglia lose their beneficial capacity for phagocytosis of Aβ [168]

and instead mediate aberrant synaptic loss leading to neurodegeneration [165, 169]. Importantly, an upregulation in iron storage genes *Fth1* and *Ftl* (ferritin) appears as a consistent marker of DAMs in transcriptomic studies [133, 170, 171], suggesting a change in microglial iron homeostasis may be a significant contributor to downstream disease development. While others have pointed out disparities in microglial phenotypes between AD mouse models and humans, this upregulation in iron storage markers has been shown as an overlapping and defining feature of mouse and human pathology [133, 146, 171].

1.8.3.1 Microglial iron and inflammation

An intimate relationship between microglial iron-handling and inflammatory status has become appreciated over the past decade [153, 172]. For example, it has been shown that excess iron load significantly increases microglial secretion of pro-inflammatory cytokines [173] and ROS [167] in response to an inflammatory stimulus. Others have also suggested that iron overload itself can provoke a cellular pro-inflammatory activation state, highlighting a close link between cellular

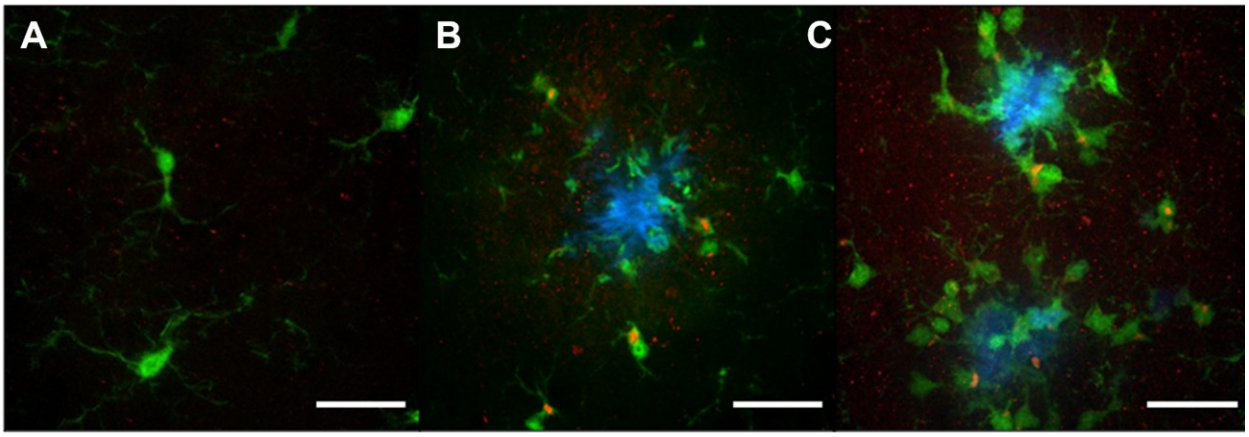

Figure 1.7. Plaque-associated, activated microglia are loaded with stored iron.
Shown are microscopic images taken of hippocampal sections from a wild-type control mouse (**a**) and the *APP/PS1* mouse model of AD (**b**) and (**c**). Microglial cells are visualized in green (endogenous GFP at the microglial *Cx3cr1* locus in both animals), Methoxy-X04 was used to visualize amyloid-β plaques (in blue), and an anti-ferritin antibody was used to visualize ferritin deposits (shown in red). Images were taken at 60x on a confocal spinning microscope, scale bar = 30 μm. Microscope images taken with the help of Julia Pinette.

iron load and inflammatory state [166, 174-177], although this has been debated recently in an iPSC model [178]. Reciprocally, inflammatory conditions promote cellular uptake of iron [179, 180]. In response to inflammatory stimuli such as bacterial LPS and Aβ, cells treated *in vitro* upregulate markers involved in iron import such as DMT1 and ferritin. In *in vivo* AD conditions, inflammatory, plaque-associated microglia are also iron-laden (which we have corroborated in my data, Fig. 1.7), suggesting a relationship between iron and inflammatory signaling in AD [50, 51]. However, it is still not fully understood how exactly iron-associated machinery and inflammation influence each other in microglia, especially during early stages of this progressive disease [128, 181]. The work in this dissertation thus aimed to determine the relationship between alterations in iron-handling machinery and inflammatory signaling in microglia during short-term inflammation and chronic disease *in vivo* (Chapters III and IV, respectively). While acute uptake of iron by macrophages and microglia may serve a protective role in the context of tissue damage (i.e., stroke) or bacterial infection (to prevent iron-aided pathogenic growth) [182], prolonged exposure to iron and inflammation such as observed in chronic AD may lead to a feed-forward loop of signaling detrimental to the cell and its surrounding environment [183] (Fig. 1.8). Although the specific interplay between microglial inflammatory signaling and iron-handling status during AD development has not been fully elucidated, microglial iron status has been suggested as a future therapeutic target for the treatment of AD [2].

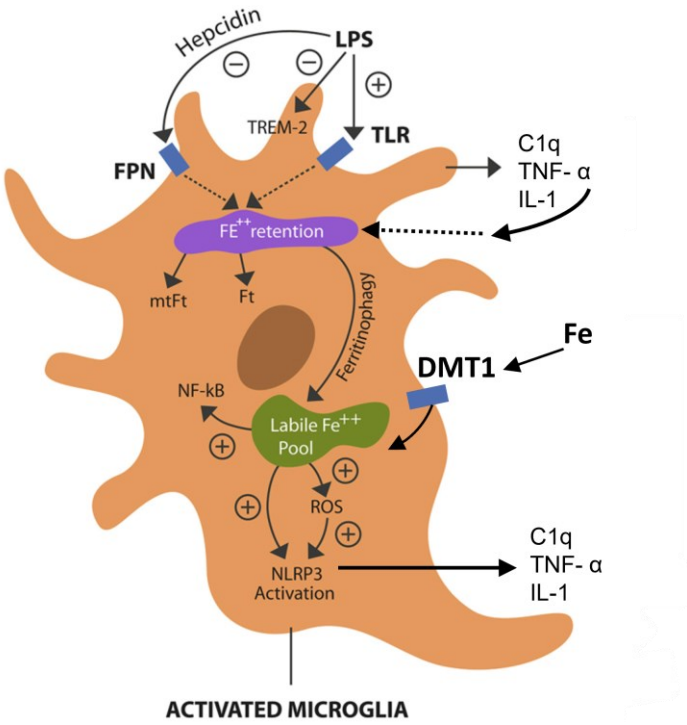

Figure 1.8. Purported iron-inflammatory feed-forward cycle in microglia.
Pro-inflammatory signals such as LPS (which activate TLR signaling) and cytokines such as IL-1β and TNFα initiate cellular iron uptake and retention. Ferroportin (iron export) is downregulated, DMT1 (iron import) is upregulated, and hepcidin is produced locally to induce iron sequestration and storage (Ft, mtFt) in these conditions. In conditions of iron overload, unbound iron augments inflammation directly and indirectly (via ROS production) through activation of nod-like receptor of pyrin domain containing 3 (NLRP3) inflammasome and nuclear factor kappa-B (NF-κB). Iron dissociation from ferritin via ferritinophagy contributes to the free iron pool ("labile iron"). NLRP3 and NF-κB activation leads to increased cytokine production of IL-1β and TNFα, which results in further iron sequestration.
Figure modified from Sfera, Gradini, Cummings, Diaz, Price, and Osorio, 2018, Figure 1, with permission [2].

Interestingly, the inflammation-induced increase in microglial iron uptake mentioned above appears to be specific to NTBI, which is reduced to Fe^{2+} at the plasma membrane before DMT1-mediated import into the cell [180]. As alluded to earlier in sections **1.4** and **1.5**, an increase in NTBI is typically observed in conditions of iron overload and represents a form of toxic iron which has a high propensity to induce ROS and cellular damage [76, 184]. It may be that detrimental DMT1-mediated increases in microglial iron contribute to the significant iron load, oxidative stress, and inflammation observed in AD brains. *In vitro* studies with AD-related

inflammatory stimulus Aβ demonstrate that microglial DMT1 is elevated in response to acute Aβ stimulation [173, 180] and inhibiting DMT1 significantly decreases the Aβ-induced inflammatory response [185]. While an association between DMT1 and inflammation related to AD in microglia has been established, a role for DMT1 in propagating microglial inflammation in the context of disease in *in vivo* systems has remained a significantly understudied area. It is not known whether altering DMT1 *in vivo* affects downstream inflammation, or whether targeting microglial DMT1 could serve as a therapeutic direction to limit disease-associated decline. This is the major focus of this dissertation.

1.9 Summary

Chapter I is a review of our current knowledge of AD pathology, iron imbalances in AD, and the roles of microglial cells in mediating neuroinflammation and iron dyshomeostasis in disease. Microglia play active and crucial roles in orchestrating inflammatory responses and associated changes in cellular iron load; thus, a deeper understanding as to how an iron-inflammatory axis in these cells may go awry in disease is of critical importance. Many questions remain as to how changes in iron homeostasis and inflammation are coordinated in the brain during disease, and especially as to how these co-pathologies may converge in microglia. In the long-standing pursuit of finding a preventative or interventive treatment for AD, targeting a pathway associated with iron-handling and inflammation in microglia may pose a new potential opportunity. The work described in this dissertation aimed to target an iron-inflammatory pathway and answer questions on how a mechanism involved in microglial iron import (via DMT1/gene, *Slc11a2*) may impact inflammatory and disease conditions *in vivo* (Fig. 1.9). In Chapter II, I describe the methodology utilized to assess the effects of targeting the microglial gene for iron importer DMT1 (*Slc11a2*) in

the context of an acute model of inflammation and a model of chronic AD. Chapter III details work showing how knockdown of microglial *Slc11a2* in mice experiencing acute inflammation leads to a significant abrogation of the neuroinflammatory response in a sex-specific manner. Chapter IV describes the impact of microglial *Slc11a2* knockdown on downstream cognition and behavior and markers of disease in a mouse model of chronic AD. Lastly, Chapter V summarizes the completed work and illuminates remaining questions and potential future directions.

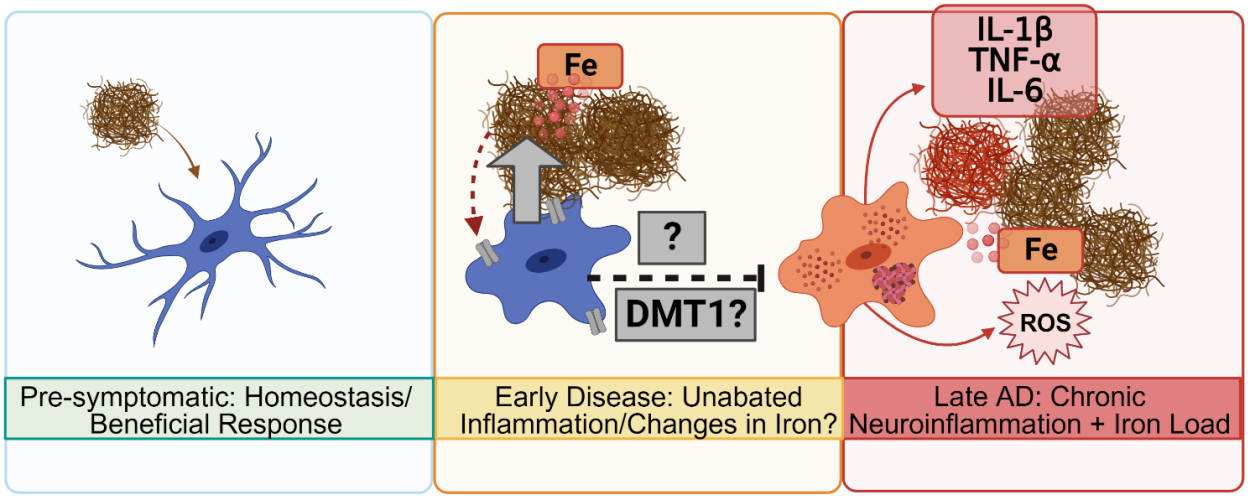

Figure 1.9. Targeting the remaining gaps in our understanding of the contribution of microglial iron importer DMT1 to disease.
In pre-symptomatic, homeostatic conditions, microglia react acutely to Aβ and effectively clear aggregates before returning to a homeostatic surveillance state. It is thought that in the transition to an early disease state, microglia become chronically activated (by a higher burden of Aβ and/or other contributing inflammatory events such as stroke, systemic inflammation). This dissertation research examines the idea that an increase in an iron-loading mechanism during this time of early disease contributes to the unabated inflammation and dysfunction of microglia observed in late-stage disease. Specifically, this research asks the question on whether targeting the microglial iron import gene for DMT1 at an early time point in disease inhibits downstream disease features including cognitive capacity and the presence of significant pro-inflammation, ROS production, and markers of iron and Aβ plaque load.
Figure made with BioRender.com, with permission.

CHAPTER 2

Materials and Methods

2.1 Animal models

All animal breeding, maintenance, and procedures were approved in advance and performed in compliance with the Institutional Animal Care and Use Committee at Vanderbilt University. Mice were weaned at 3 weeks of age and had *ad libitum* access to food (*LabDiets*, standard rodent chow 5001) and water. Both male and female mice were used in all *in vivo* experiments and were group-housed (2-5 per cage, paper bedding) by sex in transparent cages at 22-25ºC under a 12 h light/dark cycle in a specific pathogen-free facility. For studies discussed in Chapter III, an inducible model of microglial-specific knockdown of *Slc11a2* was generated. *Cx3cr1*$^{\text{Cre-ERT2}}$ (#020940, JAX) [186] and *Slc11a2-floxed* mice [96] (129S-*Slc11a2*^{tm2Nca}*/J;* #017789, JAX) were obtained from Jackson Laboratories (Bar Harbor, ME, USA). *Cx3cr1*$^{\text{Cre-ERT2}}$ mice harbor a Cre-recombinase driven by the promoter for the macrophage/microglial-specific chemokine receptor, *Cx3cr1,* fused to a mutated estrogen receptor (ER), allowing for Cre-mediated gene excision of *loxP*-containing sites upon tamoxifen exposure (agonist for the mutated ER). Homozygous *Cx3cr1*$^{\text{Cre-ERT2}}$ mice were bred in our facility with homozygous *Slc11a2-floxed* animals to obtain experimental *Cx3cr1*$^{Cre\text{-}ERT2+/WT}$*;Slc11a2*$^{fl/fl}$ animals. All genotypes were confirmed with an ear snip via Transnetyx (Cordova, TN) using real-time PCR. Experimental mice were on a mixed 129S/BL6 background and were crossed onto the C57BL/6J background over 6 different generations. For experiments conducted in Chapter IV, *Slc11a2*$^{fl/fl}$ and *Cx3cr1*$^{Cre\text{-}ERT2}$ animals were cross-bred until mice were homozygous for both genotypes (*Slc11a2*$^{fl/fl}$*;Cx3cr1*$^{Cre++}$). *APP/PS1*$^{+}$ hemizygous animals (Tg(APPswe,PSEN1dE9)85Dbo; #034832, JAX) were purchased from Jackson Laboratories and maintained in our facility. These transgenic animals express a chimeric mouse/human amyloid

precursor protein (Mo/HuAPP695swe) and a mutant presenilin-1 (PS1-dE9), as discussed in section **1.4**. *APP/PS1*$^{+}$ hemizygous animals were bred separately with *Slc11a2*$^{fl/fl}$ animals to yield *Slc11a2*$^{fl/fl}$*;APP/PS1*$^{+}$ mice. Resulting progeny from these crosses were then bred with the homozygous *Slc11a2*$^{fl/fl}$*;Cx3cr1*$^{Cre\text{-}ERT2++}$ animals to yield triple-transgenic *Slc11a2*$^{fl/fl}$*;Cx3cr1*$^{Cre\text{-}ERT2+/-}$;*APP/PS1*$^{+}$ or *APP/PS1*$^{-}$ (i.e., 'WT') mice. All mice used in experiments in Chapter IV were *Slc11a2*$^{fl/fl}$*;Cx3cr1*$^{Cre\text{-}ERT2+/WT}$ with either *APP/PS1*$^{+}$ hemizygosity or WT as littermate controls. Experimental mice were on a mixed 129S/BL6 background, with >80% BL/6J genetic makeup. For the primary cell experiments from young and aged mice in Chapter IV, young male 9-week-old control C57BL/6J mice were purchased from Jackson Laboratories (Bar Harbor, ME, USA) (#000664, JAX). C57BL/6J male mice between 27-30 months old were originally purchased from Jackson Laboratories and were aged and maintained in a Vanderbilt mouse facility (Dr. Rich Breyer). Control and experimental animals were randomly assigned across cages.

2.2 Mouse treatments

2.2.1 Tamoxifen treatment

To induce Cre-mediated knockdown of microglial *Slc11a2* in experiments for Chapters III and IV, a five-day tamoxifen treatment regimen was used. Tamoxifen (Sigma #T5648, Saint Louis, MO) was dissolved in corn oil (Sigma #C8267-2.5L, lot #MKCK6411, Saint Louis, MO) at a concentration of 20 mg/ml by stirring overnight at 37 °C. For animals in Chapter III, *Cx3cr1*$^{CreERT2/WT}$;*Slc11a2*$^{fl/fl}$ male and female mice at 9-14 weeks of age were administered a daily dose of 4 mg tamoxifen via oral gavage for five consecutive days [187] to achieve a Cre-mediated microglial knockdown of *Slc11a2* (denoted *Slc11a2*^{KD}). *Cx3cr1*$^{CreERT2/WT}$;*Slc11a2*$^{fl/fl}$ mice from the same litters given corn oil alone were used as a control for unintended Cre activity based on

recommendations in the literature [188]. Mice were allowed to rest for at least 4-5 weeks following tamoxifen or corn oil treatment before further treatment to allow for turnover of peripheral *Cx3cr1*-expressing monocytes and to restrict Cre-mediated recombination primarily to microglia [187, 189, 190]. Male and female mice in Chapter IV were administered tamoxifen with this regimen between 5-6 months of age, when Aβ plaque deposition becomes apparent in the *APP/PS1* model. These mice then remained in their cages until behavioral testing between 12-15 months of age. To confirm efficient microglial knockdown of *Slc11a2,* gene expression of *Slc11a2* was determined for each animal via RT-qPCR or bulk RNA sequencing analysis on isolated microglia depending on the experiment. Based on literature showing variability in knockdown efficiency using inducible Cre model systems [191], an *a priori* threshold of >50% *Slc11a2* knockdown was decided upon, and animals in Chapter III which did not exhibit at least a 50% knockdown of microglial *Slc11a2* compared to controls via qPCR were excluded from primary statistical analyses.

2.2.2 Lipopolysaccharide injection

For Chapter III, LPS injection was used to induce acute systemic and neural inflammation. LPS (derived from *E. coli* serotype O111:B4, Sigma #L4391, Saint Louis, MO) was dissolved in 0.9% sterile saline and fresh, single aliquots were used for each experiment. The sub-lethal dose and strain of LPS used was chosen based on previous work demonstrating a reproducible neuroinflammatory response in both sexes [192-195]. Mice were weighed the day before and morning of injection and were single-housed for accurate sickness scoring and nest building evaluations (sections **2.3** and **2.4.1**). Mice were injected intraperitoneally (i.p.) with a 2 mg/kg body weight bolus of LPS in volumes under 150 µL, or 100 µL 0.9% sterile saline as a vehicle

control. Saline and LPS mice were randomly distributed across cages prior to treatment, and the experimenter was blinded to experimental groups. Table 2.1 shows detailed numbers of animals used in the LPS experiments.

	24 h experiments	**Behavioral experiments (3-6 d post-LPS)**	**4 h experiment**
Male Control	14 Saline 14 LPS	11 Saline 13 LPS	5 Saline 5 LPS
Male *Slc11a2*^{KD}	13 Saline 14 LPS	10 Saline 11 LPS	7 Saline 7 LPS
Female Control	10 Saline 12 LPS	11 Saline 13 LPS	
Female *Slc11a2*^{KD}	12 Saline 12 LPS	11 Saline 13 LPS	

Table 2.1. Mouse numbers used for each experiment in Chapter III.
Only male mice were used for the 4 h post-LPS experiments based upon data showing that female knockdown animals were not significantly different from control female animals in LPS-induced behavioral sickness response and 24 h microglial gene expression analysis.

2.3 Sickness scoring

In Chapter III, mice were monitored for sickness behavior at baseline prior to LPS injection (0600-0730), and at 4 h, 8 h, and 24 h post-injection (injections were performed at 0800). A subset of mice was scored at 48 h and 96 h post-LPS as well. Specifically, an observer blinded to treatment groups weighed and scored the mice on the severity of sickness using a published 12-point scale of sickness behavior [196, 197], where a score of 12 represents a healthy mouse with normal activity and 0 represents a deceased mouse. Utilizing this scale, mice were evaluated for response to finger poke (4 for normal, 3 for slightly decreased, 2 for severely decreased, 1 for minimal response, and 0 for no response/dead), signs of encephalopathy (4 for normal gait, 3 for tremors or staggering, 2 for twisting movements, or 1 for falling/turning), and overall mouse appearance (score decreases by 1 each for display of piloerection, periorbital exudates, diarrhea, or respiratory

distress). Animals that received a score of 3 or below at any point post-injection were euthanized according to a humane endpoint (n = 1 euthanized male from the control-LPS group).

2.4 Behavioral assays

All behavioral assays were conducted in the Vanderbilt Murine Neurobehavioral Core laboratory after mice were acclimated to the facility for at least one-two weeks. In Chapter III, a cohort of male and female mice (n = 11-13 per group/per sex) was utilized for behavioral analyses 3-6 days after LPS injections following recovery from acute sickness behavior. In Chapter IV, all mice underwent testing by two experimenters between 12-15 months of age. The order of assays run was kept consistent for all animals in each study, and animals were run each day between 0630-1300 h with one task per day. For each task, mice were acclimated to the testing room for 30 min to 1 h prior to testing, and control and experimental groups were evenly and randomly distributed across cages, days, and time of each assay. Following completion of a trial, each apparatus was cleaned of feces, disinfected, and deodorized with an anti-bacterial spray (Peroxigard, Virox Technologies) in between animals.

2.4.1 Nest building

As a measurement of general cognition and well-being, an overnight nest building assay was used. For animals in Chapter III, nest building capacity was assessed at both 24 h post-LPS during the acute sickness phase and 72 h post-LPS following sickness recovery. In the AD model in Chapter IV, nest building assessments were performed as the first behavioral task to minimize effects of stress on the mice from other behavioral assays. Mice were single-housed and given 5 g of cotton nestlet (Ancare, Bellmore, NY) in the afternoon the day prior. The next morning, amount shredded and quality of nests was scored by a blinded observer using a 0-5 scale adapted from previous

work, in 0.5 increments [198, 199]. Following nest building assessment, mice were re-housed in groups of 4-5 for all other behavioral tasks.

2.4.2 Locomotor activity

For locomotor activity assessment, several assays were used. An elevated zero maze (white maze, width 5 cm; diameter 50 cm; wall height 15 cm, Stoelting Co. IL) was used first, where mice underwent a single 5 min trial of free exploration. Mice were video-recorded using a ceiling-mounted camera and movement was automatically tracked and scored using AnyMaze (Stoelting Co., Wood Dale, IL). Analysis parameters were set to ensure 80% of the mouse needed to be present in either the 'open' or 'closed' zone for an entry into that zone to be recorded. Total time in the open and closed zones and total distance traveled were measured. Sound-attenuating transparent open field chambers (27.5 x 27.5 cm) were used for a second measurement of baseline locomotor activity. Mice were placed in the center of the chamber and allowed to explore freely for 45 min. Distance traveled was recorded automatically via the breaking of infrared beams (MedAssociates ENV-510 software, Fairfax, VT). Additionally, time spent in the center area (19.05 x 19.05 cm) versus time in the 'surround' was calculated as a control measure of anxiety-like behavior.

2.4.3 Short-term spatial working memory

A single-trial Y-maze was used as both another measurement of baseline locomotor and exploratory behavior, as well as an assay to measure short-term working memory function. A clear plexiglass three-arm Y-maze (each arm 5 cm in width, 34.5 cm long) with differentiated arms (different colors of paper with or without patterns placed underneath the maze) was used. All mice were placed in the same point of the same arm and allowed to freely explore for 5 min. (Chapter

III) or 6 min (Chapter IV). A ceiling-mounted camera recorded video of the mice and AnyMaze automatically measured total distance traveled and order of arm entries. Entry into another arm was predicated on having at least 80% of the mouse cross into at least 1 cm of the arm. Spontaneous alternation as a measure of intact working memory was calculated by hand using arm entry order data from AnyMaze. A 'correct' alternation is defined by three consecutive entries into three different arms (e.g., ABC, BCA, CAB). Percent alternation was calculated using: ((Number of spontaneous alternations) / (Number of total arm entries – 2)) * 100.

2.4.4 Long-term memory (inter-session habituation)

In Chapter III, mice were returned to open field locomotion chambers two weeks following their initial exposure and the change in total distance traveled from the first session was recorded as a measure of longer-term memory with *Slc11a2* knockdown and post-LPS [200].

2.4.5 Morris water maze

The mice used in Chapter IV also underwent testing in the Morris water maze (MWM) to assess the effect of *Slc11a2* knockdown on learning and memory [201]. Briefly, a circular pool approximately 1 m in diameter filled approximately 30 cm deep with 22-27°C water was used for this task. A white round platform (10 cm in diameter) was used to provide animals an escape from the water. Mice first underwent two visual training days, where the platform jutted above the water with a pole attached to allow mice to see the target platform. This platform was moved around to each of the four quadrants on each session during training days to allow the opportunity for each animal to swim and survey the room, which contained multiple visual spatial cues kept constant throughout. Each training day comprised four trials per mouse, and each mouse was given 60 sec to find the platform. If a mouse did not reach the platform in 60 sec, it was guided to and placed

on the platform for at least 5 sec. On subsequent days following the two visual training days, the water was made opaque with non-toxic tempura white paint, and the platform was submerged approximately 0.5 cm under the water. The platform was kept in the same location for each trial and day, and mice were randomly placed in different locations in the pool so that the use of spatial cues for navigation was necessitated. Mice underwent four trials per day for five days, with each trial lasting 60 sec to assess learning and short-term memory. If mice did not find the platform within 60 sec, they were guided to the platform and escape latency was recorded as 60 sec. Following the final day of testing, the platform was removed and mice were allowed to swim freely for 60 sec. Total time spent in the target quadrant where the platform used to be, time spent around the location of the platform, swim speed, total distance traveled, and time spent in perimeter were recorded as measurements of platform location memory.

2.4.6 Fear conditioning assay

Following completion of all other behavioral tasks, a fear conditioning assay was conducted in the animals in Chapter IV to assess differences in fear-associated memory. Mice were placed in sound-attenuating chambers with a wire grid floor. On the first day (training trial), mice were placed in the chambers for 8 min and allowed to run around freely. Every 2 min, a 30 sec tone was played, followed immediately by a small shock administered through the wire floor (1 sec, 0.5 mA). This tone-shock pairing occurred 3 times during the training trial. To assess contextual fear conditioning, mice were placed back into the same chamber the next day and allowed to run around freely for 4 min with no tone or shock presented. Total time freezing – indicative of fear memory – was recorded automatically (VideoFreeze, MedAssociates). To assess cued fear conditioning (memory of the tone), mice underwent a second testing trial. This trial included a different experimenter handling the mice, significant alterations to the chamber with white walls, white

floor inserts, and red light, and the scent of vanilla placed in an open tube outside the chamber. Mice freely explored the chamber for 2 min before the tone was administered for the final 2 min (without a shock pairing). Total time spent freezing during the no-tone and tone segments were recorded as a measurement of cued fear memory.

2.5 Mouse euthanasia and tissue collection

At the time of euthanasia, mice were deeply anesthetized with isoflurane and 500-700 μL of blood was collected via cardiac puncture. Immediately following blood collection, mice were trans-cardially perfused with 20 mL of cold 1x Dulbecco's phosphate-buffered saline (DPBS) to remove circulating blood and decapitated for rapid brain removal. Whole brains were either placed on ice for mincing and processing for cellular isolation, or the hippocampus and cortical regions were isolated first before proceeding to cellular isolation. A subset of brains from females in chapter IV were extracted carefully following transcardial perfusion with ice-cold 4% paraformaldehyde (PFA) and immediately fixed in 4% PFA for 24 h at 4°C before transferring to a 1x PBS with 0.02% sodium azide solution. These brains were used for tissue clearing using the SHIELD method [202] following manufacturer's instructions (Life Canvas Technologies, Cambridge, MA) and imaged with a light sheet microscope at the Vanderbilt Neurovisualization Core (Dr. Jose Maldonado).

2.6 Plasma collection and cytokine analysis

Blood was collected into EDTA-coated syringes from the right ventricle following cardiac puncture and immediately placed into EDTA-coated (25 mM, 20-30 μL evaporated overnight) tubes on ice to prevent coagulation. Samples were then centrifuged at 4°C (2500 rcf, 10 min) for

plasma isolation. Plasma was aliquoted into separate tubes and stored at -80°C for further analysis. A cohort of male mice in Chapter III (n = 5-7/group) was utilized to assess the acute systemic cytokine response 4 h after LPS. Only male mice were assessed based on multiple data points from earlier experiments indicating a significant effect of knockdown on the LPS-induced response only in the males. Plasma cytokines IFNγ, IL-1β, IL-10, MCP-1, IL-6, and TNFα were measured via a Luminex multiplex cytokine panel performed by the Vanderbilt University Medical Center Hormone Assay and Analytical Services Core. To stay within standard curves, un-diluted samples were used for IFNγ, IL-1β, IL-10, and MCP-1, and a 1:5 dilution was used for IL-6 and TNFα. Additionally, levels of TNFα and IL-6 were confirmed by ELISA according to manufacturer's instructions (BioLegend, TNFα, #430904; IL6, #431304, San Diego, CA).

2.7 Microglial isolation

2.7.1 Tissue digestion and single-cell suspension preparation

Brains were rapidly removed and briefly placed in 3 mL cold, sterile 1x Hank's buffered saline solution (HBSS, Gibco, #14175095) containing 1% fetal bovine serum (FBS, heat-inactivated; Gibco, #10082147) to remove any residual blood. Microglia isolation was performed following published protocols, with slight modifications [203-205]. Briefly, whole brains were transferred and finely minced with scissors in cold, sterile "IMG media" [Dulbecco's modified Eagle's medium (DMEM) with high glucose (4.5 g/L) and L-glutamine media (Gibco, #11965092) containing 10% FBS and 1% penicillin-streptomycin (Gibco, #15140122). Minced tissue was transferred into 50 mL conical tubes and 5 mL of digestion media (IMG media + 100 units Papain, #LK003176; 500 Kunitz units DNase, #LK003170, Worthington Biochemicals, Lakewood, NJ) was added to each tube. Samples were enzymatically-dissociated by placing in an orbital shaker

for 1 h at 37°C, diluted with 10 mL IMG media, and strained through 70 μm sterile filters (Corning, #431751). Samples were further processed at 4°C unless otherwise indicated.

2.7.2 Percoll gradient

Cells were centrifuged for 5 min at 500 x g, and re-suspended in a solution of 30% isotonic Percoll and IMG media (Cytiva, #17-0891-01) and slowly layered onto a 70% Percoll gradient with HBSS + 1% FBS. HBSS + 1% FBS (without Percoll) was layered on top, and samples were centrifuged for 15 min at room temperature at 600 x g with the brake set to the lowest setting to allow for density separation. The supernatant containing myelin and neuronal debris was removed, and cells at the interface between the 30-70% gradients were carefully collected and placed on ice into 8mL HBSS + 1% FBS in a fresh tube to wash residual Percoll. Cells were centrifuged at 500 x g for 5 min at 4°C, and pelleted cells were re-suspended in appropriate media for downstream assays.

2.7.2.1 Plating and treatment for primary cell experiments

For experiments conducted in isolated primary cells from young and aged mice in Chapter IV, all steps above were performed under sterile conditions in a cell culture hood with autoclaved tools and sterile-filtered reagents. Glial cells isolated and pelleted from the Percoll gradient were re-suspended in 1 mL IMG media for counting and plating. Cells were counted using the Nexcelom Cellometer Auto T4 Cell Counter (Nexcelom Biosciences) and plated at a density of 100,000 cells per well in poly-L-lysine-coated 48-well plates in pre-warmed sterile IMG media containing 5 ng/mL GM-CSF (R&D Systems, #415-ML-010). Media was changed the next day, and then every other day for five days before stimulation, described below in section **2.10.2**.

2.7.3 CD11b immunomagnetic microglial isolation

For experiments in Chapter III (**sections 3.2.2 and 3.2.5**) and **section 4.2.5** of Chapter IV, Percoll-isolated glial samples were further processed for enrichment of $CD11b^+$ microglia. Following Percoll gradient separation, centrifugation, and pelleting, cells were re-suspended in 400 µL cold "MACS" buffer (1x PBS containing 0.5% FBS and 2 mM EDTA) and transferred to 5 mL tubes. Cells were centrifuged at 4°C for 5 min at 500 x g, pelleted, and re-suspended in 90 µL MACS buffer for magnetic labeling and separation according to manufacturer's instructions (Miltenyi Biotec, Bergisch Gladbach, Germany). Briefly, samples were incubated with magnetic anti-CD11b MicroBeads (Miltenyi Biotec, #130-093-634; 10 µl per 90 µl buffer/brain) for 15 min at 4°C. Magnetic separation was performed utilizing MS columns, and $CD11b^+$ cells and the effluent non-magnetic fractions ($CD11b^-$ cells) were obtained. Following a final centrifugation for 5 min at 500 x g, cells were immediately re-suspended in RLT lysis buffer (Qiagen, #74004) supplemented with 1% beta-mercaptoethanol, briefly vortexed, and flash-frozen in liquid nitrogen. Samples were stored at -80°C until RNA isolation.

2.8 RNA isolation, cDNA synthesis, and RT-qPCR

Lysed cell samples ($CD11b^+$ and $CD11b^-$ fractions) were processed for total mRNA using an RNeasy Micro Kit with DNase treatment according to the manufacturer's protocol (Qiagen, Hilden, Germany, #74004). Following on-column RNA purification and elution, cellular RNA was reverse transcribed into cDNA at equal concentrations across samples using iScript Reverse Transcriptase (BioRad, Hercules, CA). RT-qPCR was conducted to assess the expression of several genes and confirm *Slc11a2* knockdown using FAM-conjugated TaqMan Gene Expression Assay primers (Thermofisher) and iQ Supermix (BioRad). PCR reactions were performed in duplicate

under thermal conditions: 95°C for 10 min, followed by 40 cycles of 95°C for 15 s, and 60°C for 45 s. The expression of each gene measured was normalized to a housekeeping gene (either *18S* or *ActinB* where indicated), and relative expression values were analyzed utilizing the comparative cycle threshold $2^{-\Delta\Delta CT}$ method [206].

2.9 RNA sequencing

2.9.1 Library preparation and RNA sequencing

Following on-column purification and DNase treatment with the Qiagen Rneasy Micro Kit, total mRNA extracted from $CD11b^+$ samples was submitted to the Vanderbilt Technologies for Advanced Genomics (VANTAGE) Core facility for sample quality control assessment and RNA Sequencing (RNASeq). The concentration of RNA samples was determined by NanoDrop (ThermoScientific). Sample Quality Control analysis was assessed using fluorometry Qubit and integrity by BioAnalyzer, and a RIN value of >7 was confirmed for all samples before proceeding to library preparation and sequencing. One sample (n =1) was excluded from the male samples in Chapter III due to low RNA quality. Paired-end sequencing libraries were constructed using a standard mRNA NEBNext Poly(A) selection Library Prep Kit (Illumina). Library Quality Control analysis was performed by using Qubit and BioAnalyzer to determine the concentration and size bp. Samples were then sequenced at multiplex Paired-End 150 bp using the Illumina NovaSeq 6000 sequencing platform targeting an average of 50M reads per sample. To confirm sequencing quality, Illumina Quality Scores were calculated utilizing the following equation: $Q = -10\log_{10}I$. All samples sequenced reached sequencing quality of at least Q(30).

2.9.2 Sequencing analysis: alignment, mapping, quantification, differential expression

For RNASeq data in Chapter III, gene alignment, read mapping, and reads quantification were conducted using Illumina's automated Dragen RNA-Seq pipeline version 3.6.3 with the mouse reference genome Mouse mm10. Files were generated and deposited in BaseSpace Sequence Hub via Illumina's automated workflow. A .csv file describing the number of reads mapped to each gene for each sample was then utilized as input for an RNA-Seq data analysis pipeline. Differential expression for gene read counts were analyzed with DESeq2 version 1.36 [207] using R version 4.2.2. In brief, gene counts were normalized by a negative binomial distribution model to account for overdispersion, followed by Bayesian shrinkage estimators for effect sizes using the Approximate Posterior Estimation for the GLM (apeglm) package [208]. Differential expression analyses between Control vs. *Slc11a2*^{KD} in the LPS studies was completed using the Wald test in DESeq2, and corrected for multiple comparisons (p.adjust) using the Benjamini and Hochberg method [209, 210]. RNASeq data discussed as a future direction in Chapter V will be from hippocampal CD11b^{+} microglia isolated from female control and experimental mice following findings of significant behavioral differences in *Slc11a2* knockdown female *APP/PS1* animals. Gene alignment, read mapping, and gene counts quantification were conducted at the Creative Data Solutions (CDS) Core at Vanderbilt using mouse reference genome mm39.

2.10 *In vitro* cells and experimental treatments

The immortalized microglial cell line, "IMG" [211], was used for *in vitro* experiments to assess the effect of pharmacological inhibition of DMT1 on Aβ-induced inflammation. IMG cells were purchased from Millipore (Cat. #SCC134, RRID:CVCL_HC49), and cultured as described using

Accutase for dissociation and passaging [185]. Cells used in experiments were cultured up to a maximum of 10 passages in sterile IMG media (described in section **2.7.1**).

2.10.1 Ebselen treatment of IMG cells

IMG cells were plated and grown in six-well tissue culture plates the day before ebselen treatment in IMG media. Ebselen was purchased from Focus Biomolecules (#10-2288) and re-suspended in sterile dimethyl sulfoxide (DMSO; Sigma, #276855). A 25 μM concentration of ebselen was chosen as the treatment, following preliminary experiments indicating this dose decreased cellular iron content and following similar reported doses from previous work [89]. After 24 h treatment with either ebselen or control DMSO, cells were treated as described below in section **2.10.2**.

2.10.2 Amyloid-β and iron treatments

In both IMG cells and the primary isolated glia in Chapter IV, amyloid-$\beta_{1\text{-}42}$ was used as an acute AD-associated inflammatory stimulus. Aβ (HFIP-treated, rPeptide #A-1163-2) and a scrambled Aβ (rPeptide #A-1004-2) were purchased from rPeptide and 5 mM stock solutions were prepared with anhydrous DMSO (Sigma #276855) and sonicated for 15 min before storing aliquots at -20°C. The day before cell stimulation, oligomeric $A\beta_{1\text{-}42}$ was prepared as previously described [173] using cold, sterile phenol-free Ham's F-12 media (R&D Systems, #M25350) and allowed to rest at 4°C for 24 h. The next day, cells were treated with 1 μM $A\beta_{1\text{-}42}$ or scrambled Aβ for 24 h before lysis and collection for RNA isolation as described above in section **2.8**. For *in vitro* experiments in IMG cells, ferric ammonium citrate (FAC, Sigma, #F5879) was used as a non-transferrin-bound form of iron. FAC was re-suspended fresh in sterile RNase-free water immediately before each experiment, and cells were treated with 50 μM FAC based on literature recommendations [173, 178] or water (control), with or without Aβ.

2.11 Data and statistical analyses

Data are presented as mean ± S.E.M. All experiments were analyzed using analysis of variance (ANOVA) for multiple comparisons followed by appropriate post-hoc analyses unless otherwise noted. Male and female data were first compared using ANOVA (2(Sex) x 2(Genotype) x 2(Treatment), followed by Sidak's corrections for multiple comparisons and analysis of interaction effects. After observing sex differences particularly in LPS-induced *Slc11a2* expression when directly comparing male and female data in Chapter III, most primary analyses were conducted within each sex separately to assess the effect of *Slc11a2* knockdown in each sex. To do this, a 2(Genotype) x 2(Treatment) ANOVA followed by Sidak's corrections was used. In analyzing sickness scoring data from Chapter III, repeated measures ANOVA (2(Genotype) x 2(Treatment) x 4(Time)) was used to analyze scoring data from multiple time points and Tukey's post-hoc analysis was used following significant F values to establish differences among all groups. Data from primary cell and IMG cell experiments in Chapter IV were analyzed using either 2(Treatment) x 2(Age) ANOVA or 3(Treatment) x 2(ebselen/DMSO) ANOVA, respectively. Sidak's post-hoc analysis was used for interaction effects and corrections for multiple comparisons. Statistical outliers within each group for all studies were identified using the ROUT method for multiple outliers and excluded from statistical analyses. GraphPad Prism 9 (GraphPad Software, San Diego, CA, USA) was used for statistical analyses outside of RNASeq analyses conducted in R. Differences among groups were considered significant at values of $p<0.05$.

CHAPTER 3

Microglial-specific knockdown of iron import gene, *Slc11a2,* blunts LPS-induced neuroinflammatory responses in a sex-specific manner

Adapted from Volk Robertson, K., et al. *Brain Behavior and Immunity,* 2024. February 2024. doi: 10.1016/j.bbi.2023.12.020

3.1 Introduction

Excessive iron deposition in the brain is strongly associated with several neurodegenerative diseases, including Alzheimer's disease (AD), Huntington's disease, and Parkinson's disease [104, 212-214]. While iron is critical for mitochondrial metabolism, neurotransmitter synthesis, and myelination in the brain; excess iron is associated with chronic neuroinflammation and the toxic production of reactive oxygen species (ROS), which can ultimately lead to DNA and protein damage, lipid peroxidation, and cell death often seen in disease [52, 184].

Microglia, the resident innate immune cells of the central nervous system (CNS), play a critical role in tightly regulating brain iron levels to maintain neural homeostasis and orchestrate appropriate responses to CNS injury [153]. While microglial cell-mediated neuroinflammation has been widely recognized as a prominent feature of neurodegenerative disease pathology [215, 216], more recent work suggests that iron loading in activated microglia is also a prominent hallmark of both mouse and human disease pathology [2, 50, 146]. Work over the last decade has highlighted an intimate relationship between inflammatory signaling and iron-handling status at the cellular level [2, 172]. Microglial iron retention often occurs during a shift towards a pro-inflammatory cellular state [50, 51, 160], and increased iron import has been shown to enhance microglial secretion of pro-inflammatory cytokines and ROS production in response to inflammatory stimuli

[167, 173, 217]. While iron load enhances inflammation, *in vitro* studies also demonstrate that acute inflammatory signals, such as bacterial lipopolysaccharide (LPS) and AD-associated amyloid-β, increase microglial import and sequestration of local non-transferrin-bound iron (NTBI) [179, 180]. Specifically, these inflammatory signals upregulate the microglial ferrous iron (Fe^{2+}) importer, divalent metal transporter 1 (DMT1; gene name, *Slc11a2*) [167, 173, 180]. DMT1 is a widely-expressed proton-coupled ferrous iron transporter critical for life [92], and is found on both the cellular plasma membrane as well as the endosomal membrane. While this transporter is important for the immediate import of extracellular iron reduced to Fe^{2+} at the plasma membrane, it also plays an essential role in the endosome, where it transports Fe^{2+} (the usable form of iron in the cell) into the cytosol after reduction in the endosome [79]. Inflammation-induced increases in DMT1, and the reported effects of iron on augmenting inflammation suggest a reciprocal, feed-forward relationship between inflammatory signaling and changes in iron import machinery in these cells. Despite the greater attention brought to the role of iron in exacerbating neuroinflammation during the last decade, the bidirectional relationship between changes in cellular iron import mechanisms and inflammatory signaling is not fully understood [172].

Considerable evidence demonstrates that systemic inflammation triggers microglial activation and accelerates neurodegeneration in rodent models [218, 219] and humans [220, 221]; however, it is not known how or whether microglial iron-handling machinery and systemic inflammatory signaling influence each other. Few studies have examined directly how a shift in a microglial iron import gene might affect downstream inflammatory processes *in vivo.* In the present study, we sought to determine the effects of directly altering a microglial iron import gene, via microglial-specific knockdown of iron importer *Slc11a2*, on downstream inflammatory events in a rodent model of LPS-induced inflammation. The endotoxin, LPS, is the major surface

membrane component of Gram-negative bacteria, and is a widely used stimulus to experimentally induce neuroinflammation associated with increases in key pro-inflammatory cytokines, such as interleukin (IL)-1β, IL-6, and tumor necrosis factor-α (TNF-α) [59, 222, 223]. To determine the *in vivo* effects of decreased *Slc11a2* on the inflammatory response in both sexes, we generated a novel model of inducible microglial *Slc11a2* knockdown in both male and female mice. After challenging mice with systemic LPS, we investigated whether microglial *Slc11a2* knockdown alleviated acute LPS-induced inflammation and altered downstream cognitive function following a period of short-term recovery.

3.2 Results

3.2.1 Microglial *Slc11a2* knockdown improves acute sickness response post-LPS injection in male, but not female, mice

Following i.p. injection of LPS (2 mg/kg body weight, initial body weights shown in Table 3.1), male and female mice were monitored for signs of sickness behavior at 4, 8, and 24 h post-LPS before euthanasia and CD11b+ microglial isolation for *Slc11a2* gene expression analysis (experimental diagram, Fig. 3.1a).

	Control + Saline	***Slc11a2*^{KD} + Saline**	**Control + LPS**	***Slc11a2*^{KD} + LPS**
Males	28.82 ± 0.71	29.38 ± 0.67	29.03 ± 0.56	28.92 ± 0.78
Females	24.98 ± 0.68	25.16 ± 0.60	25.43 ± 0.48	24.80 ± 0.46

Table 3.1. Body weights were assessed immediately prior to injections of saline or LPS. The data are presented as average weight in grams ± S.E.M. for 21-33 mice per group.

As expected, isolated microglial cells from animals treated 4-5 weeks prior with tamoxifen exhibited a significant decrease in *Slc11a2* gene expression in both males and females, indicating efficient cellular knockdown of *Slc11a2* (Fig. 3.1b; *Knockdown,* $F(1,88) = 163.6$, $p < 0.0001$).

Specifically, we were able to achieve between an 80-90% knockdown of *Slc11a2* in most mice. At 24 h post-LPS injection, microglia from control male mice exhibited a >2-fold increase in *Slc11a2* expression compared to saline controls (Fig. 3.1b; $p<0.0001$), reproducing *in vivo* what has been shown *in vitro* [180]. This upregulation was only observed in cells isolated from males (*Sex,* $F(1,88) = 10.17$, $p = 0.002$, *Treatment x Sex,* $F(1,88) = 7.78$, $p=0.007$), as microglia from females showed no upregulation in microglial expression of *Slc11a2* in response to LPS (Fig. 3.1b; Female Saline vs Female LPS, $p>0.999$). Indeed, female microglia express significantly lower levels of *Slc11a2* in response to LPS when compared directly to their male counterparts (Fig. 3.1b, Males Control LPS vs. Females Control LPS, $p<0.0001$). Furthermore, this LPS-induced *Slc11a2* response in males appears to be primarily a microglial response, as the CD11b-negative neural cell fraction isolated from this timepoint did not exhibit a significant increase in *Slc11a2* (Fig. 3.2). As expected, LPS significantly worsened sickness score in control male and female mice at all time points (Fig. 3.1c, *Time* $F(2.6, 202.6) = 90.62$, $p<0.0001$ compared to baseline, Fig. 3.1d, Males; *Treatment* $F(1, 77) = 64.75$, $p<0.0001$, *Time x Treatment* $F(3, 231) = 28.39$, $p<0.0001$; 4 h: $p<0.0001$; 8 h: $p<0.0001$; 24h: $p = 0.0002$; Fig, 3.1e, Females; *Treatment* $F(1,72) = 53.73$, $p<0.0001$; *Time x Treatment* ($F(3, 216) = 22.75$, $p<0.0001$). When comparing males and females directly post-LPS, we did not observe a statistically significant difference in LPS-induced sickness scores at 4, 8, or 24 h in control animals (Fig. 3.1c, *Sex,* $p>0.05$), demonstrating the robust effect of this LPS dose in provoking significant sickness behavior compared to baseline and saline controls in both sexes. However, there was a significant interaction between *Sex* and *Knockdown* in the LPS-provoked sickness response (Fig. 3.1c; *Sex x Knockdown,* $F(1,77) = 8.34$, $p = 0.005$). Specifically, male mice with microglial *Slc11a2* knockdown showed an acute significant improvement in overall sickness score compared to littermate *Slc11a2*-intact control animals at 4

and 8 h post-LPS (Fig. 3.1c, d; *Knockdown x Treatment* $F(1, 77) = 12.52$, $p<0.001$), *Time x Knockdown x Treatment* ($F(3, 231) = 4.142$, $p<0.01$; 4hr: $p = 0.003$, 8hr: $p = 0.056$). In fact, the sickness response observed in male *Slc11a2*^{KD} animals following LPS treatment was not significantly different from male control animals administered saline during the acute phase post-LPS (Fig. 3.1d; 4 h: $p = 0.412$; 8 h: $p = 0.252$). This modulatory effect of microglial *Slc11a2* knockdown was only observed in male mice, as *Slc11a2*^{KD} females exhibited similar LPS-induced sickness behavior as both control females and males at all time points post-LPS (Fig. 3.1c, 4 h: Female KD LPS vs. Female control LPS, $p>0.99$, Female KD LPS vs. Male control LPS, $p = 0.57$; 8 h: Female KD LPS vs. Female control LPS, $p>0.99$, Female KD LPS vs. Male control LPS, $p = 0.70$; 24 h: Female KD LPS vs. Female control LPS, $p = 0.98$, Female KD LPS vs. Male control LPS, $p>0.99$; Fig. 3.1e; *Treatment* $F(1,72) = 53.73$, $p<0.0001$; *Time x Treatment* ($F(3, 216) = 22.75$, $p<0.0001$; *Knockdown x Treatment* $F(1,72) = 0.003$, $p = 0.96$). This demonstrates the sex-specific effect of the *Slc11a2* knockdown in modulating the acute male sickness behavioral response to LPS.

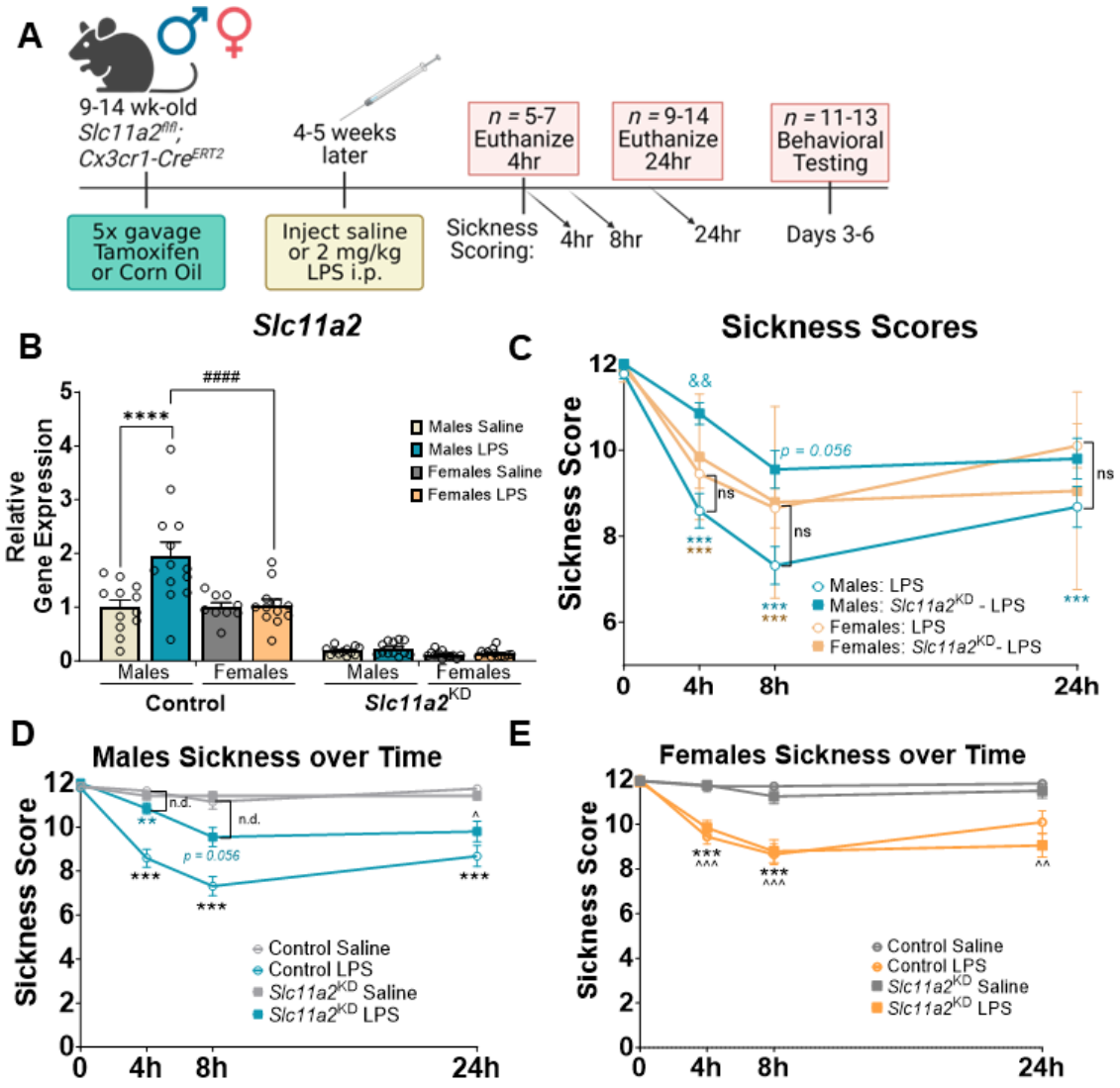

Figure 3.1. Microglial *Slc11a2* knockdown improves acute LPS-induced sickness response in male, but not female, mice.

a) Experimental design: Male and female *Slc11a2*$^{fl/fl}$;*Cx3cr1*$^{Cre\text{-}ERT2+/WT}$ mice were given tamoxifen or corn oil vehicle (p.o.) to induce Cre-mediated *Slc11a2* gene knockdown. After 4-5 weeks, control and knockdown mice received saline control or LPS (i.p., 2 mg/kg) before downstream assessments at various timepoints. **b)** *Slc11a2* gene expression was measured via RT-qPCR from whole-brain isolated CD11b+ microglia 24 h after LPS injection. Data represent the mean ± S.E.M. of 9-14 mice per group. Three-way ANOVA, ****p<0.0001 effect of LPS Treatment in males, $^{\#}$p<0.05, $^{\#\#\#\#}$p<0.0001 effect of Sex x Treatment in females, $^{\&\&}$p<0.01 effect of male knockdown on LPS-induced response. **c)** Behavioral sickness response scores at baseline and 4, 8, and 24 h post-LPS injection in male and female mice. $^{\&\&}$p<0.01 male *Slc11a2*^{KD} compared to control LPS, ***p<0.001 compared to baseline for both sexes labeled in corresponding color, 'ns' = not significant, no significant differences found between males and females in the LPS-induced response in controls. Data represent the mean ± S.E.M of 17-22 mice per group. **d)** Male behavioral sickness response scores at baseline and 4, 8, and 24 h post-LPS, including saline groups. *denotes differences between Control-LPS and Saline, *denotes differences between *Slc11a2*^{KD}-LPS vs. Control-LPS in corresponding color, $^{\wedge}$denotes differences between Slc11a2^{KD}-LPS vs. Saline, 'n.d.', no difference between *Slc11a2*^{KD}-LPS and Saline mice, **p<0.01, ***p<0.01, $^{\wedge}$p<0.05. Data represent the mean ± S.E.M. of 19-22 mice per group. **e)** Female behavioral sickness response scores at baseline, 4, 8, and 24 h post-LPS, including saline groups. *denotes differences between Control-LPS and Saline, $^{\wedge}$denotes differences between *Slc11a2*^{KD}-LPS and Saline, no differences detected between *Slc11a2*^{KD}-LPS and Control-LPS, ***p<0.001, $^{\wedge\wedge}$p<0.01, $^{\wedge\wedge\wedge}$p<0.001. Data represent the mean ± S.E.M of 17-20 mice per group.

Figure 3.1a was generated using BioRender.com, with permission.

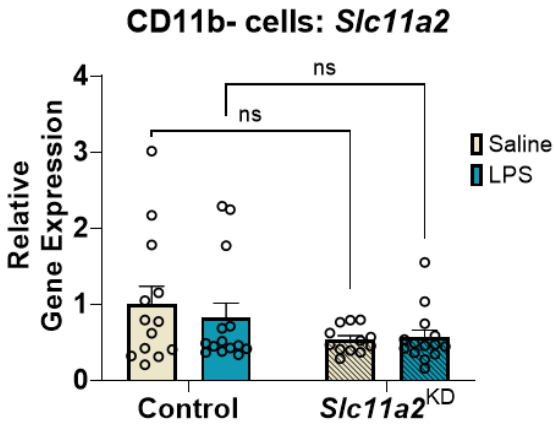

Figure 3.2. CD11b-negative cells do not exhibit changes in *Slc11a2* in males 24 h post-LPS. Cells from the whole brain were magnetically-sorted for CD11b, and the negative fraction was isolated for RT-qPCR gene expression. Data are normalized to housekeeping gene *18S* and represent the mean ± S.E.M of 11-14 mice per group. ns = not significant.

3.2.2 LPS-induced pro-inflammatory gene expression is significantly decreased in isolated microglia from *Slc11a2* knockdown male mice.

To assess molecular changes that underlie the blunted LPS-induced sickness response in *Slc11a2*-knockdown male animals, mice were euthanized 24 h following saline or LPS injections and whole-brain CD11b$^+$ microglia were collected for RT-qPCR gene expression analyses of several pro-inflammatory markers. As expected, LPS treatment significantly upregulated the expression of *Il-1β* in both male and female controls, albeit to a lesser degree in females (Fig. 3.3a, Males; *Treatment,* p = 0.0005; Fig. 3.3d, Females; p = 0.012). Female microglia overall displayed a lower LPS-induced cytokine response in *Il-1β* and *Il6* compared to males in the control groups (Fig. 3.4a-b; *Il-1β,* Males LPS vs. Females LPS, p = 0.056; *Il6,* Males LPS vs. Females LPS p = 0.015), which has been reported by others [224-226]. Microglial *Slc11a2* knockdown had a modulatory effect on LPS-induced *Il1β* and *Il6* expression only in male microglia, as *Slc11a2* knockdown significantly attenuated the LPS-induced upregulation in *Il1β* (Fig. 3.3a; *Interaction*, F(1, 46) = 9.15, p = 0.0041) and *Il6* expression in isolated male *Slc11a2*^{KD} microglia (Fig. 3.3b; *Interaction*,

F(1, 48) = 7.07, p = 0.011; Fig. 3.4a-b, *Il1β*: *Knockdown x Treatment x Sex,* F(1,83) = 3.52, p = 0.064; *Il6*: *Knockdown x Treatment x Sex,* F(1,86) = 9.40, p = 0.003). *Tnfα* was significantly upregulated in female and male microglia in response to LPS compared to their control counterparts (Fig. 3.4c; *Treatment,* F(1,81) = 7.49, p = 0.008); however, there were no significant differences in LPS-induced *Tnfα* expression due to knockdown in either sex (Fig. 3.3c, f; Fig. 3.4c). Female *Slc11a2* knockdown microglia given LPS exhibited no difference compared to female LPS controls in any of the measured LPS-induced cytokines (Fig. 3.3d-f, p>0.05), suggesting this is a sex-specific effect of *Slc11a2* knockdown on markers of LPS-induced pro-inflammation in microglia.

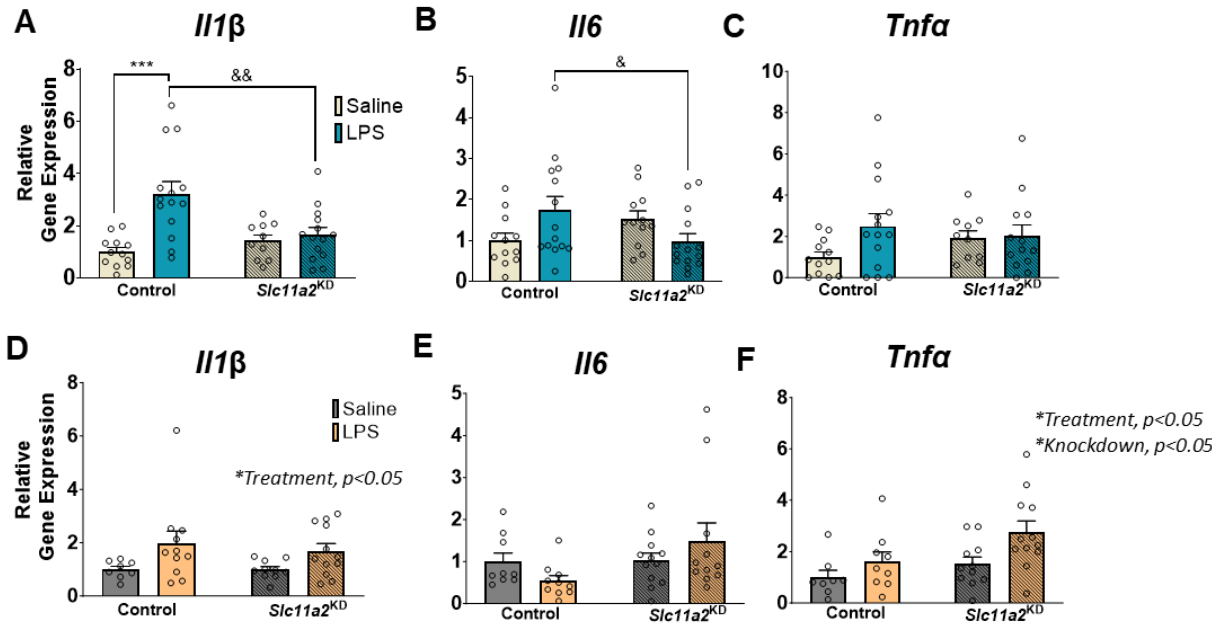

Figure 3.3. *Slc11a2* knockdown blunts pro-inflammatory gene expression in isolated microglia 24 h post-LPS in male, but not female, mice.
a-c) CD11b^{+} microglia were isolated from the brains of *Slc11a2*-knockdown and corn oil control animals 24 h following saline or LPS injection for RNA extraction and RT-qPCR analysis. *Il1β*, *Il6,* and *Tnfα* gene expression from male microglia 24 h post-LPS. **d-f)** *Slc11a2, Il1β*, *Il6,* and *Tnfα* gene expression from female microglia 24 h post-LPS. *denotes *Treatment* effect, $^{\&}$denotes *Interaction* effect, $^{**}p < 0.01$, $^{***}p < 0.001$; $^{\&}p < 0.05$, $^{\&\&}p < 0.01$, $^{\&\&\&}p < 0.001$, 'n.d.' = no difference. Data represent the mean ± S.E.M of 8–14 mice per group.

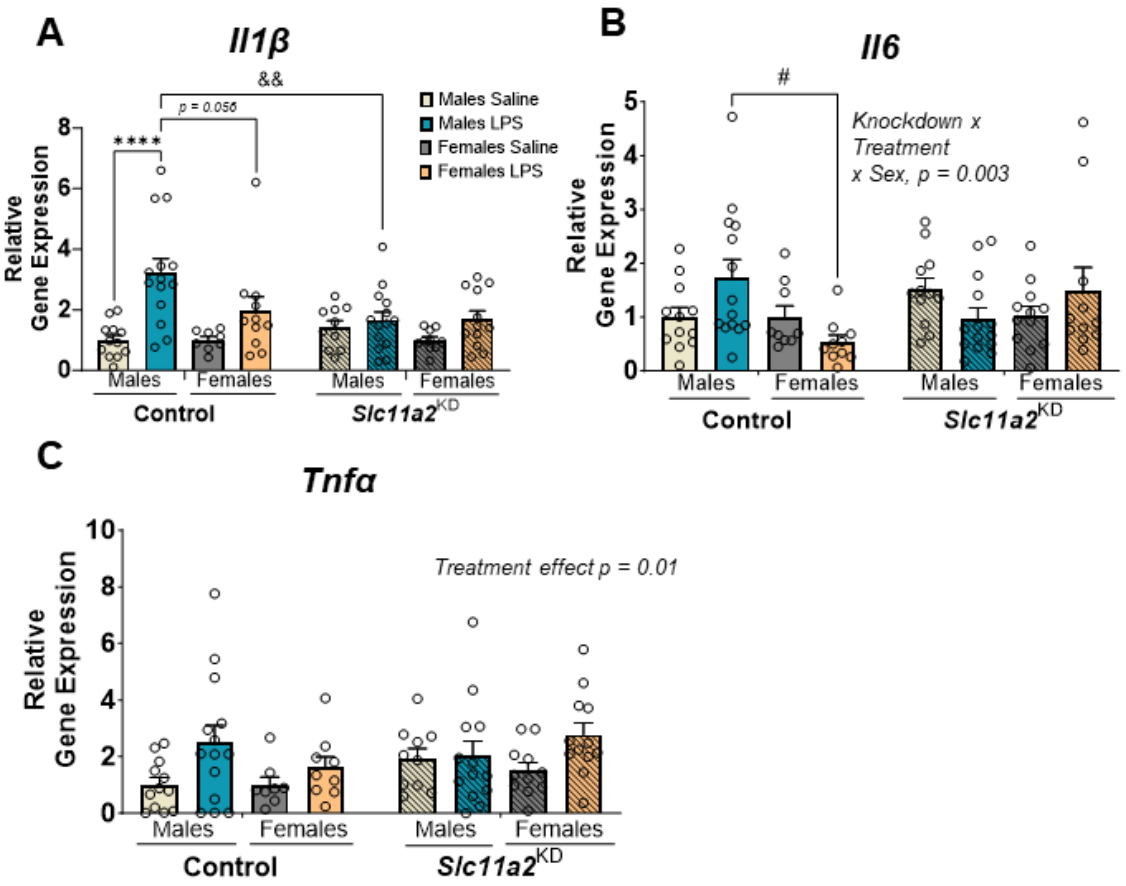

Figure 3.4. Changes in gene expression in response to LPS in microglial *Slc11a2* knockdown animals are sex-specific.
a-c) CD11b+ microglia were isolated from whole brains 24 h after LPS injection, and gene expression was measured via RT-qPCR. Data represent the mean ± S.E.M. of 9-14 mice per group. Three-way ANOVA, ****p<0.0001 effect of LPS Treatment in males, #p<0.05 effect of Sex x Treatment in females, &&p<0.01 effect of male knockdown on LPS-induced response. Outliers were removed using ROUT's test for multiple outliers.

3.2.3 *Slc11a2* knockdown did not significantly affect downstream changes in behavior after sickness recovery from LPS treatment.

Previous research has reported longer-term alterations in behavior and cognition in rodents administered LPS [227, 228]. Thus, we aimed to determine whether LPS and/or *Slc11a2* knockdown affected longer-term behavior and cognition following sickness recovery in our studies. To do this, a subset of male and female mice was administered 2 mg/kg LPS and allowed

to recover from sickness for 72 h before beginning a behavioral testing battery (complete sickness curves shown in Fig. 3.5a and d). An acute difference in sickness response was again observed only in the knockdown males (Fig. 3.5a, *Time x Knockdown x Treatment* $F(6,250) = 3.11$, $p = 0.006$; 4 h: $p = 0.048$). Female mice given LPS recovered more quickly overall compared to male LPS control mice (Fig. 3.6a, *Time x Sex* $F(6,274) = 2.53$, $p = 0.021$), replicating what others have shown [229, 230]. However, most animals were fully recovered by the 72 h time point, and there were no significant differences based on knockdown in the later time points of recovery in either sex (Fig. 3.5a and d, monitored to 96 h post-LPS, $p>0.05$). To determine whether LPS and/or *Slc11a2* knockdown affected downstream general cognition and wellbeing in these mice, we utilized a nest building assay, where mice were given 5 g of nestlets overnight following sickness recovery (72 h after LPS), and nests were scored the following morning. All groups of mice performed similarly on nest building capacity, with no significant differences between sexes (Fig. 3.6b). When analyzing the sexes separately, we found a statistically significant improvement in nest scores in the female knockdown animals given LPS compared to their control LPS counterparts (Fig. 3.5b, males, Kruskal-Wallis statistic = 0.44, $p = 0.93$ and Fig. 3.5e, females, Kruskal-Wallis statistic = 7.92, $p = 0.048$, compared to control-LPS group). Next, as LPS significantly decreases locomotor activity in the acute sickness phase [231], (*which we corroborated*, *data not shown*) we determined whether LPS and/or knockdown had a lasting effect on spontaneous locomotor activity following recovery from acute sickness. Four days following LPS treatment, mice were placed into open field chambers and allowed to run freely for 45 min. Female mice overall traveled less than male mice across treatments (Fig. 3.6c, *Sex* $F(1,84) = 6.34$, $p = 0.014$); however, neither LPS nor *Slc11a2* knockdown had a significant effect on total distance traveled between any groups at this time point in either sex (males, Fig. 3.5c; *Treatment* $F(1, 41)$

= 0.12, p = 0.73, *Knockdown* F(1, 41) = 0.055, p = 0.82; females, Fig. 3.5f; *Treatment* F(1, 44) = 0.48, *Knockdown* F(1, 44) = 0.13, p = 0.72).

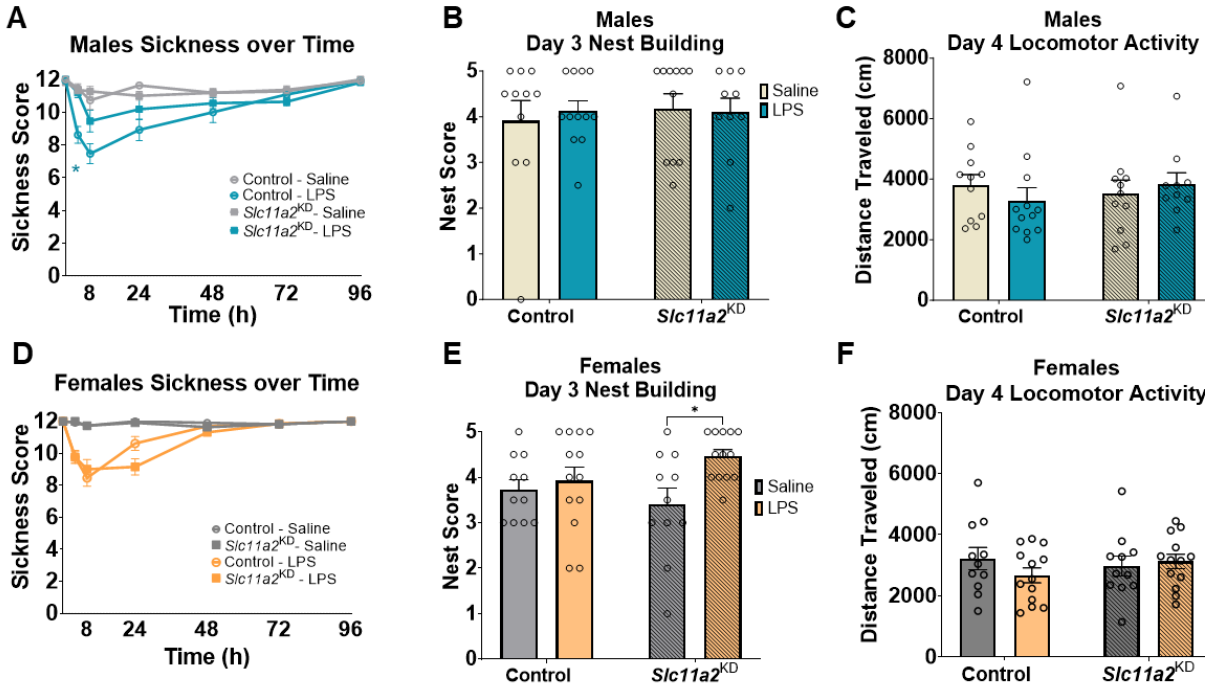

Figure 3.5. *Slc11a2* knockdown had no significant effect on longer-term behavioral recovery post-LPS.

a, d) Sickness behavior was monitored in a subset of control and knockdown male and female mice at 4, 8, 24, 48, 72, and until 96 h post-LPS injection. *denotes difference between *Slc11a2*^{KD}-LPS vs. Control-LPS at 4 h post-LPS. No significant differences were found in overall sickness recovery between 24 and 96 h in any of the groups. **b, e**) At 72 h following LPS administration, single-housed mice were given 5 g of nestlet overnight and nest building capacity was scored the next morning. *denotes *Interaction* effect, *p < 0.05. **c, f**) At 96 h following LPS injection, mice were placed in open field locomotor activity chambers and activity was recorded for 45 min. Total distance traveled in cm is shown; no significant differences were detected. Data represent the mean ± S.E.M. of 10–14 mice per group.

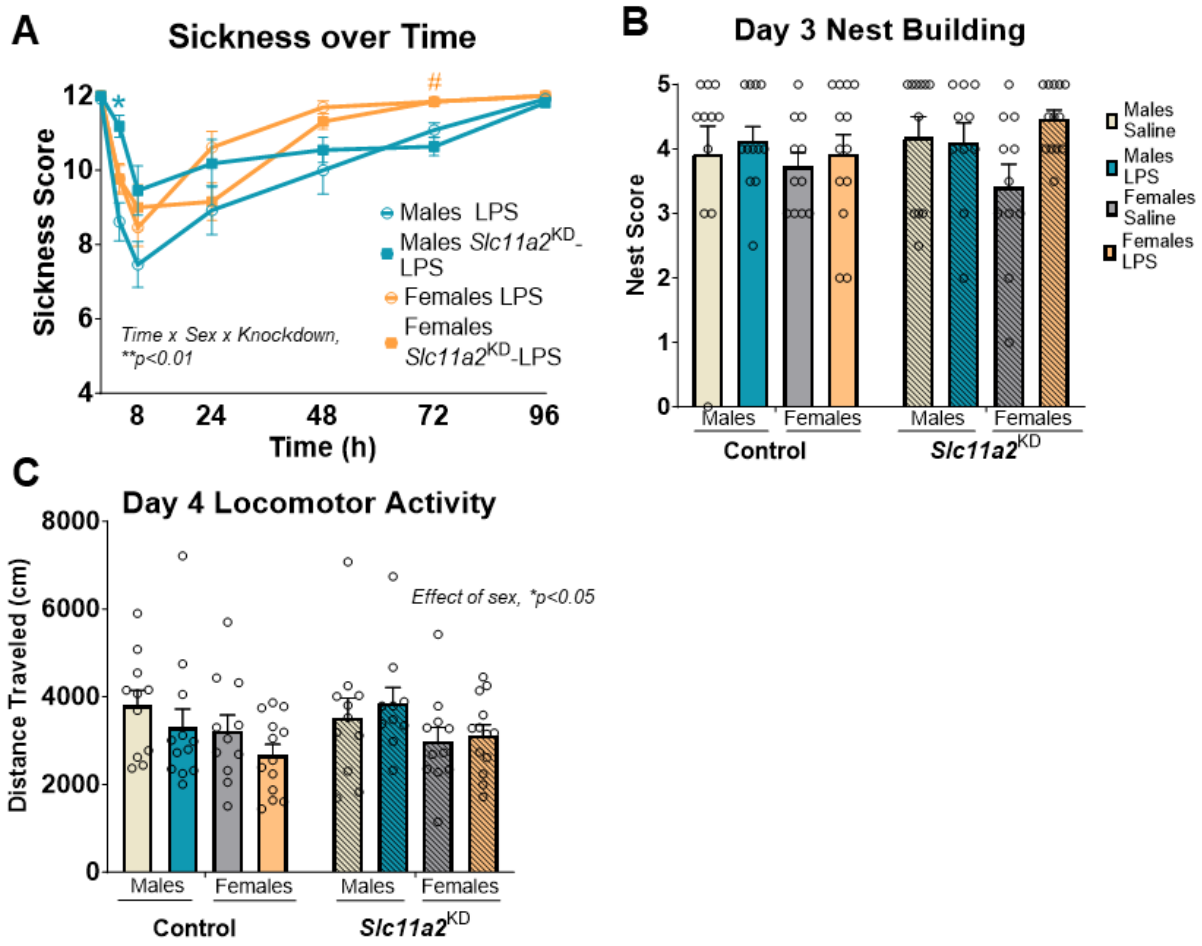

Figure 3.6. Neither LPS nor *Slc11a2* knockdown had a significant effect on behavioral phenotypes (tested within one week of LPS injection) in males or females.
a) Sickness scores were measured at baseline, 4, 8, 24, 72, and 96 h post-LPS injection in male and female animals with or without *Slc11a2* knockdown. Three-way RM ANOVA, *p<0.05 compared to control LPS animals, #p<0.05 compared to males. **b**) Mice were given 5g nestlets overnight three days after LPS and nests were scored the following morning. No significant differences found between sexes or due to knockdown. **c**) Four days following LPS, mice were placed in transparent open field chambers to move about freely for 45 min. Total locomotor activity was calculated in cm distance traveled. Three-way ANOVA, *$p<0.05$ effect of sex. Data represent the mean ± S.E.M. of 10-13 mice per group.

To assess any changes in longer-term memory, we placed mice back into the same open field chambers two weeks after this initial session, and allowed free exploration for 45 min. The change in distance traveled between first exposure and this second session was calculated as a measure of inter-session habituation and long-term memory [200]. Although LPS treatment

decreased the change in distance traveled between sessions – indicative of an LPS-induced deficit in both sexes (Fig. 3.7c, *Treatment* F(1,83) = 5.32, p = 0.024) – there was no significant effect of *Slc11a2* knockdown in either sex on this measurement of long term context-dependent memory (Fig. 3.7c, 3.8c, 3.9c; Males: *Treatment* F(1,39) = 1.83, p = 0.18, *Knockdown* F(1,39) = 1.11, p = 0.30; Females: *Treatment* F(1,44) = 3.68, p = 0.062, *Knockdown* F(1,44) = 0.082, p = 0.78). Data

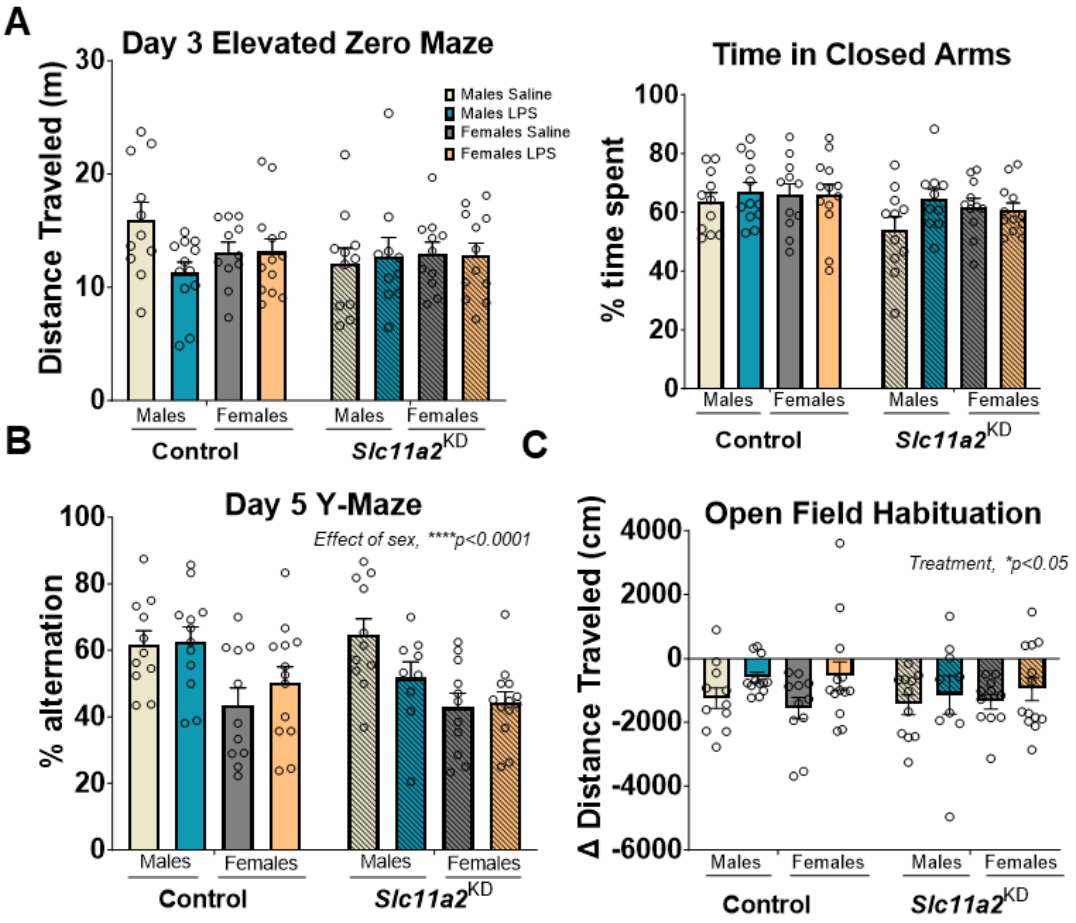

Figure 3.7. *Slc11a2* knockdown had no significant effect on behavioral phenotypes (tested 3-5 days or 2 weeks following LPS injection) in males or females. a) Control and knockdown male and female animals freely explored an elevated zero maze for 5 min. 3 days post-saline or LPS. There were no significant differences in total distance traveled (m) or time spent in closed arms among groups or between sexes. **b**) Mice freely explored a three-arm Y-maze for 5 min., and spontaneous alternation capacity was calculated as a measurement of spatial working memory. Mice with fewer than eight total arm entries were excluded from analysis. Three-way ANOVA, ****p<0.0001, effect of sex. **c**) Two weeks following initial open field assessment, mice were placed back into the same open field chambers and allowed to move freely for 45 min. Change in distance traveled compared to the original session (four days after LPS) was calculated. Three-way ANOVA, *p<0.05, effect of LPS Treatment; no significant differences due to knockdown or sex. Data represent the mean ± S.E.M. of 9-13 mice per group.

from additional assays including elevated zero maze and Y-maze spontaneous alternation in our behavioral battery revealed no significant differences as an effect of LPS treatment or *Slc11a2* knockdown (Fig. 3.7-3.9, $p>0.05$).

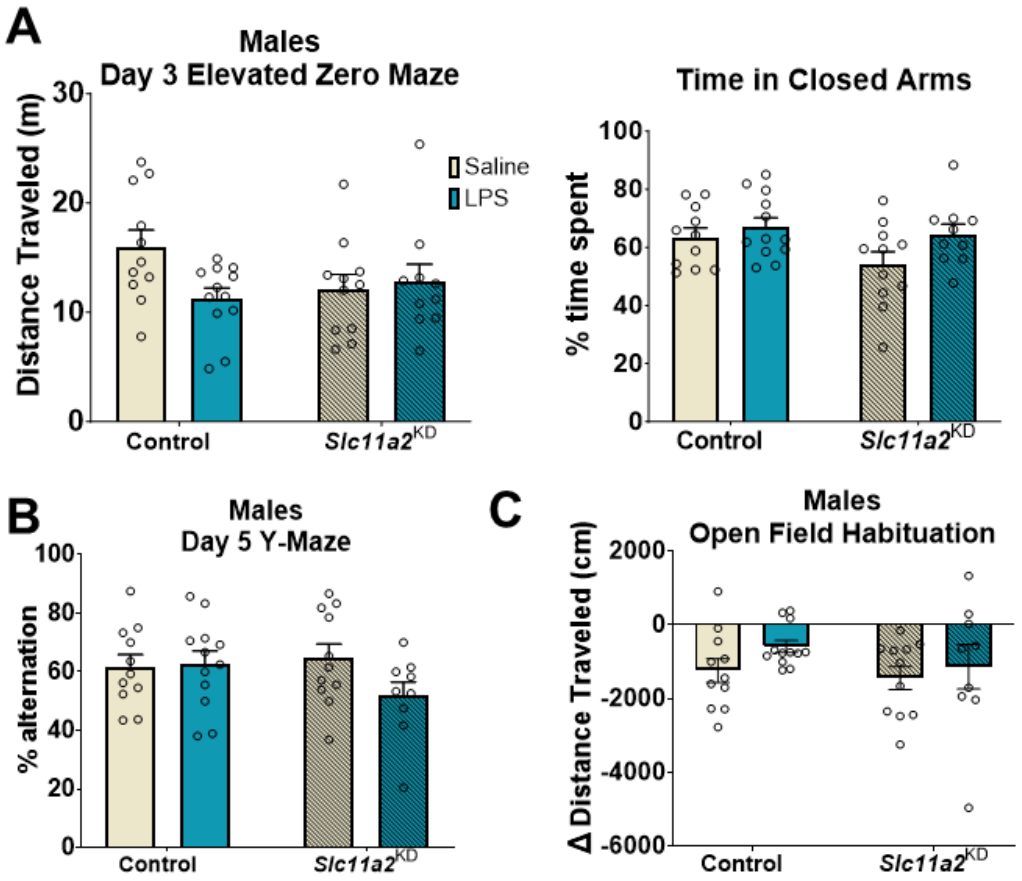

Figure 3.8. Neither LPS nor *Slc11a2* knockdown had a significant effect on behavioral phenotypes (tested 3-5 days or 2 weeks following LPS injection) in males. a) Male control and knockdown animals freely explored an elevated zero maze for 5 min. 3 days following saline or LPS injection. There were no significant differences in total distance traveled (m) or time spent in closed arms. **b**) Male animals freely explored a three-arm Y-maze for 5 min., and spontaneous alternation capacity was calculated as a measurement of spatial working memory. There were no significant differences found. **c**) Two weeks following initial open field assessment, mice were placed back into the same open field chambers and allowed to move freely for 45 min. Change in distance traveled from the original session four days after LPS was calculated. No significant differences. Data represent the mean ± S.E.M. of 9-13 mice per group.

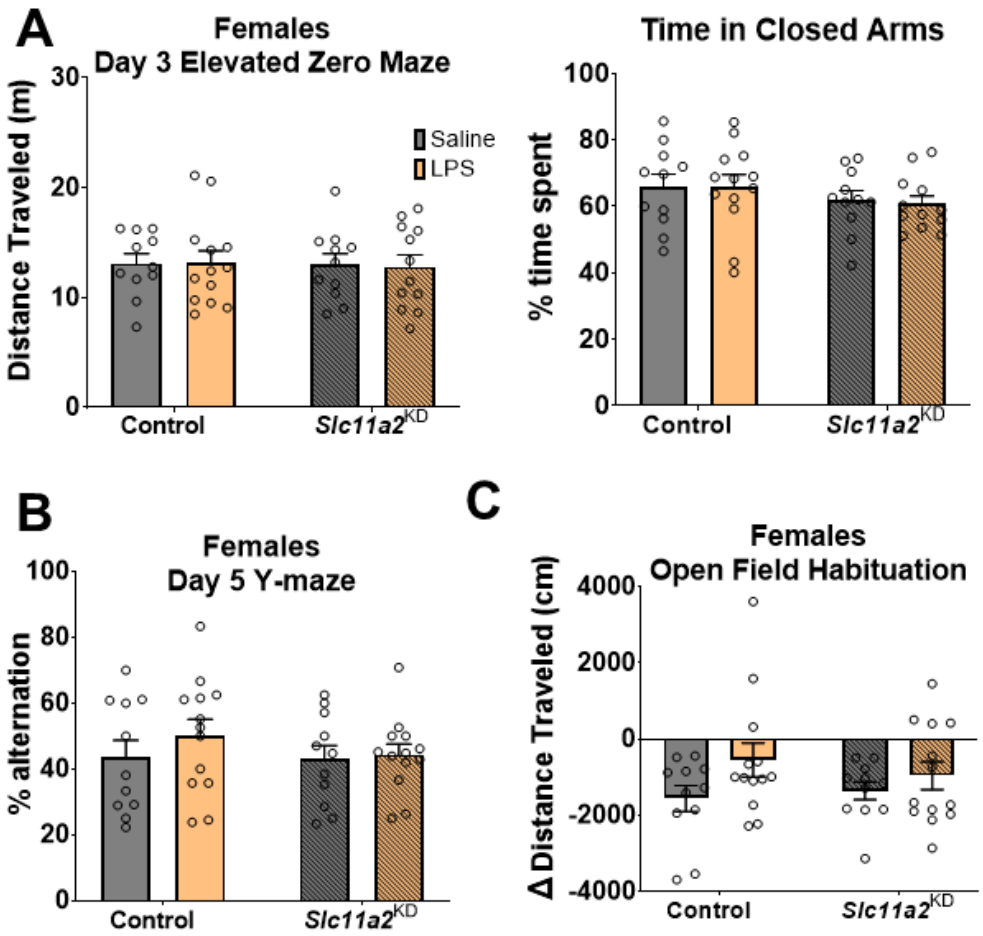

Figure 3.9. Neither LPS nor *Slc11a2* knockdown had a significant effect on behavioral phenotypes (tested 3-5 days or 2 weeks following LPS injection) in females. a) Female control and knockdown animals freely explored an elevated zero maze for 5 min. 3 days following saline or LPS injection. There were no significant differences in total distance traveled (m) or time spent in closed arms. **b)** Female animals freely explored a three-arm Y-maze for 5 min., and spontaneous alternation capacity was calculated as a measurement of spatial working memory. There were no significant differences found. **c)** Two weeks following initial open field assessment, mice were placed back into the same open field chambers and allowed to move freely for 45 min. Change in distance traveled from the original session four days after LPS was calculated. There was a trend towards an LPS-induced deficit ($p = 0.0617$); however there was no significant difference due to knockdown. Data represent the mean ± S.E.M. of 11-13 mice per group.

3.2.4 *Slc11a2* knockdown is associated with a significant blunting of the acute systemic inflammatory response post-LPS in males.

Murine plasma levels of LPS-induced inflammatory cytokines typically peak between 2-6 h post-LPS, depending on the cytokine [195, 232]. We observed the greatest difference in LPS-induced sickness response during the acute phase of sickness immediately following LPS administration only in male mice (4-8 h, shown earlier). As female mice had shown no significant changes in response to *Slc11a2* knockdown in sickness behavior or LPS-provoked pro-inflammatory cytokines to this point, we focused on how *Slc11a2* knockdown affected the immediate LPS-induced inflammatory response in a separate cohort of male animals. This cohort of mice was administered LPS and euthanized 4 h post-injection for the assessment of systemic inflammatory cytokines in plasma and for microglial isolation.

We found a striking decrease in several pro-inflammatory cytokines in plasma collected from male *Slc11a2* knockdown animals compared to their littermate controls given 4 h LPS, (Fig. 3.10). In particular, knockdown males exhibited a significant decrease in LPS-induced plasma IFNγ, which was indistinguishable from the control animals administered saline only (Fig. 3.10a; *Interaction* $F(1,15) = 8.67$, $p=0.01$). As expected, LPS induced a robust increase in plasma cytokine levels of monocyte-chemoattractant protein 1 (MCP-1), IL-1β, IL-6, and TNFα in our control animals, which were also significantly blunted in male *Slc11a2* knockdown animals (Fig. 3.10b-f; MCP-1: *Interaction* $F(1,15) =21.12$, $p=0.00034$; IL-1β: *Interaction* $F(1,15) = 11.39$, $p=0.0042$; IL-6: *Interaction* $F(1,17) = 84.54$, $p<0.0001$; TNFα: *Interaction* $F(1,17) = 50.90$, $p<0.0001$). Plasma IL-10 was also measured, as secreted levels have been shown to coincide with a rise in TNFα in the coordinated LPS-induced response [233], and we observed a significant decrease in LPS-provoked IL-10 levels in knockdown samples (Fig. 3.10c; *Interaction* $F(1,15) =$

99.54, p<0.0001). To confirm that this blunted systemic inflammatory response is not a result of deficient *Slc11a2* presence in peripheral monocytes – which also express *Cx3cr1* in the Cre-lox system used – we isolated peripheral blood monocytes (PBMCs) in a different subset of knockdown mice. *Slc11a2* expression levels in PBMCs were not different between control and knockdown groups (Fig. 3.11), suggesting that the microglial-specific *Slc11a2* inhibition contributed to the blunted LPS-induced systemic response of several cytokines in male knockdown mice.

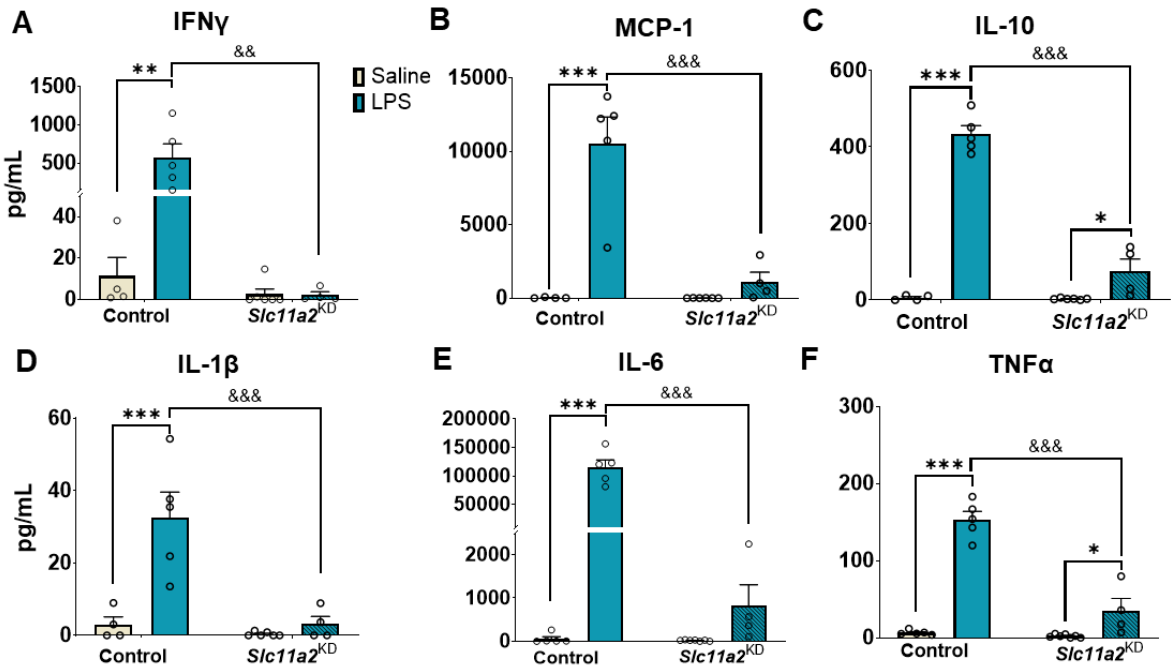

Figure 3.10. Microglial *Slc11a2* knockdown in males significantly blunts LPS-induced pro-inflammatory cytokines in plasma collected 4 h post-LPS. a-f) Male mice were euthanized 4 h following LPS injection and blood was collected immediately via cardiac puncture. Isolated plasma was assayed for presence of inflammatory cytokines via Luminex multi-plex panel. The LPS-induced increases in plasma IFNγ, MCP-1, IL-10, IL-1β, IL-6, and TNFα were significantly abrogated in *Slc11a2*^{KD} mice. Samples which were below the limit of detection in the assay were given a numerical value of 0. *denotes *Treatment* effect, *p < 0.05, **p < 0.01, ***p < 0.001; $^{\&}$denotes *Interaction* effect, $^{\&\&}$p < 0.01, $^{\&\&\&}$p < 0.001. Data represent the mean ± S.E.M. of 4–7 mice per group.

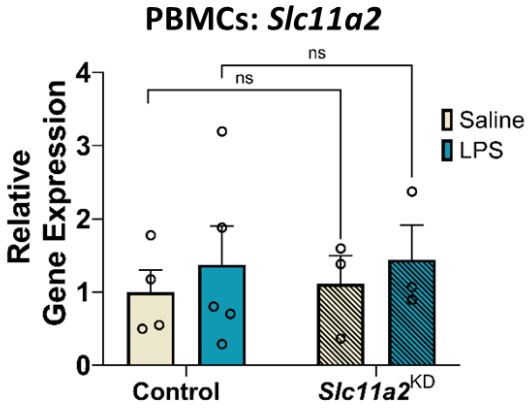

Figure 3.11. No significant differences in *Slc11a2* expression levels were found between treatment or knockdown groups in peripheral blood mononuclear cells (PBMCs). A subset of male mice was euthanized and PBMCs collected for RT-qPCR analysis of *Slc11a2* gene expression. ns = not significant. Data are normalized to housekeeping gene *18S* and represent the mean ± S.E.M. of 3-5 mice per group.

Furthermore, corroborating the work of others [234], in a separate group of control C57BL/6J male mice we confirmed that tamoxifen alone does not have a significant effect on LPS-induced cytokine production in males (Fig. 3.12), further suggesting that this result is due to the microglial knockdown of *Slc11a2* and not a delayed response to tamoxifen injection.

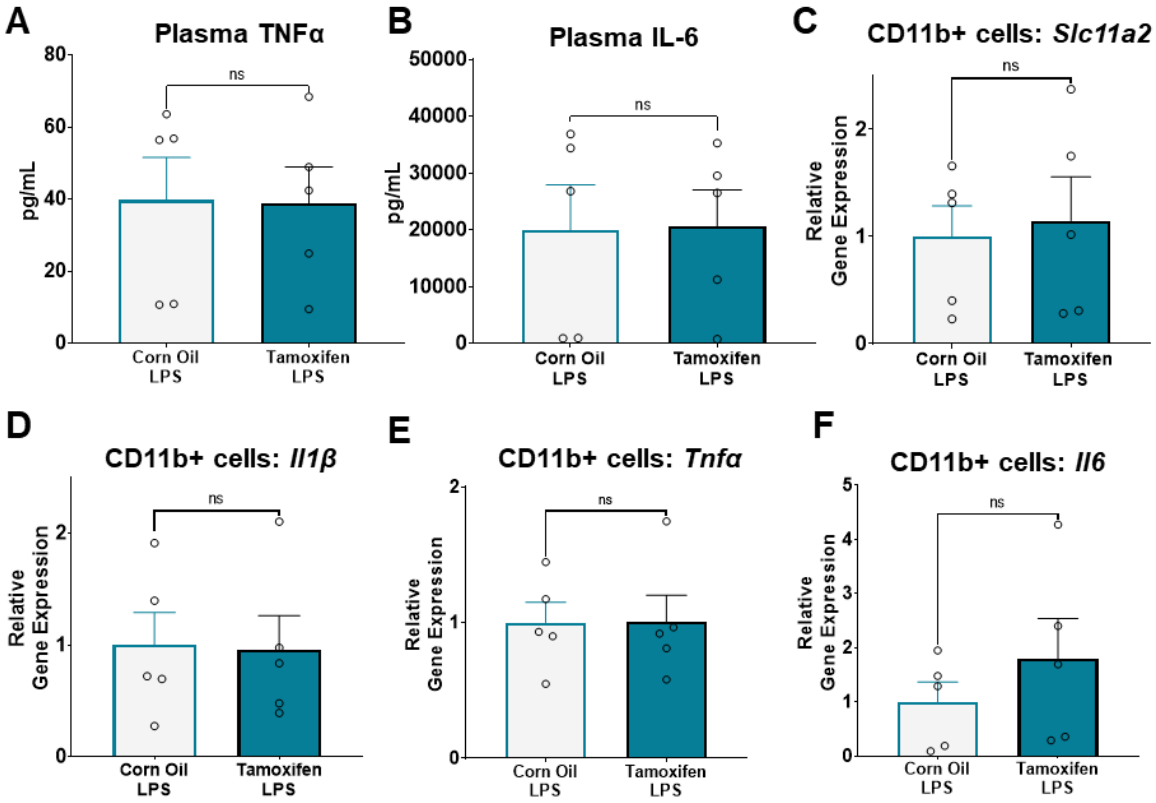

Figure 3.12. Tamoxifen alone does not have a significant effect on markers of LPS-induced pro-inflammation in male mice. A control experiment was conducted in male C57BL/6J mice to assess for effects of tamoxifen alone. Nine-week-old male mice were given five doses of tamoxifen (1x/day for five days, 20mg total by end of treatment) and treated with i.p. LPS (2 mg/kg) 4 ½ weeks later. **a-b)** 4 h plasma cytokines were measured via ELISA, and **c-f)** CD11b+ microglia were isolated for gene expression analyses via RT-qPCR (data normalized to housekeeping gene *18S*). ns = not significant. Data represent the mean ± S.E.M. of 5 mice per group.

3.2.5 Microglial *Slc11a2* knockdown significantly alters acute transcriptional response in microglia isolated 4 h post-LPS in males.

Along with the systemic response following 4 h LPS, we also determined the effect of *Slc11a2* knockdown on transcriptional changes in isolated microglia from the males, during peak transcriptional stimulation in the brain post-LPS [222, 235]. To determine global transcriptional changes in microglia from these mice, which may underlie the systemic differences we observed, brains were rapidly collected at 4 h post-injection and CD11b+ cells were magnetically-sorted for mRNA isolation and microglial bulk RNASeq analyses. We first confirmed *Slc11a2* knockdown

in our samples. Three mice in the '*Slc11a2*^{KD}' group given LPS exhibited a <50% knockdown of *Slc11a2* in our sequencing data (shown as triangles in Fig. 3.13a), and thus were excluded from primary statistical analyses at the 4 h timepoint based on an *a priori* threshold of at least 50% knockdown efficiency and data were analyzed separately (plasma cytokine data from these animals is shown in Fig. 3.14). Interestingly, the three mice in this cohort which had insufficient microglial

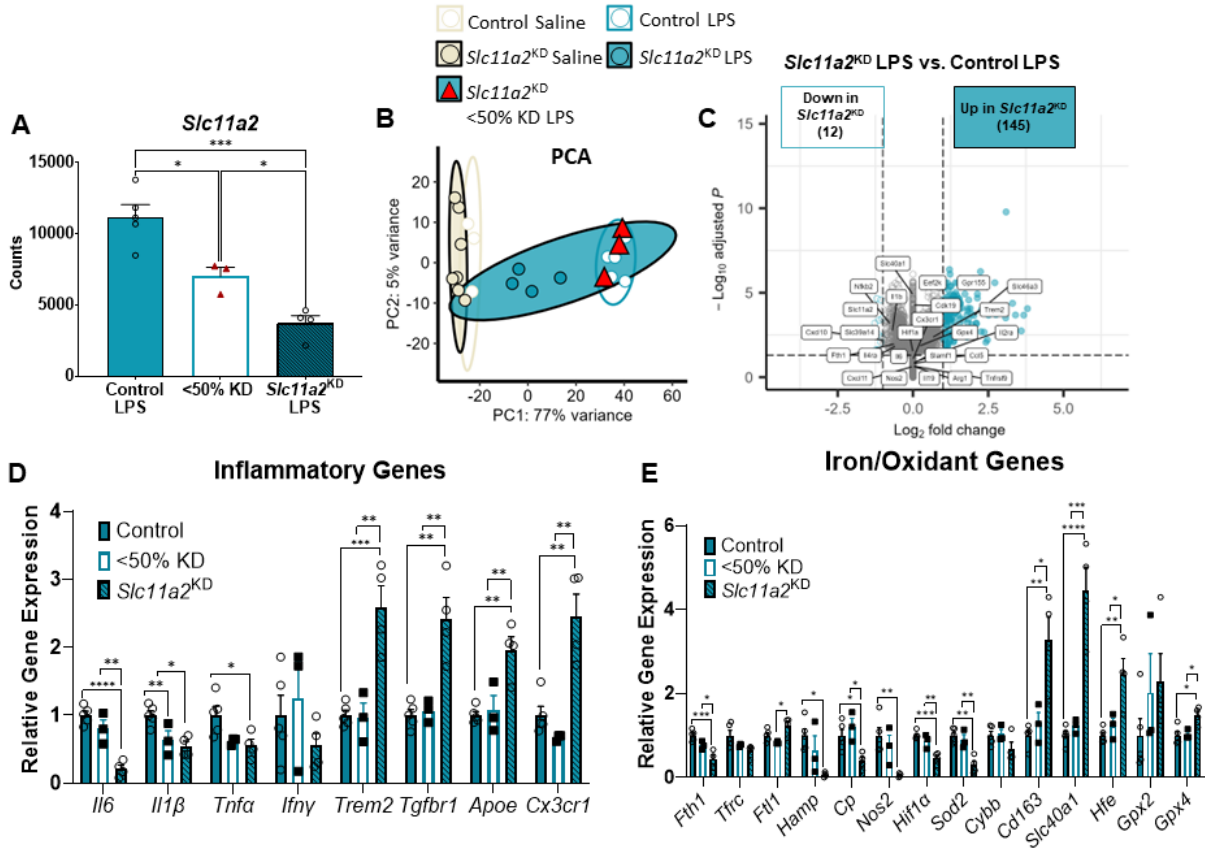

Figure 3.13. Males with < 50% *Slc11a2* knockdown exhibit microglial gene expression patterns similar to control animals following 4 h LPS. a) Microglia were CD11b-magnetically isolated 4 h post-saline or LPS injection and analyzed via bulk RNASeq. Counts of *Slc11a2* were assessed to confirm sufficient knockdown. Three samples in the knockdown group (red triangles) did not exhibit at least a 50% knockdown in gene expression. **b)** PCA plot showing the three samples with <50 % knockdown of *Slc11a2* in red triangles. These samples cluster closely with control-LPS samples shown in white circles. **c)** Volcano plot with differentially-expressed genes between knockdown LPS and control LPS groups when the three samples without sufficient knockdown are included. **d-e)** Targeted relative gene expression analysis of inflammatory markers, iron-handling, and oxidative stress markers using RNASeq counts. The three samples with < 50% knockdown exhibit significant differences in gene expression for several genes measured compared to the full-knockdown samples, more closely mirroring levels observed in control LPS samples. $^{*}p < 0.05$, $^{**}p < 0.01$, $^{***}p < 0.001$, $^{****}p < 0.0001$. Data represent the mean ± S.E.M. of 3–7 mice per group.

Slc11a2 knockdown also exhibited an overall gene expression profile more similar to control LPS mice (PCA plot in Fig. 3.13b, differentially-expressed genes in 3.13c - e) and levels of LPS-induced plasma cytokines that were more similar to control animals given LPS (Fig. 3.14). This suggests a close association between microglial *Slc11a2* expression levels and the inflammatory response 4 h post-LPS.

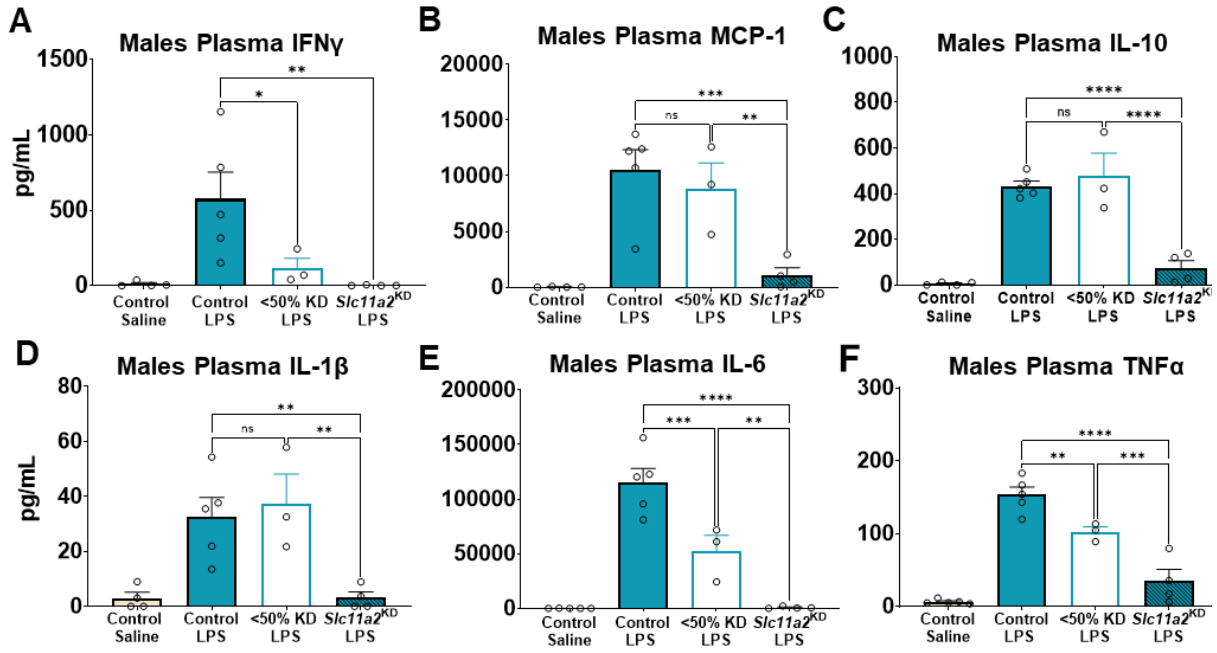

Figure 3.14. Male mice exhibiting insufficient knockdown (<50% *Slc11a2* microglial knockdown) display similar LPS-induced systemic cytokine profile as control mice 4 h post-LPS treatment. **a-f)** Luminex multiplex cytokine data from plasma isolated 4 h post-saline or LPS injection. The three male mice with <50% *Slc11a2* knockdown as assessed via RNASeq are shown here, labeled "<50% KD LPS" group. For figure clarity, statistical differences between Control-Saline vs. Control-LPS are not shown here; however, there was a significant LPS treatment effect for all cytokines in the control animals, $p<0.05$. Additionally, the <50% knockdown LPS group was statistically different from the Control Saline group for all cytokines except for IFNγ. $^{*}p<0.05$, $^{**}p<0.01$, $^{***}p<0.001$, ns = not significant. Data represent the mean ± S.E.M. of 3-5 mice per group.

Principal component analysis in mice with >50% (between 60-80%) knockdown of *Slc11a2* revealed distinct sample population clusters in the male mice. Specifically, we observed both saline groups (control animals and knockdown animals) clustered together similarly,

suggesting minimal differences in gene expression due to knockdown alone (Fig. 3.15b). As expected, control animals given LPS exhibited a significantly different transcriptional profile from both saline groups. In the *Slc11a2* knockdown + LPS group, we observed a unique cluster of samples, which appeared transcriptionally distinct from control animals administered LPS and from saline controls (Fig. 3.15b). To define specific differences in the microglial response to LPS in our knockdown animals, we then calculated $\log_2$ fold change and adjusted *p*-values of differential gene expression between groups. In control animals given LPS we identified 3,843 genes significantly altered compared to their vehicle saline counterparts (adj. *p*-value threshold < 0.05; Fig. 3.15c).

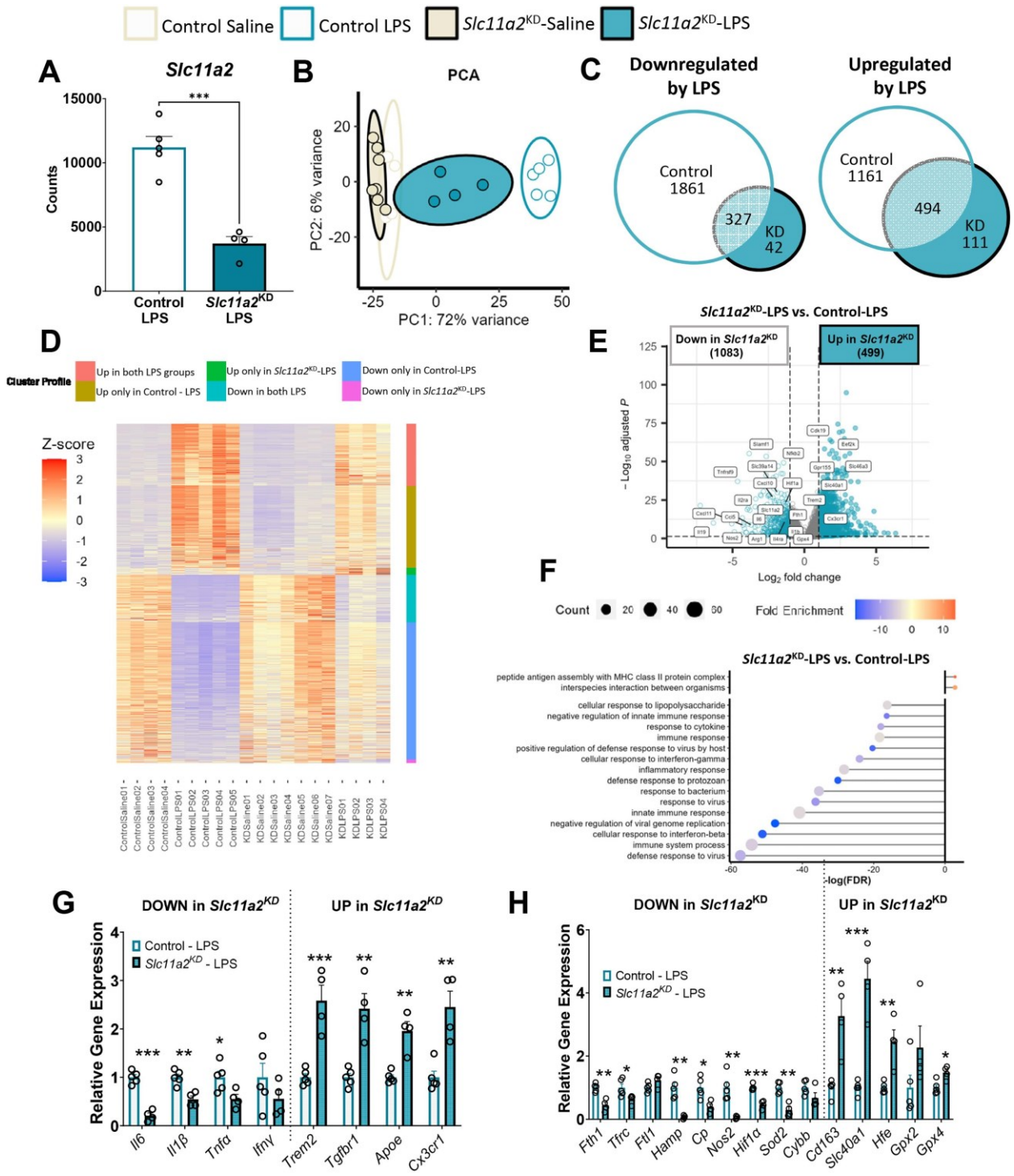
Control Saline
Control LPS
Slc11a2KD-Saline
Slc11a2KD-LPS
A
Slc11a2
***
Counts
15000
10000
5000
0
Control LPS
Slc11a2KD LPS
B
PCA
PC2: 6% variance
PC1: 72% variance
C
Downregulated by LPS
Upregulated by LPS
Control 1861
327
KD 42
Control 1161
494
KD 111
D
Cluster Profile
Up in both LPS groups
Up only in Control - LPS
Up only in Slc11a2KD-LPS
Down in both LPS
Down only in Control-LPS
Down only in Slc11a2KD-LPS
Z-score
E
Slc11a2KD-LPS vs. Control-LPS
Down in Slc11a2KD (1083)
Up in Slc11a2KD (499)
F
Count
Fold Enrichment
Slc11a2KD-LPS vs. Control-LPS
peptide antigen assembly with MHC class II protein complex
interspecies interaction between organisms
cellular response to lipopolysaccharide
negative regulation of innate immune response
response to cytokine
immune response
positive regulation of defense response to virus by host
cellular response to interferon-gamma
inflammatory response
defense response to protozoan
response to bacterium
response to virus
innate immune response
negative regulation of viral genome replication
cellular response to interferon-beta
immune system process
defense response to virus
-log(FDR)
G
DOWN in Slc11a2KD
UP in Slc11a2KD
Control - LPS
Slc11a2KD - LPS
Relative Gene Expression
Il6
Il1β
Tnfα
Ifnγ
Trem2
Tgfbr1
Apoe
Cx3cr1
H
DOWN in Slc11a2KD
UP in Slc11a2KD
Control - LPS
Slc11a2KD - LPS
Relative Gene Expression
Fth1
Tfrc
Ftl1
Hamp
Cp
Nos2
Hif1α
Sod2
Cybb
Cd163
Slc40a1
Hfe
Gpx2
Gpx4

Figure 3.15. *Slc11a2* knockdown significantly alters microglial transcriptional landscape 4 h post-LPS in male mice. a) CD11b + microglia were sorted from whole brains of control and knockdown male mice 4 h following saline or LPS for bulk RNASeq analysis. *Slc11a2* expression levels (gene counts) were significantly decreased in the knockdown group administered LPS compared to controls. **b)** Principal component analysis plot reveals distinct sample clusters from each group. *Slc11a2*^{KD} samples administered LPS exhibited a transcriptional profile distinct from saline control and control LPS groups. **c)** Venn diagram of differentially-expressed genes (DEGs) following LPS. **d)** Heat map of genes significantly altered by LPS in control versus knockdown samples reveals a significant blunting of LPS-induced transcriptional changes in the *Slc11a2*^{KD} LPS samples compared to controls. **e)** Volcano plot with significant DEGS between control LPS and *Slc11a2*^{KD} LPS samples. **f)** Gene ontology analysis of pathways differentially altered in *Slc11a2*^{KD} samples in response to LPS. **g-h)** Targeted expression analyses comparing relative counts of genes from RNASeq data between *Slc11a2*^{KD} and control cells post-LPS. $^{*}p < 0.05$, $^{**}p < 0.01$, $^{***}p < 0.0001$. Data represent the mean ± S.E.M. of 4–7 mice per group.

As expected, many of the genes significantly upregulated in response to LPS in the control animals included pro-inflammatory markers such as *Il1β, Il6,* and *Il19* (Fig. 3.16a). Gene ontology (GO) analysis identified a robust upregulation of genes associated with immune-related and inflammatory response pathways in response to LPS in our controls (Fig. 3.16b). Downregulated pathways included several related to lipid-handling, fatty acid metabolism, and cholesterol transport in response to LPS (Fig. 3.16b), which are pathways typically associated with inflammatory resolution [236, 237]. In addition to changes in inflammatory signaling, data from the control animals administered LPS also demonstrate significant changes in the cellular transcriptional iron-handling phenotype, with alterations in genes such as *Slc40a1* (iron exporter, ferroportin) and *Fth1* (ferritin heavy chain, iron oxidation and storage). Importantly, *Slc11a2* increased in response to LPS in our control animals at 4 h (adj. $p<0.0001$; Fig. 3.16a*),* further demonstrating a significant shift in the expression of this cellular iron import gene associated with the acute inflammatory stimulus.

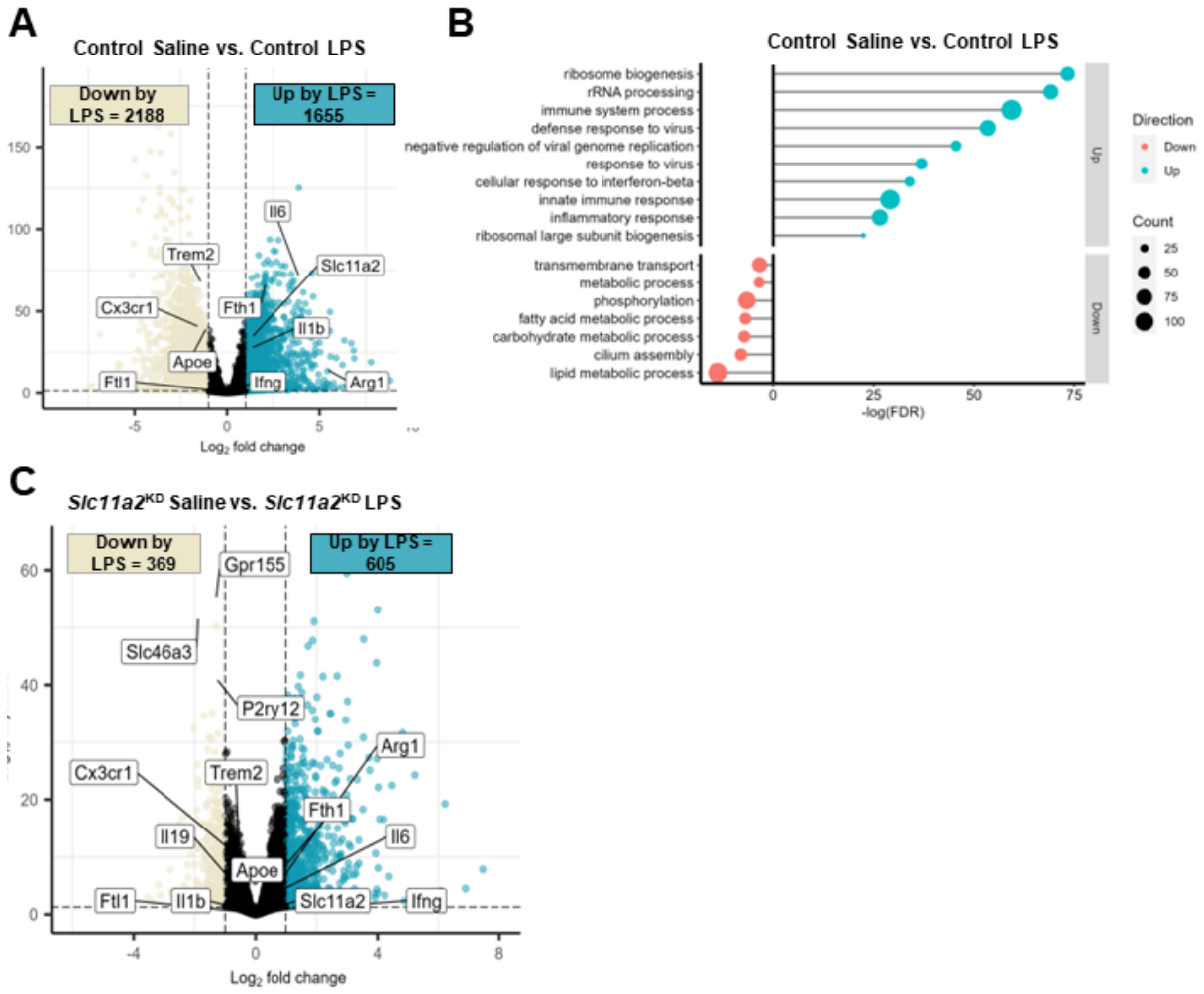

Figure 3.16. LPS induces significant and widespread changes in gene expression in male control animals.
Microglia were CD11b-magnetically isolated 4 h following saline or LPS injection for bulk RNASeq analysis. **a)** Volcano plot showing significant differentially-expressed genes between Control Saline and Control LPS animals; adjusted p-value <0.05. **b)** Gene ontology pathway analysis reveals a significant upregulation in immune processes and the inflammatory response, and a downregulation in lipid-related signaling in control cells given LPS compared to saline-treated animals (p<0.05). **c)** Volcano plot showing significant differentially-expressed genes between *Slc11a2*^{KD} samples given saline and *Slc11a2*^{KD} samples given LPS; adjusted p-value <0.05. Data are shown from 4-7 mice per group.

When we compared *Slc11a2* knockdown saline-treated animals with knockdown animals given LPS, we observed a significant decrease in the number of genes altered by LPS treatment (974 genes compared to 3,843 in our control LPS animals, Fig. 3.15c, volcano plot in Fig. 3.16c). In fact, there were 3,022 genes uniquely affected by LPS treatment in our control animals which

were not found in *Slc11a2* knockdown animals (1861 up and 1161 down), suggesting a significant effect of the knockdown in modulating LPS-induced alterations in microglial gene expression (Fig. 3.15c). Indeed, when visualizing differential gene expression across groups via heatmap (Fig. 3.15d), we observed a significant overall blunting of LPS-induced changes in the knockdown animals. When we directly compared gene expression in microglia from control and *Slc11a2* knockdown animals treated with LPS, we observed a significant difference in the transcriptional profiles. Specifically, we identified 1,582 genes significantly altered in *Slc11a2* knockdown cells compared to control cells post-LPS (Fig. 3.15e). We observed a robust decrease in LPS-induced pro-inflammatory cytokines such as *Il1β, Tnfα, Il6,* and *Ifnγ* in knockdown cells compared to controls (Fig. 3.15e), which recapitulates our RT-qPCR data observed in male microglia 24 h post-LPS shown earlier. GO analysis of these knockdown cells reveals an overall marked inhibition of pathways involved in the innate immune response, inflammatory processes, and cytokine and chemokine-related signaling following LPS compared to controls (Fig. 3.15f). In conjunction with this decrease in pro-inflammatory gene expression, we also observed a significant upregulation in anti-inflammatory cellular markers such as *Trem2, Tgfbr1, Pparγ, Apoe,* and homeostatic microglial marker *Cx3cr1* in *Slc11a2* knockdown cells compared to control samples given LPS (Fig. 3.15g).

To assess whether alterations in cellular iron-related genes are associated with this decrease in the immune response, we determined differences in markers of iron homeostasis between control cells and knockdown cells post-LPS. Critically, *Slc11a2* knockdown cells exhibited a shift in overall iron-related gene profile. Along with the expected decrease in *Slc11a2* gene expression levels (Fig. 3.15a, as shown earlier), these cells also exhibited a significant decrease in iron storage marker *Fth1* (a key marker of 'disease-associated microglia', DAMs [133, 134]). In general,

knockdown cells exhibited markers indicative of a robust shift towards a more iron-recycling and pro-resolving cell, displaying significant increases in iron export gene *Slc40a1* and hemoglobin-haptoglobin scavenger receptor gene *Cd163,* which are both associated with tissue repair and the resolution phase of inflammation [182, 238, 239] (Fig. 3.15h). Furthermore, knockdown cells exhibited a robust increase in the homeostatic *Hfe* gene, which is typically associated with maintenance of iron homeostasis, and pronounced decreases in iron-related genes *Hamp* (hepcidin) and *Cp* (ceruloplasmin) (Fig. 3.15h).

Interestingly, in isolated cells which did not display efficient knockdown of *Slc11a2,* we observed expression levels of pro-inflammatory markers and iron-relevant genes that were more similar to control LPS cells (Fig. 3.13d - e). This suggests that the degree of *Slc11a2* knockdown corresponds with a decrease in the LPS-induced inflammatory and iron-related gene response in these microglial cells, at least at the transcriptional level.

3.3 Discussion

Neuroinflammation and associated microglial activation have long been recognized as key features of the neurodegenerative process in several neurodegenerative diseases, including AD, Huntington's disease, and Parkinson's disease. Recent publications have suggested that dysfunctional iron homeostasis in the brain coincides with this aberrant activation of microglia in disease [50, 154, 240]. In particular, it has been suggested that iron accumulation, specifically in microglial cells, is associated with increased cellular inflammation and dysfunction in disease [146, 156]. Furthermore, an increase in markers of cellular iron storage (via *Ftl* and *Fth1* upregulation) is a key signature of disease-associated microglia in AD models [133, 137, 146]. *In vitro* work in primary mouse microglia has shown a specific upregulation in the microglial iron

importer, DMT1/*Slc11a2*, in response to inflammatory signals [180] (*corroborated by us also, data not shown)*. This acute response to an inflammatory challenge is thought to be an innate mechanism intended to prevent pathogenic access to iron needed for growth and proliferation [68, 241, 242]. However, prolonged exposure to inflammation may also lead to an aberrant increase in DMT1, which could further exacerbate inflammation and cellular dysfunction in a vicious cycle. Others have targeted microglial DMT1/*Slc11a2* in cell culture systems and observed a significant decrease in cellular inflammatory signaling when DMT1 expression is inhibited [89, 173]. However, few studies have examined a direct role for this microglial gene in inflammatory contexts *in vivo,* and no studies to our knowledge have examined whether genetically suppressing microglial DMT1 (gene, *Slc11a2*) *in vivo* impacts downstream neuro-inflammatory responses. Additionally, some work has been completed to elucidate sex differences in the inflammatory response; however, none to our knowledge has explored a sex-specific role for a microglial iron import gene during inflammation. We therefore sought to elucidate the effects of microglial *Slc11a2* suppression on downstream inflammatory responses *in vivo* in both male and female mice.

Here, we established a novel mouse model of tamoxifen-inducible microglial-specific *Slc11a2* knockdown utilizing the $Cx3cr1^{Cre\text{-}ERT2}$ and $Slc11a2^{floxed}$ mouse lines. We used a well-established model of LPS-induced inflammation, in which others have highlighted a critical role for microglia in mediating the neuroinflammatory response [56, 243]. In this model, we examined behavioral, systemic, and cellular effects of knocking down microglial *Slc11a2* on subsequent LPS-induced inflammatory responses in both male and female mice. First, we found a sex-specific increase in microglial *Slc11a2* expression levels only in male microglia isolated 24 h after LPS injection. Corresponding with this data, we observed a significant effect of *Slc11a2* knockdown in the LPS-induced inflammatory response only in male mice, despite achieving a robust knockdown

of microglial *Slc11a2* in both sexes. We showed that microglial *Slc11a2* knockdown decreased the overall inflammatory response in male mice and had no effect on LPS-induced inflammatory markers in females. Following both 4 h and 24 h LPS administration, we observed a significant downregulation in pro-inflammatory cytokine expression in isolated microglia from knockdown male animals, including *Il1β* and *Il6*. We also found a significant decrease in several plasma cytokines (IFNγ, TNFα, IL-6, IL-10, IL-1β, and MCP-1) in male knockdown animals 4 h following LPS, suggesting a fascinating interplay between microglial *Slc11a2* and the systemic inflammatory response in our acute model. In fact, it was striking to see that male samples without sufficient microglial *Slc11a2* knockdown (<50% as assessed via RNASeq data) also exhibited LPS-provoked plasma cytokines similar to control LPS animals.

We confirmed absence of the knockdown in CD11b-negative cells isolated from the brain, as well as PBMCs isolated from the periphery, suggesting that this effect on cytokine levels in the males is related to a knockdown found primarily in CD11b+ brain mononuclear cells. In accordance with this, a study by Zhang *et al*. recently demonstrated an inflammatory pathway of communication from the CNS to the periphery [244], and others have also suggested a bi-directional relationship, such that changes in the brain may regulate peripheral responses to inflammation [245, 246]. While extensive work has shown the effects of systemic inflammation on neural signaling, fewer studies have documented a central-to-peripheral inflammatory pathway. Our work suggests that a change in microglial inflammatory signaling could contribute, in part, to the whole-body immune and behavioral sickness response to LPS.

In addition to the changes observed in male microglia 24 h following LPS, our RNASeq data also illuminated a variety of cellular changes in male knockdown microglia 4 h post-LPS. Specifically, *Slc11a2* knockdown led to a similar significant decrease in pro-inflammatory

cytokine signaling (*Il6, Il1β, Tnfα*) after 4 h of LPS, corroborating the gene expression analyses conducted at the 24 h time point. This decrease in inflammatory markers in response to LPS paralleled a shift in the expression of cellular iron-related genes, as male knockdown microglia exhibited a significant downregulation in markers of cellular iron-storage genes such as *Fth1, Ftl1,* and *Tfrc.* Instead, *Slc11a2* knockdown cells upregulated genes typically associated with iron-recycling, the resolution of inflammation, and tissue repair (*Cd163* and *Slc40a1*). We also observed a dramatic decrease in *Hamp* levels in the knockdown cells compared to the controls following LPS. Hepcidin (protein for *Hamp*) plays a prominent role in cellular iron import and storage, as it degrades iron exporter ferroportin to limit iron export and to induce cellular iron sequestration [247]. It is primarily produced by the liver to assist in systemic iron regulation [248]. However, more recently, hepcidin has emerged as an important mediator during brain inflammation, and it is still not fully understood how hepcidin is produced locally in the brain in response to damage or inflammation [249]. The alterations we observed in LPS-induced *Hamp* levels in microglia from our mice may suggest a critical role microglia play in producing *Hamp* to mediate local iron homeostasis in the brain, particularly in response to inflammation. The robust decrease in *Hamp* in the knockdown cells reflects a significant shift in the cellular transcriptional profile as the cells express increased markers related to iron-releasing and iron-recycling compared to controls. Interestingly, we also observed a decrease in *Cp* (ceruloplasmin) expression in the knockdown microglia. Ceruloplasmin is a critical ferroxidase, important for catalyzing the conversion of ferrous to ferric iron and facilitating cellular iron export. While it initially surprised us to observe a decrease in *Cp* associated with the knockdown microglia, it may be that *Cp* is playing a role in the inflammatory response outside of its role in helping to mediate iron export. Indeed, it has been shown that *Cp* plays a role in potentiating iNos signaling in microglia [250]; thus, a decrease in

Cp in the knockdown cells may be associated with the overall marked inhibition of the inflammatory response we observed.

Our RNASeq data also revealed a significant upregulation in anti-inflammatory, pro-resolving, and lipid-handling genes (*Trem2, Pparγ, Apoe*) in the male *Slc11a2* knockdown microglia compared to their control counterparts administered LPS. These changes corresponded with a shift to a more homeostatic microglial signature, marked by increased expression of genes such as *Cx3cr1, Tgfbr1, Tmem119,* and *P2ry12.* These data suggest that decreasing *Slc11a2* in male microglia during a bout of acute inflammation is associated with a significant shift of the transcriptional profile towards a cell state more closely associated with iron-recycling, debris clearance, and resolution of inflammation. Additionally, we found significant downregulation in several genes related to oxidative stress in knockdown cells, such as *Cybb, Sod2, Nos2,* and *Hif1α.* Increased *Hif1α* has been associated with detrimental increases in intracellular ROS production [251] and both *Hif1α* and *Cybb* are core transcriptional markers of DAMs [252, 253]. Thus, it may be that these alterations in the cellular oxidative stress signature provide an important link between changes in iron-associated machinery and inflammation and may partially underlie the differences we observed in *Slc11a2* knockdown cells. Taken together, our bulk RNASeq data reflect significant transcriptional changes to the oxidative, inflammatory, and iron-handling machinery in these cells. Significant technical challenges limited us to gene expression analyses in these studies, and we note that quantifying cellular iron levels and changes in iron transport and/or handling itself are important future directions. It is intriguing to consider whether the knockdown of *Slc11a2* has an effect on cellular iron import, or whether the knockdown affects iron and/or other metal localization within the cell. *In vitro* work has shown that inhibiting microglial DMT1 decreases iron uptake in response to LPS [180], and future work will aim to characterize metal load in

knockdown cells *in vivo*. Nonetheless, the association between relative gene levels of *Slc11a2* and alterations in LPS-induced plasma cytokines and cellular iron-related and oxidative stress genes is compelling to suggest a role for *Slc11a2* in the inflammatory response.

The LPS-induced sickness response has been extensively characterized and is thought to be a brain-mediated behavioral response to a bout of systemic inflammation [223, 254]. Corresponding with our gene expression and cytokine analyses, we found that male *Slc11a2* knockdown animals exhibited a significant improvement in sickness scores, particularly during the peak of LPS-induced sickness. These sickness scores in the knockdown males did not significantly differ from control animals given saline, demonstrating a robust blunting of the typical behavioral response to LPS. Although we observed this difference in behavior immediately following LPS injection, we did not find any significant changes in cognitive performance following sickness recovery due to knockdown in either sex. Others have shown that LPS administration can induce robust behavioral changes and lasting cognitive deficit in murine models [54, 255, 256], and we found an overall LPS-induced deficit in long term memory in both sexes. However, it may be that this acute model of LPS was not sufficient to induce lasting changes in cognition due to knockdown.

The sex differences we found in the knockdown animals are particularly noteworthy. Female and male mice often exhibit profound differences in the immune response to LPS [224, 257]; thus, we also aimed to explore whether microglial *Slc11a2* knockdown had a different effect within each sex. Coupled with sex differences typically observed in the inflammatory response to LPS [258], our data show that the cellular *Slc11a2* response to inflammation may also be sex-dependent, as male, but not female, microglia upregulate *Slc11a2* in response to LPS. Furthermore, when challenged with the same moderate-high dose of LPS, only male mice exhibited an effect of

microglial *Slc11a2* knockdown, as female control animals and knockdown animals produced the same inflammatory response to LPS. It is intriguing to consider a differential role for microglial *Slc11a2* in partially mediating this inflammatory response in each of the sexes. Sex differences in brain ferritin iron levels in humans have been observed, such that males have higher brain ferritin iron than women in several regions [259]. It has been suggested that these increased iron levels may contribute to the risk for males of developing neurodegenerative diseases at earlier ages compared to females [260]. However, others have presented mixed results, showing that female mice accumulate more brain iron compared to their male littermates when injected with iron [261], suggesting sex differences in brain iron uptake, but not in total levels per se. While the specific association between sex and brain iron status is still unclear, the sex difference we report in the microglial *Slc11a2* response points to another site of differential regulation of the mechanisms involved in the cellular iron-associated response between males and females. Interestingly, we observed this difference in LPS-induced microglial *Slc11a2* expression *in the absence of additional excess iron.* Thus, our data suggest a sex-specific microglial response in which inflammatory signals and changes in cellular iron-handling machinery at the transcriptional level are intimately connected, particularly in male mice. As young female mice typically respond less robustly than males to a variety of acute inflammatory or infectious stimuli [262, 263] – likely due in part to estrogenic and neurotrophic effects [264-266] – it may be that a significantly higher dose of LPS (closer to lethal) or an additional challenge (e.g., age) could evoke a role for microglial *Slc11a2* in the inflammatory response in the females; however, this remains to be determined. Nevertheless, it is intriguing to consider the implications of these data to our understanding of the baseline differences between females and males in the development of diseases of concomitant iron dys-homeostasis and inflammation.

CHAPTER 4

Microglial-specific knockdown of *Slc11a2* worsens behavioral phenotypes in female mice in the *APP/PS1* model of Alzheimer's disease

4.1 Introduction

Alzheimer's disease (AD) is one of the most common neurodegenerative diseases and most frequent cause of dementia. The disease is primarily characterized by the accumulation of extracellular amyloid-beta (Aβ) plaques and intraneuronal neurofibrillary tau tangles, which ultimately results in neuronal loss and debilitating impairments in memory and cognition [7]. Over the past decade, mounting evidence has shown that excessive iron deposition in the brain is strongly associated with AD pathogenesis [62, 184, 213]. Iron levels in the brain increase significantly with age [267, 268] and studies in patients with AD demonstrate that the degree of iron load in disease-associated brain regions (i.e., the hippocampus and frontal cortex) positively correlates with aberrant protein aggregation and severity of cognitive decline [155, 269, 270]. Furthermore, iron directly binds to and exacerbates the toxicity of Aβ [108, 109] and has been found in dense core plaques and in tau tangles in the brains of AD patients and mouse models [106, 212, 271]. Although iron is critical for myelination, neurotransmitter synthesis, and mitochondrial metabolism in the healthy brain, excessive levels of iron can result in the harmful formation of toxic free radicals and production of reactive oxygen species (ROS), which can ultimately lead to lipid peroxidation, cellular damage, and ultimately cell death [272].

Microglial cells are the primary resident innate immune cell of the central nervous system (CNS) and play essential roles in brain development, maintenance of neural homeostasis, and response to injury and disease in the CNS. While it was been widely appreciated that microglial-

mediated neuroinflammation is a key pathological hallmark of AD [127, 128], more recent work has begun to also highlight the prominent role microglia play in mediating brain iron dysregulation in disease [50, 153]. Microglia are equipped with all the necessary machinery to import, store, and export and/or recycle iron [1, 153, 180]. In fact, others have suggested that iron transport occurs preferentially in microglia compared to other cell types in the brain [147-149]. Despite their high capacity to handle and store iron, microglia have been shown to be particularly susceptible to iron-induced damage compared to other neural cells [273] and Ryan et al. recently demonstrated a predominant role for microglia in mediating the harmful effects of excess iron on other neural cells in a tri-culture system [161]. Microglia have been found loaded with iron in AD and other neurodegenerative diseases [51, 146, 154, 159, 274] and one of the key transcriptional changes in clusters of disease-associated microglia ('DAM's) identified by several groups in both humans and mice is an alteration in iron-storage genes such as *Fth1* and *Ftl* [133, 171]. While microglial iron loading has been more widely recognized as a key component of AD pathology, it is still not understood how exactly microglial iron loading contributes to overall disease progression [62, 168, 275].

At the cellular level, an intimate relationship between microglial iron load and inflammatory signaling has been established. In a reciprocal manner, iron has been shown to enhance markers of inflammation and oxidative stress in some systems [50, 167, 173] and inflammatory signals induce the cellular uptake and storage of iron [179, 180]. Specifically, microglia preferentially upregulate iron importer divalent metal transporter 1 (DMT1; gene name, *Slc11a2*) in response to acute inflammatory stimuli such as lipopolysaccharide (LPS) and Aβ [179, 180, 276]. DMT1 is a widely-expressed proton-coupled ferrous iron (Fe^{2+}) importer essential for life, found on both the cellular plasma membrane and endosomal membrane [277]. This importer

plays a role in both transferrin-bound and non-transferrin-bound iron uptake, as it mediates the immediate import of ferrous iron at the cell surface, and also transports iron reduced in the endosome into the cytosol so it can be utilized by the cell [79]. Previous work has targeted DMT1/*Slc11a2* in cell culture systems, and observed a significant decrease in *Il1β* signaling in response to an acute stimulus of Aβ [185]. Furthermore, our prior work showed that knocking down *Slc11a2* in a short-term *in vivo* model of LPS-induced inflammation blunted the systemic and neural inflammatory response in male, but not female, mice [276]. These results were observed in the absence of an additional iron load, suggesting a role for microglial DMT1/*Slc11a2* in helping to drive the baseline inflammatory response.

With these findings, it is intriguing to consider a role for microglial DMT1/*Slc11a2* in a disease of chronic cellular iron load and inflammation. However, to our knowledge, no studies have investigated whether targeting this microglial iron importer alters disease pathogenesis *in vivo.* These studies aimed to determine how directly decreasing a microglial cell iron import gene, via genetic knockdown of *Slc11a2,* impacts cellular inflammatory and oxidative stress status and cognitive function in a mouse model of AD. We generated an inducible, microglial-specific knockdown of *Slc11a2* in a model of AD in both male and female mice and investigated whether microglial *Slc11a2* knockdown alleviated markers of disease including microglial inflammatory and oxidative stress markers and changes in behavior and cognition.

4.2 Results

4.2.1 Age and Aβ stimulation synergize to increase microglial *Slc11a2* in primary isolated microglia.

To assess a potential role for microglial iron and *Slc11a2* in aging and amyloid-related pathology, we isolated microglia from young and aged mice for primary cell *in vitro* experiments. First, glia from young and aged mice were isolated for imaging of ferritin (FtL) as a marker of iron load. We observed significant FtL protein deposits in isolated aged cells compared to young cells (Fig. 4.1a-b), demonstrating, as others have shown, a key iron-loading microglial phenotype in aging [164, 168]. To determine whether *Slc11a2* may contribute to this age-associated increase in iron and whether the transporter gene plays a role in amyloid-related disease conditions, isolated microglia from young and aged mice were treated *ex vivo* with an acute stimulus of 1 μM oligomeric Aβ for 24 h and gene expression of *Slc11a2* was measured. As others have also shown [180, 185], there was a significant increase in microglial *Slc11a2* in response to acute Aβ exposure (Fig. 4.1c, *Treatment,* $F(1,35) = 48.91$, $p<0.0001$). Additionally, glia from the aged mice exhibited an augmented Aβ-induced *Slc11a2* response, which was significantly greater than the response observed in the cells from young mice (*Age,* $F(1,35) = 11.21$, $p=0.002$; young vs. old Aβ, $p=0.005$). This suggests a synergistic relationship between age and Aβ on increasing microglial *Slc11a2* expression. In addition, there was a robust increase in pro-inflammatory cytokines *Tnfα, Il1β,* and *Il6* in response to Aβ (Fig. 4.1d-f, *Il6: Treatment,* $F(1,32) = 41.20$, $p<0.0001$; *Il1β:* $F(1,34) = 24.23$, $p<0.0001$; *Tnfα:* $F(1,34) = 77.83$, $p<0.0001$), which was even higher in the aged glia compared to the young glia (significant only for *Tnfα: Age,* $F(1,34) = 6.52$, $p=0.015$, *Interaction* $F(1,34) = 5.57$, $p=0.024$; young vs. aged Aβ $p=0.005$). Along with differences in *Slc11a2* gene levels in the aged glia in response to Aβ, there was a significant increase in iron-storage genes *Ftl* and *Fth1* in

response to Aβ only in the aged cells (Fig. 4.1g-h). Specifically, Aβ induced an increase in *Fth1* in the aged glia (*Age,* $F(1,29) = 12.46$, $p=0.001$, *Treatment,* $F(1,29) = 13.67$, $p=0.0009$), and *Fth1* and *Ftl* were significantly higher in response to Aβ in the aged cells when compared to the young cells (*Fth1,* young vs. aged, $p=0.01$; *Ftl: Age,* $F(1,34) = 7.92$, $p=0.008$, young vs. aged, $p=0.02$). There were no differences in *Tfrc* gene expression – another main iron importer –due to age or Aβ treatment (Fig. 4.1i, $p>0.05$), suggesting that a specific increase in *Slc11a2* may accompany age- and Aβ-related changes in cellular iron and inflammatory status. Aβ also decreased *Slc40a1* levels (gene for ferroportin, main iron exporter) to a similar degree in the young and aged cells (Fig. 4.1j, *Treatment,* $F(1,30) = 23.40$, $p<0.0001$), further suggesting that a specific alteration in *Slc11a2* in response to age and amyloid may be involved in the progression of disease.

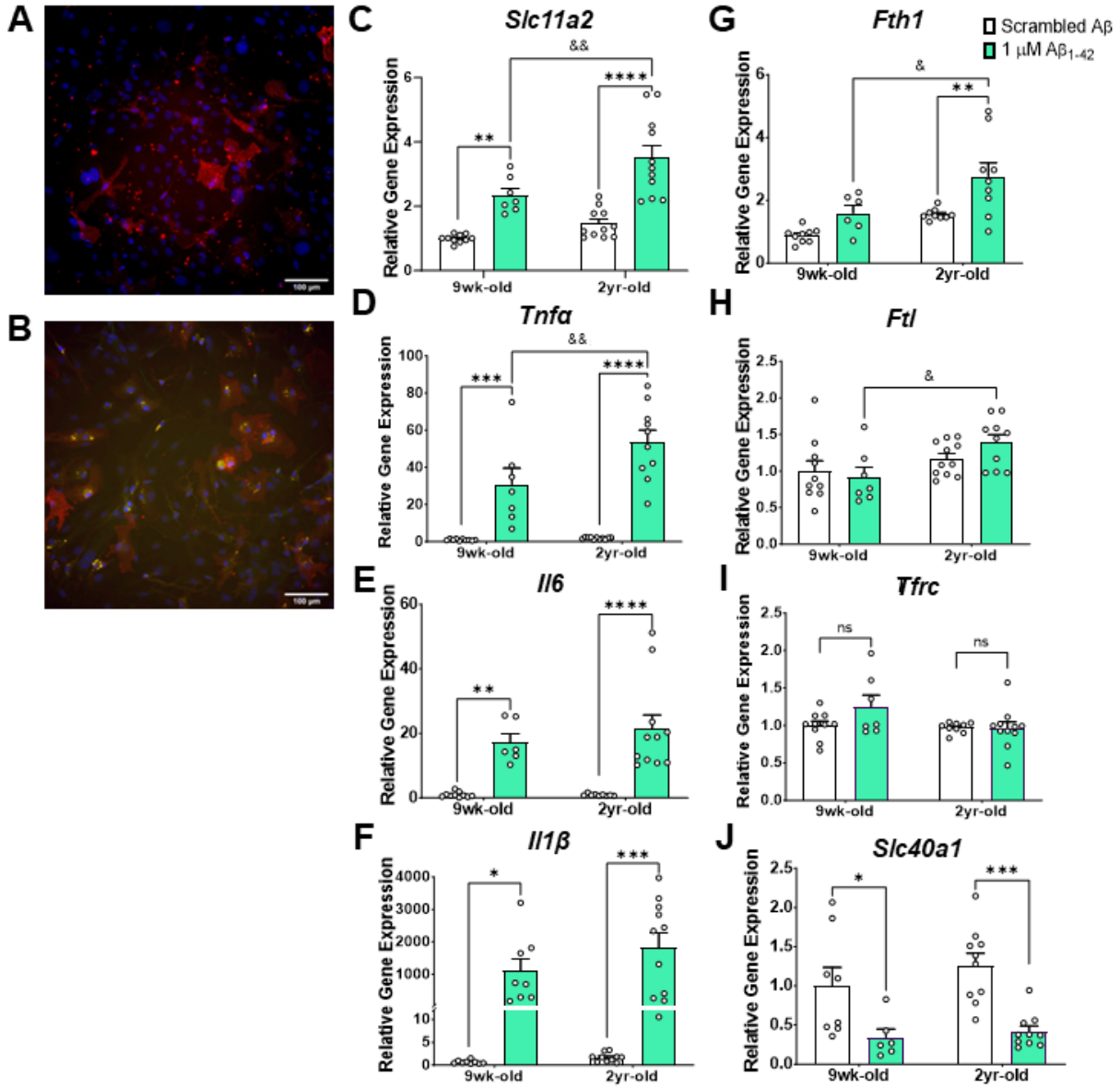

Figure 4.1. Age and Aβ stimulation synergize to increase *Slc11a2* in cultured primary microglia from adult mice.

a) Representative image of isolated primary microglia from 9-week-old C57BL/6J mouse, visualizing microglia (red, F4/80), ferritin (green, FtL), and DAPI (blue, nuclear stain). **b)** Representative image of isolated microglia from two-year-old aged C57BL/6J mouse showing ferritin deposits (green) in microglia (red), with DAPI (blue). Microscope images taken with 20x magnification, scale bar = 100 μm. **c-j)** Gene expression analysis via RT-qPCR in microglia isolated from young (9-wk-old) and aged (2-yr-old) mouse brains following 24 h stimulation with 1μm $A\beta_{1\text{-}42}$ or control scrambled Aβ. *p<0.05, **p<0.01, ***p<0.001, ****p<0.0001, ns = not significant. *asterisks, *Aβ Treatment effect*; &ampersand, *Age x Aβ Treatment Interaction* effect. Data represent the mean ± S.E.M. of 6-10 mice per group.

4.2.2 DMT1 inhibition *in vitro* significantly decreases Aβ-induced inflammation in immortalized microglia.

Based on the purported roles for DMT1/*Slc11a2* in Aβ stimulation and iron load, we characterized the effect of inhibiting DMT1 on Aβ and iron-induced inflammation in an *in vitro* system. This preliminary work has been replicated in two separate experiments, and further work will repeat the experiment at least once more before our manuscript is submitted for publication to ensure statistical power. Cells from the murine immortalized microglial cell line, "IMG" cells [211], were treated with ebselen, a pharmacological inhibitor of DMT1 [278], before subsequent treatment with scrambled Aβ, $A\beta_{1\text{-}42}$ alone, or iron (50 μM FAC) + $A\beta_{1\text{-}42}$. Preliminary results showed that Aβ stimulation leads to a robust increase in microglial pro-inflammatory *Il1β, Tnfα,* and *Il6* transcription, as expected (Fig. 4.2a-c). Simultaneous treatment with FAC alongside Aβ resulted in a blunting of Aβ-induced *Tnfa* and *Il6* transcription. Ebselen profoundly decreased the Aβ-induced pro-inflammatory cytokine response for all three cytokines assayed, even in the Aβ alone condition with no iron added (Fig. 4.2a-c). As expected, Aβ induced a significant upregulation in *Slc11a2* and ebselen exacerbated this increase (Fig. 4.2d), likely reflecting a compensatory upregulation of gene expression following ebselen-mediated DMT1 inhibition. Interestingly, the decrease in inflammatory cytokine transcription observed in response to ebselen treatment occurred in the absence of excess iron added to the media and without a significant change in total intracellular iron in the Aβ-alone condition (as measured via ICP-MS) (Fig. 4.2e). This suggests that a change in total intracellular iron content is not necessary for ebselen to exert its anti-inflammatory effects in these cells. Similar to our previous *in vivo* work using LPS as a neuroinflammatory stimulus [276], these preliminary data suggest a critical role for DMT1 in

mediating the baseline inflammatory response to Aβ in microglia, even without significant changes in total iron content.

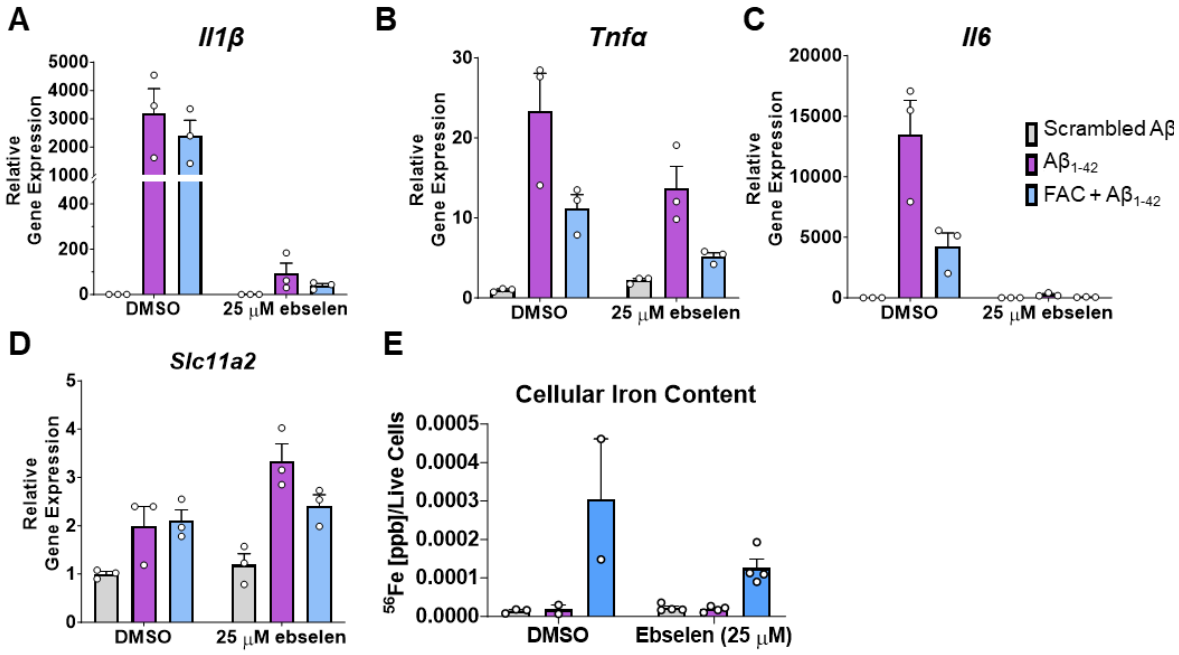

Figure 4.2. Ebselen-mediated DMT1 inhibition significantly abrogates Aβ-induced inflammatory cytokine expression in IMG cells.
a) *Il1β* gene expression via RT-qPCR from IMG cells treated for 24 h with DMSO control or 25 μM ebselen, followed by 24 h treatment with scrambled Aβ, 1 μM oligomeric $Aβ_{1-42}$, or 50 μM FAC with 1μM oligomeric $Aβ_{1-42}$. **B)** *Tnfα* gene expression via RT-qPCR following cell treatments. **c)** *Il6* gene expression via RT-qPCR following cell treatments. **d)** *Slc11a2* gene expression via RT-qPCR following cell treatments. **e)** Total cellular iron content assessed via ICP-MS in IMG cells treated for 24 h with DMSO or 25 μM ebselen, followed by 24 h treatment with scrambled Aβ, $Aβ_{1-42}$, or FAC + $Aβ_{1-42}$. Data shown represent an *n* of 3 technical replicates from one experiment. This experiment was repeated twice.

4.2.3 Microglial *Slc11a2* knockdown produces a hyperactive phenotype in female *APP/PS1* mice and worsens hyperactivity in male *APP/PS1* mice at 12-15 months.

Between 12-15 months of age, male and female mice were run through a series of behavioral assays to assess the effect of microglial *Slc11a2* knockdown on aspects of behavior and cognition. First, to assess locomotor activity, mice were run through an elevated zero maze (EZ maze, 5 min), open field chambers (45 min), and a one-trial spontaneous alternation Y-maze test (6 min) and total distance traveled was measured.

In females, *APP/PS1* mice did not exhibit differences in baseline locomotor activity compared to control WT female mice in any of the assays tested (Fig. 4.3a-f; $p>0.05$). However, female *APP/PS1* animals with microglial *Slc11a2* knockdown exhibited a significant increase in distance traveled in all three activity measurement assays compared to their non-*APP/PS1* counterparts (Fig. 4.3a, c-f; activity measurements, EZ maze: *APP/PS1,* $F(1,39) = 7.55$, $p=0.01$, *Interaction effect,* $F(1,39) = 10.21$, $p=0.003$; open field: *Interaction,* $F(1,39)=5.36$, $p=0.03$; Y-maze activity: *APP/PS1,* $F(1,40) = 5.23$, $p=0.03$, *Interaction,* $F(1,40) = 5.92$, $p=0.02$; arm entries in Y-maze: *APP/PS1,* $F(1,40) = 5.76$, $p=0.02$, *Interaction,* $F(1,40) = 7.93$, $p=0.008$). As control measurements to assess for anxiety-like behavior, the amount of time spent in the open arms of the EZ maze (Fig. 4.3b, $p>0.05$) or in the center area of the open field chambers were not significantly different (Fig. 4.3d, $p>0.05$). Additionally, there were no significant differences in Y-maze spontaneous alternation capacity between any groups (Fig. 4.3g, $p>0.05$).

Male *APP/PS1* mice exhibited a significant increase in activity in the EZ maze compared to controls, suggesting a sex-specific effect on baseline activity in this *APP/PS1* disease model at this age (Fig. 4.4a; EZ Maze: *APP/PS1 effect,* $F(1,48) = 22.61$, $p<0.0001$). There was a significant main effect of *Slc11a2* knockdown on activity in the EZ maze in males (*Knockdown effect,* $F(1,48)$

= 8.18, p =0.0063), and post-hoc analyses revealed that *Slc11a2* knockdown had a greater effect on the hyperactive phenotypes observed in the *APP/PS1* males compared to corresponding controls (Fig. 4.4a, EZ maze: Control vs. *APP/PS1,* p=0.013, *Slc11a2*^{KD} Control vs. *Slc11a2*^{KD} *APP/PS1,* p=0.0006). This was observed in the absence of a significant anxiety-like phenotype, with no difference in time spent in the open arms of the EZ maze (Fig. 4.4b). Male *APP/PS1* mice did not show any significant differences in total distance traveled or anxiety-like behavior in the open field chambers over 45 min (Fig. 4.4c,d, p>0.05). However, there was a significant *APP/PS1*-associated increase in activity in a 6 min Y-maze in the males (Fig. 4.4e; Y-maze: *APP/PS1 effect,* F(1,46) = 8.40, p=0.006), which was exacerbated in the *Slc11a2* knockdown animals (Fig. 4.4e, Y-maze activity post-hoc comparisons: Control vs. *APP/PS1,* p=0.39, *Slc11a2*^{KD} Control vs. *Slc11a2*^{KD} *APP/PS1,* p=0.012; Fig. 4.4f, Y-maze arm entries: F(1,46) = 5.65, p = 0.02; post-hoc comparisons: Control vs. *APP/PS1*, p=0.61, *Slc11a2*^{KD} Control vs. *Slc11a2*^{KD} *APP/PS1,* p=0.03). There were no significant differences in Y-maze spontaneous alternation capacity as a measure of working memory (Fig. 4.4g). Overall, these data suggest that microglial *Slc11a2* knockdown is associated with an exaggerated hyperactive phenotype in the *APP/PS1* animals, particularly in female mice.

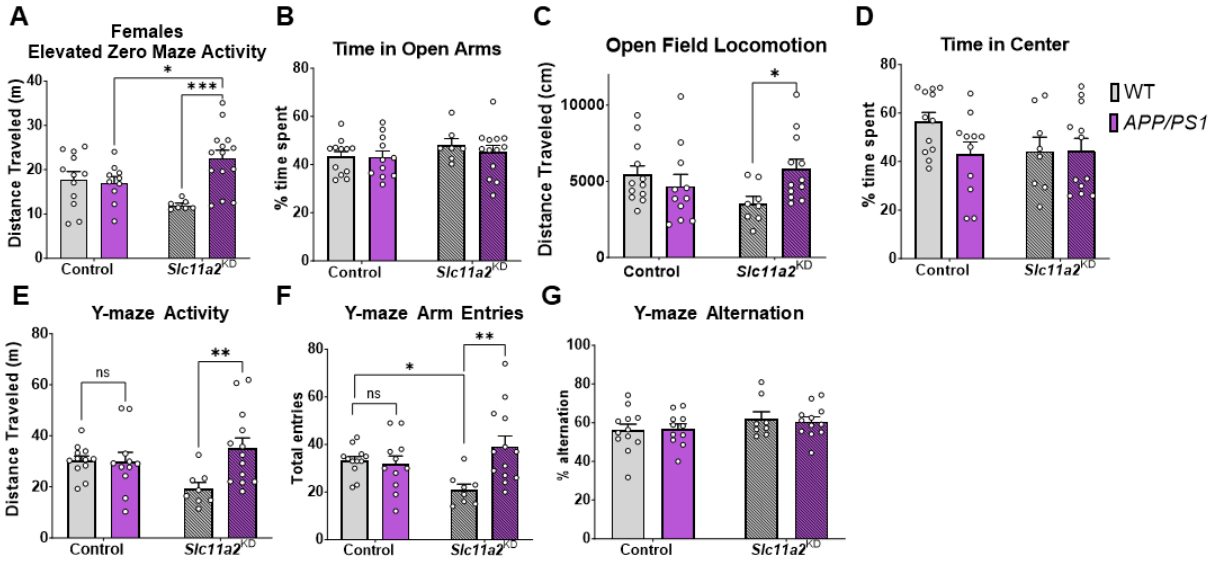

Figure 4.3. Microglial *Slc11a2* knockdown produces hyperactive phenotype in female *APP/PS1* mice.

a) Total distance traveled (m) in a 5-min elevated zero maze between control and *APP/PS1* females with or without *Slc11a2* knockdown. **b)** Percent time spent in open arms of elevated zero maze during the 5 min trial. **c)** Total distance traveled (cm) in open field transparent chambers during a 45 min trial of free locomotion. **d)** Percent time spent in center square area of open field chamber during 45 min session. **e)** Total distance traveled (m) in a 6 min trial of Y-maze. **f)** Number of arm entries in 6 min Y-maze trial. **g)** Percent spontaneous alternation in 6 min three-arm Y-maze trial. *p<0.05, **p<0.01, ***p<0.001, ns = not significant. Data represent the mean ± S.E.M. of 8-13 mice per group.

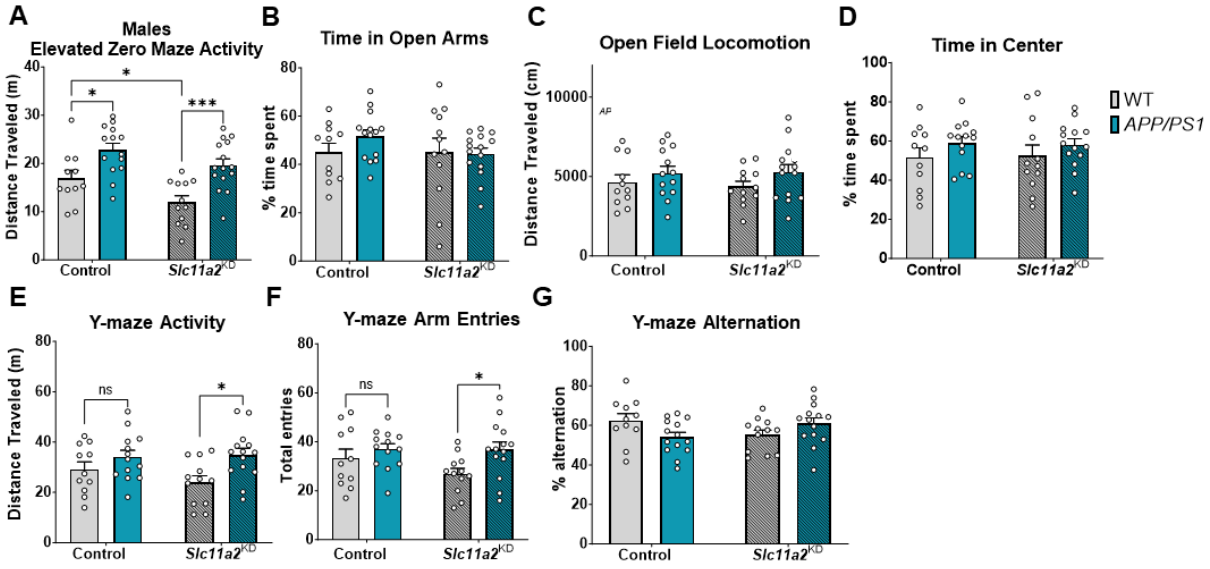

Figure 4.4. Microglial *Slc11a2* knockdown exacerbates hyperactivity in male *APP/PS1* mice. **a)** Total distance traveled (m) in a 5 min elevated zero maze between control and *APP/PS1* male mice with or without microglial *Slc11a2* knockdown. **b)** Percent time spent in the open arms of elevated zero maze. **c)** Total distance traveled (m) in open field chambers during a 45 min session. **d)** Percent time spent in center square of open field chambers during 45 min session. **e)** Total distance traveled (m) during 6 min Y-maze trial. **f)** Number of total arm entries explored during 6 min Y-maze. **g)** Percent spontaneous alternation in 6 min Y-maze trial. *p<0.05, **p<0.01, ***p<0.001, ns = not significant. Data represent the mean ± S.E.M. of 11-15 mice per group.

4.2.4 *Slc11a2* knockdown results in worsened performance in Morris Water Maze and fear conditioning assay in female *APP/PS1* animals.

To determine whether *Slc11a2* knockdown affected measurements of well-being, cognition, and longer-term learning and memory, several behavioral tasks were utilized. An overnight nest building assay revealed a significant *APP/PS1*-associated deficit in nestlet amount shredded in both females and males (Fig. 4.5a; Females: *APP/PS1 effect,* $F(1,38) = 43.54$, $p<0.0001$, Fig. 4.6a; Males: *APP/PS1 effect,* $F(1,47) = 9.15$, $p = 0.004$); however, there were no additional effects of knockdown on this measurement of cognition and well-being in either sex ($p>0.05$). To assess learning and spatial memory, mice underwent five days of trials to find a hidden platform in Morris water maze (MWM), a widely used test for hippocampal-dependent spatial navigation and

memory. Over the course of five days, all mice (both males and females regardless of *APP/PS1* genotype or knockdown), effectively learned the location of the platform compared to their baseline on day one, exhibiting significantly shorter path lengths to find the platform by day five (Fig. 4.5b, 4.6b; Females: *Day effect,* $F(2.75, 110.1) = 11.38$, $p<0.0001$; Males: *Day effect,* $F(2.891, 135.9) = 20.45$, $p<0.0001$). Female *APP/PS1* mice were not different than control females at finding the hidden platform during training days. However, female *APP/PS1* animals with microglial *Slc11a2* knockdown exhibited slightly longer path lengths to find the hidden platform, although this was not significant ($p = 0.1$). Furthermore, in accordance with data from earlier tasks assessing locomotor activity, female *Slc11a2* knockdown *APP/PS1* mice were significantly more hyperactive in the water maze (i.e., greater average swim speed) compared to all other groups (Fig. 4.5c; *Knockdown x APP/PS1 Interaction,* $F(1,40) = 5.45$, $p = 0.025$Mice underwent one 60 sec probe trial for memory of platform location 24 h after the last set of training trials, in which the platform was removed from the pool and mice were allowed to swim freely. There were no significant differences in time spent in the target quadrant where the platform location was previously (Fig. 4.5d, $p>0.05$); however, female *APP/PS1* mice overall exhibited a significant decrease in time spent around the exact platform location (1.5 cm radius) compared to littermate controls (Fig. 4.5e; Females: *APP/PS1 effect,* $F(1,35) = 11.45$, $p = 0.002$). Female *APP/PS1* mice with *Slc11a2* knockdown exhibited a significant further reduction in time spent around the platform location, suggesting an exacerbated loss of memory function in these animals (Females: *post hoc analysis:* Control WT vs. Control *APP/PS1,* $p = 0.39$; *Knockdown* WT vs. *Knockdown APP/PS1,* $p = 0.003$). To further assess the effects of *Slc11a2* knockdown on memory function, we utilized a fear conditioning assay. In a contextual fear conditioning assay, female *APP/PS1* mice exhibited a disease-associated deficit in fear memory (Fig. 4.5f, *APP/PS1 effect,* $F(1,39) = 12.26$,

p = 0.0012); although, there was no additional effect of *Slc11a2* knockdown. However, in a cued fear conditioning memory task, female *APP/PS1* mice with *Slc11a2* knockdown displayed a significant worsening in fear memory associated with presentation of a tone (Fig. 4.5g, *Knockdown x APP/PS1 Interaction,* $F(1,39) = 4.19$, $p = 0.047$). Indeed, although all females exhibited an increase in freezing in response to the presentation of the tone (*Tone,* $F(1,39) = 145.2$, $p<0.0001$), female *Slc11a2* knockdown *APP/PS1* mice were significantly less responsive compared to all other groups (Fig. 4.5h; *Interaction of Knockdown x APP/PS1,* $F(1,39) = 5.39$, $p = 0.026$). It is unlikely that this effect was due to a hearing phenotype, as all groups significantly increased freezing in response to the tone in this trial and also in response to the tone by the third tone presentation in the initial training session, albeit *APP/PS1* females overall froze less over the course of the 8 min training session (Fig. 4.5i, *Time effect,* $F(6.9, 279.3) = 41.1$, $p<0.0001$; *Interaction of Time x APP/PS1,* $F(15,600) = 4.91$, $p<0.0001$).

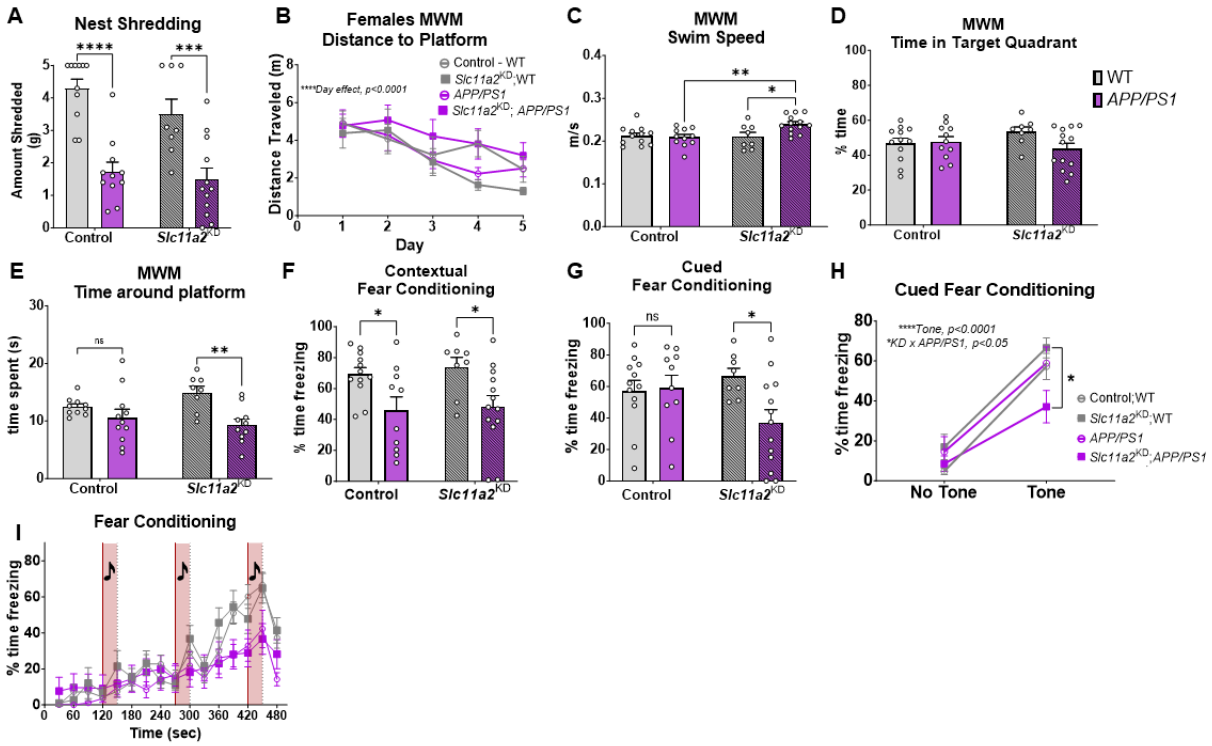

Figure 4.5. Microglial *Slc11a2* knockdown in *APP/PS1* females results in worsened performance in Morris water maze and fear conditioning assay compared to controls.
a) Total amount of 5 g nestlet shredded in overnight nest building assay. **b)** Total distance traveled (i.e., path length in m) during learning days 1-5 of Morris Water Maze (MWM). ****p<0.0001, *effect of day.* **c)** Average swim speed (m/sec) during the 60 sec probe trial of MWM. **d)** Percent time spent in the target quadrant where platform location previously was during 60 sec probe trial of the MWM. **e)** Total time spent (sec) in the 1.5 cm radius around and including the previous platform location during the memory probe trial of MWM. **f)** Percent time spent freezing during 4 min of contextual fear conditioning memory task (mice were placed in the same chamber in which they received tone-shock pairings the day prior). **g)** Percent time spent freezing during re-presentation of a tone during a cued fear conditioning memory task (mice were placed in an unfamiliar environment (chamber walls were changed to plastic white, vanilla scent added, lights off, new experimenter) the day after receiving tone-shock pairings). **h)** Change in percent time spent freezing between 2 min of no tone and 2 min of re-presentation of the tone (paired with a shock the day prior) during a cued fear conditioning memory task. **i)** Percent time freezing over 8 min fear conditioning training session with three tone-shock pairings. Red boxes represent a 30 sec tone, at the end of which was a 1 sec shock (black dotted line). *p<0.05, **p<0.01, ***p<0.001, ****p<0.0001, ns = not significant. Data represent the mean ± S.E.M. of 8-13 mice per group. Statistical outliers removed using ROUT's test.

APP/PS1 males exhibited significantly longer path lengths to find the hidden platform compared to male littermate controls during the five MWM training days (Fig. 4.6b; *APP/PS1* effect, $F(1, 47) = 5.99$, $p = 0.018$). This behavioral phenotype was observed in the absence of

differences in swim speeds between groups (Fig. 4.6c, $p>0.05$), demonstrating a disease model-associated learning deficit in the males. In the MWM probe trial, there were no significant differences between groups in time spent in the target quadrant of the previous platform location (Fig. 4.6d, $p>0.05$); however, male *APP/PS1* mice overall spent significantly less time around the remembered platform location (within 1.5 cm radius) compared to littermate controls (Fig. 4.6e; Males: *APP/PS1 effect,* $F(1,47) = 5.06$, $p = 0.03$). There were no differences in male knockdown animals compared to *Slc11a2*-intact control animals in MWM. Furthermore, there were no significant difference between any groups of the males in the contextual fear conditioning assay (Fig. 4.6f, $p>0.05$), although male *APP/PS1* mice overall performed worse on the cued fear conditioning task for memory (Fig. 4.6g-h, *APP/PS1 effect,* $F(1,46) = 4.15$, $p = 0.047$; Fig. 4.6i, *Interaction of Time x APP/PS1,* $F(15, 705) = 2.25$, $p = 0.004$). *Slc11a2* knockdown had no effect on performance in these assays in the males. Overall, these data suggest that a decrease in microglial *Slc11a2* is associated with significant worsening of cognitive dysfunction in several tasks in a sex-specific manner, particularly in female *APP/PS1* animals.

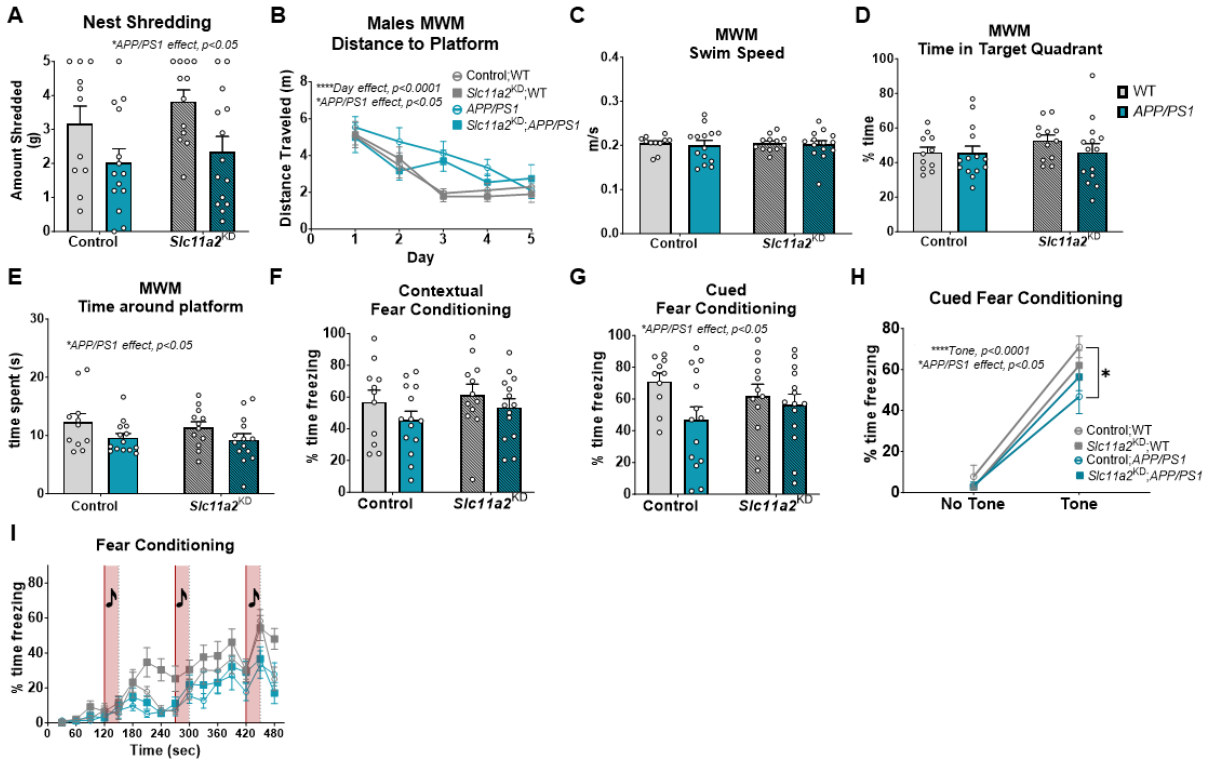

Figure 4.6. Microglial *Slc11a2* knockdown had no significant effect on performance in Morris water maze and fear conditioning assay in *APP/PS1* males.
a) Total amount of 5 g nestlet shredded overnight in nest building assay. *p<0.05, *effect of APP/PS1*. **b)** Total distance traveled (path length, m) during learning days 1-5 in MWM in males. ****p<0.0001, *effect of day,* *p<0.05, *effect of APP/PS1*. **c)** Average swim speed in 60 sec MWM probe trial (m/sec). **d)** Percent time spent in target quadrant of previous platform location during 60 sec probe trial for memory in MWM. **e)** Total time spent (sec) in the area of where the platform location was previously (radius of 1.5 cm) in a 60 sec MWM probe trial for memory. *p<0.05, *effect of APP/PS1*. **f)** Total percent time spent freezing in a contextual fear conditioning assay. Mice moved freely for 4 min in the same chambers as the day before, where they had received a tone-shock pairing. **g)** Total percent time spent freezing in a cued fear conditioning assay. Mice were placed in a novel environment and re-presented with a tone that had been paired with a shock the day prior. *p<0.05, *effect of APP/PS1.* **h)** Change in percent time freezing during 2 min of no tone presentation versus 2 min of tone re-presentation the day after mice experienced a tone-shock pairing. **i)** Percent time spent freezing during 8 min fear conditioning training session with three tone-shock pairings. Red boxes = 30 sec tone presentation, immediately followed by a 1 sec shock, shown in black dotted lines. *p<0.05, **p<0.01, ***p<0.001, ****p<0.0001 *effect of Tone.* Data represent the mean ± S.E.M. of 11-15 mice per group.

4.2.5 *Slc11a2* knockdown is associated with significantly lower microglial *Ftl1* expression levels in *APP/PS1* animals.

Following significant behavioral differences observed in female *APP/PS1* animals with *Slc11a2* knockdown, we aimed to assess changes in microglia from these animals, which may in part

underlie the worsened cognitive performance observed. Specifically hippocampal microglia were isolated, as the hippocampus is a primary brain region involved in learning, memory formation, and consolidation [279, 280]. Bilateral hippocampi were extracted from female control and experimental animals and hippocampal $CD11b^+$ microglia were isolated using magnetic sorting. These samples will be utilized for bulk-RNASeq analysis in a future direction, described in Chapter V. $CD11b^+$ cells were also collected from the remaining whole brain from males and females for preliminary RT-qPCR analysis of overall changes to microglia due to *Slc11a2* knockdown. In whole-brain $CD11b^+$ cells, there was an *APP/PS1*-associated increase in *Slc11a2,* which was significant in male, but not female, microglia (Fig. 4.7a, b; Females: *Knockdown,* $F(1,26) = 270$, $p<0.0001$, *Interaction,* $F(1,26) = 7.23$, $p = 0.01$, WT vs. APP, $p = 0.07$; Males: *Knockdown,* $F(1,35) = 66.77$, $p<0.0001$, *Interaction,* $F(1,35) = 4.06$, $p=0.05$, WT vs. APP, $p = 0.038$). *Il1β* and *Cybb* were also measured in whole-brain microglia to determine whether *Slc11a2* knockdown affects *APP/PS1*-associated inflammation and oxidative stress, respectively. Both female and male microglia isolated from *APP/PS1* mice exhibited a robust upregulation in pro-inflammatory cytokine *Il1β*, as expected (Fig. 4.7c, d; Females: *APP/PS1* effect, $F(1,30) = 24.2$, $p<0.0001$; Males: *APP/PS1* effect, $F(1,36) = 27.81$, $p<0.0001$). *Slc11a2* knockdown had no additional effect on this marker of inflammation in either sex ($p>0.05$). In measuring *Cybb* as a marker of oxidative stress, there was a significant increase in *APP/PS1*-induced *Cybb* in male microglia, but not female microglia, with no effect of *Slc11a2* knockdown (Fig. 4.7e, f; Females, $p>0.05$; Males: *APP/PS1* effect, $F(1,34) = 13.73$, $p=0.0007$).

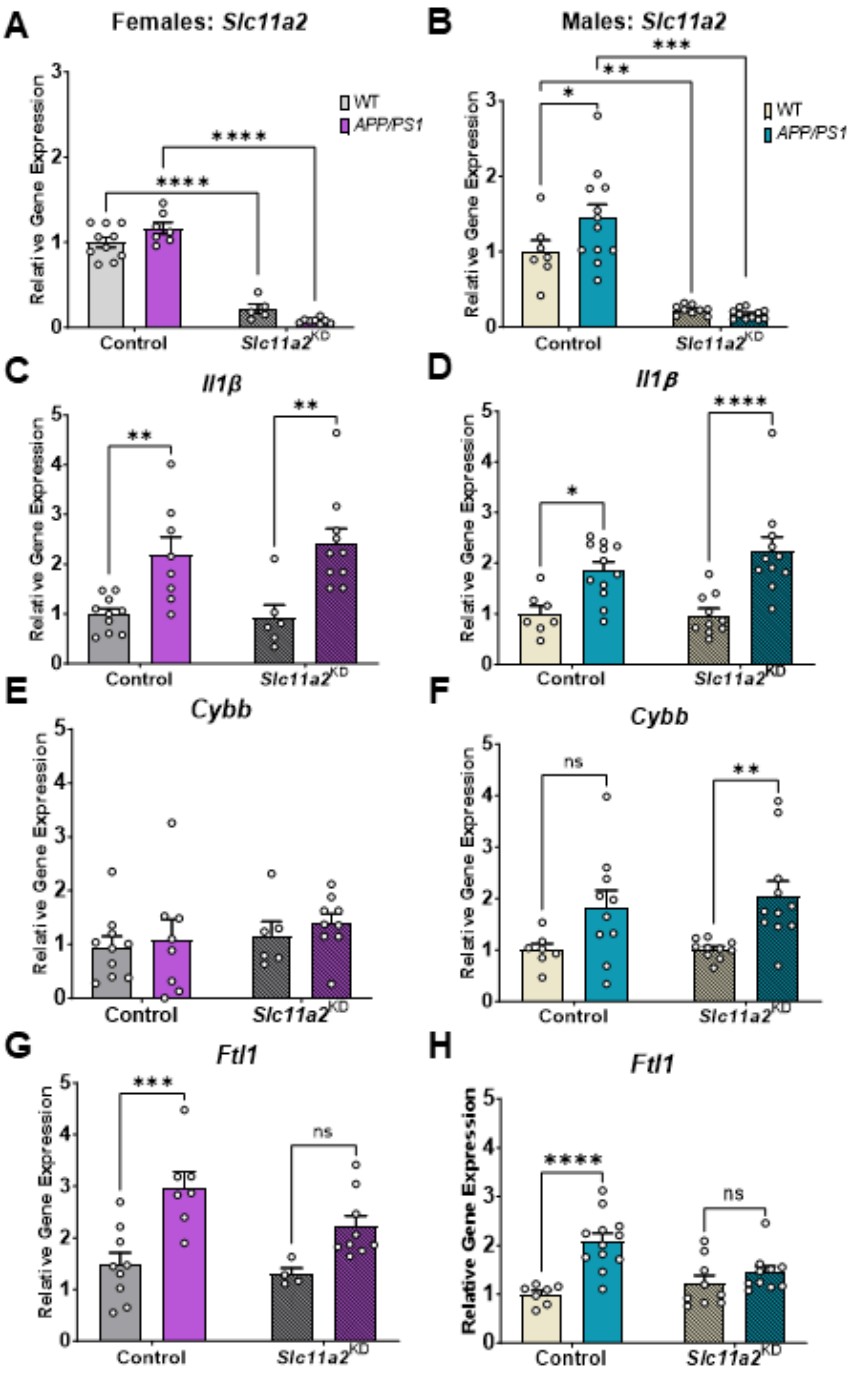

Figure 4.7. *Slc11a2* knockdown blunts *APP/PS1*-induced *Ftl1* upregulation in microglia isolated from whole brains of male and female mice.
a) RT-qPCR gene expression of *Slc11a2* from microglia isolated from WT or *APP/PS1* female mice with or without microglial *Slc11a2* knockdown. **b)** RT-qPCR gene expression of *Slc11a2* from microglia isolated from WT or *APP/PS1* male mice with or without microglial *Slc11a2* knockdown. **c)** *Il1β* expression in female microglia. **d)** *Il1β* expression in male microglia. **e)** *Cybb* expression in female microglia. **f)** *Cybb* expression in male microglia. **g)** *Ftl1* gene expression in isolated microglia from females. **h)** *Ftl1* gene expression in isolated microglia from males. *p<0.05, **p<0.01, ***p<0.001, ****p<0.0001, ns = not significant. Data represent the mean ± S.E.M. of 4-12 mice per group.

Lastly, disease-associated microglia isolated from brains of AD model mice and humans consistently display a robust upregulation in *Ftl* gene expression across multiple datasets [133, 134, 146, 281]; thus, *Ftl* gene expression was measured in these cells. Microglia isolated from brains of *APP/PS1* females and males exhibited a significant increase in *Ftl1* expression compared to WT controls (Fig. 4.7g, h; Females: *APP/PS1* effect, $F(1,25) = 21.28$, $p<0.0001$; Males: *APP/PS1* effect, $F(1,34) = 18.60$, $p<0.0001$). *Slc11a2* knockdown blunted this *APP/PS1*-induced upregulation of microglial F*tl1* in both sexes, albeit to a greater degree in the males (Females: *Interaction,* $F(1,25) = 3.22$, $p = 0.08$, Control *APP/PS1* vs. *Slc11a2*^{KD} *APP/PS1* $p = 0.064$, 25% decrease in *Ftl1* expression in *Slc11a2*^{KD} *APP/PS1* compared to control *APP/PS1*; Males: *Interaction,* $F(1,34) = 7.94$, $p = 0.008$, Control *APP/PS1* vs. *Slc11a2*^{KD} *APP/PS1* $p=0.005$, 34% decrease in *Ftl1* expression in *Slc11a2*^{KD} *APP/PS1* vs. control *APP/PS1*). As the greatest differences in behavior due to *Slc11a2* knockdown were observed in female mice, further analysis of transcriptional changes of female hippocampal CD11b^{+} microglia via RNAseq is a future direction.

4.2.6 Determining differences in brain-wide distribution of Aβ, ferritin, and microglia using brain clearing and light sheet microscopy.

To determine global and region-specific changes in microglia, iron, and Aβ in the brains of female *Slc11a2* knockdown mice compared to controls, we also conducted brain clearing and light sheet microscopy. Female WT and *APP/PS1* mice with or without *Slc11a2* knockdown were used for whole brain isolation and tissue clearing using SHIELD method. This work is in its preliminary stages; however, we have been able to visualize Aβ plaques, microglia (via Iba1 antibody staining), and ferritin deposits (via ferritin antibody staining) throughout the brain, which all colocalize in *APP/PS1* female brains (Fig. 4.8). Our future work aims to utilize these images to quantify

differences in regional amyloid deposition, ferritin immunoreactivity, and microglial number by brain region (total number and average number of cells surrounding plaques). It may be that the *Slc11a2* knockdown in microglia is associated with decreased microglial ferritin staining, and questions remain on the implications that might have on microglial reactivity and plaque deposition *in vivo* in these brains. This light sheet microscopy work will allow us to delve deeper into understanding the changes underlying the altered cognition observed in the female *APP/PS1 Slc11a2* knockdown animals.

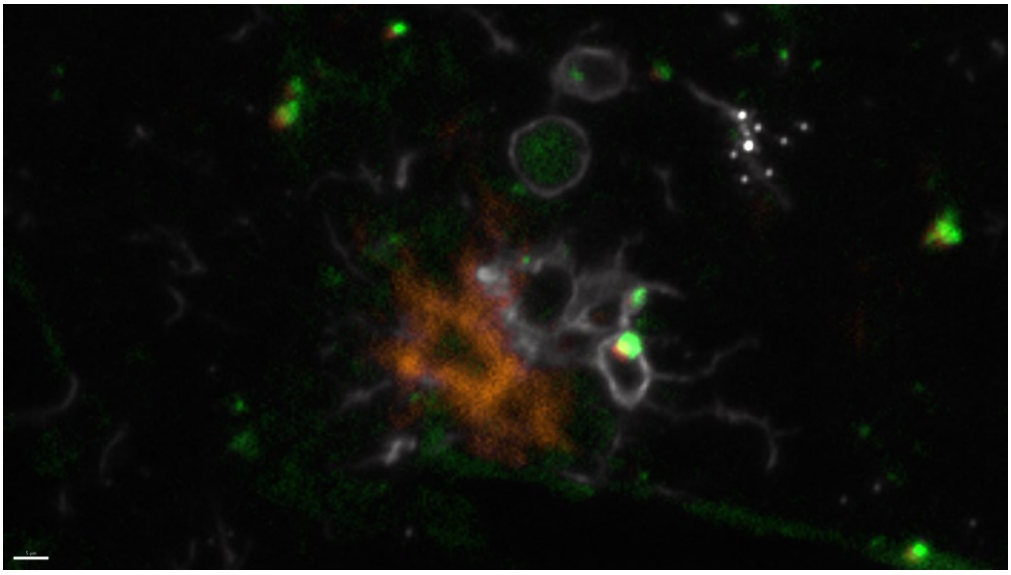

Figure 4.8. Microglia, ferritin, and Aβ can be visualized in a brain cleared using SHIELD. Image shows an Aβ plaque (stained with an anti-amyloid antibody, orange), microglial cells (probed with an anti-Iba1 antibody, white), and ferritin deposits (stained with anti-ferritin antibody, green) from the brain of an *APP/PS1* female mouse at 15 months of age. Image taken by Dr. Jose Maldonado with light sheet microscope at 15x, scale bar = 5 μM.

4.3 Discussion

Iron-loaded microglia are a significant hallmark of several neurodegenerative diseases, including AD [282-284]. Reactive microglia surrounding Aβ plaques exhibit a significant upregulation in ferritin-L (*Ftl1*) across AD mouse models and human patients and is thus a defining feature of DAMs across multiple disease models [133, 134, 146, 171]. At the *in vitro* level, we and others have shown that inflammatory signals and iron import mechanisms are intimately connected in microglial cells [[153, 180], our data also in IMG cells]. AD-associated pro-inflammatory signals such as Aβ and bacterial lipopolysaccharide upregulate microglial iron importer DMT1 and increased iron levels lead to enhanced secretion of pro-inflammatory cytokines [185], toxic ROS production [167], and cellular senescence and dysfunction [164, 166]. Furthermore, recent *in vitro* work has shown that iron loading specifically in microglia underlies subsequent neurotoxicity and cell death in a tri-culture system [161].

In studies in primary isolated microglia from aged and young mice, we demonstrated significant ferritin deposits in aged cells compared to young cells, replicating what others have shown in aged human populations [164]. After treating the isolated cells *in vitro* with pro-inflammatory oligomeric $A\beta_{1\text{-}42}$, we found a significant Aβ-induced increase in *Slc11a2,* which was exacerbated in aged microglia compared to young cells. Interestingly, this Aβ and age-induced upregulation in iron import machinery was specific to *Slc11a2,* as we observed no changes in the other primary iron importer *Tfrc,* at least at the transcriptional level. This age-associated increase in *Slc11a2* expression was accompanied by a significant upregulation in iron storage genes *Ftl1* and *Fth1* and augmented Aβ-induced inflammatory markers in the aged cells. This exacerbated Aβ-provoked response in the aged glia has been similarly observed by others [285, 286] and suggests a primed cellular inflammatory state**.** These preliminary findings in primary cells

demonstrate an association between iron loading markers and Aβ-induced inflammation in aged cells and suggest that changes in microglial DMT1/*Slc11a2* may be uniquely associated with the development of these hallmarks in age and disease.

In our previous work, we showed that knocking down *Slc11a2* in an LPS-induced acute inflammatory model *in vivo* led to a decrease in microglial pro-inflammatory markers, suggesting a key role for DMT1 in mediating the inflammatory response [276]. To examine whether altering DMT1 might affect downstream disease-associated parameters associated with Aβ, *in vitro* experiments were first conducted to inhibit DMT1 in an immortalized microglial cell line (IMGs) before treating the cells with oligomeric Aβ. Pharmacological inhibition of DMT1 using ebselen resulted in a robust abrogation of Aβ-induced pro-inflammatory cytokine expression. These data, in correspondence with our previous work, suggest a critical role for DMT1 in mediating inflammatory responses to multiple stimuli (i.e., LPS and Aβ). However, no studies to our knowledge have directly examined whether altering microglial iron-handling machinery affects the development of chronic inflammation and disease-associated hallmarks *in vivo.*

In these studies, we generated a novel model of inducible, microglial-specific knockdown of DMT1 (gene, *Slc11a2*) in the *APP/PS1* mouse model of AD. Microglial *Slc11a2* knockdown was induced in male and female mice at an early stage of plaque development (5-6 months of age) and downstream cognitive function, behavior, and markers of disease were assessed when mice were 12-15 months of age. We observed a significant worsening of behavioral phenotypes and cognitive function in female *APP/PS1* mice with *Slc11a2* knockdown. Specifically, female *APP/PS1* knockdown animals were significantly more hyperactive than all other female groups in multiple assays conducted, including EZ maze, open field locomotion, and spontaneous Y-maze. Interestingly, these data showed that female *APP/PS1* mice at 12-15 months of age do not exhibit

differences compared to controls in baseline locomotor activity; however, the substantial hyperactive phenotype emerged in females with *Slc11a2* knockdown. In males, *APP/PS1* mice overall were significantly hyperactive and *Slc11a2* knockdown further increased hyperactive behavior in EZ maze and Y-maze, but not in open field. This may reflect a significant change in hyperactive behavior exercised in a novel environment, as the open field test we used consists of a longer 45 min bout of activity. Previous studies have demonstrated significant hyperactivity in mouse models of AD [287-290] and AD human patients often exhibit disruptions in psychiatric behaviors such as hyperactivity, impulsivity, and disinhibition [291]. Thus, microglial *Slc11a2* knockdown exacerbates disruptions in these neuropsychiatric-like symptoms, particularly in female *APP/PS1* mice.

To assay for changes in memory function in these mice, we utilized the MWM test for memory – a gold standard for testing hippocampal-dependent spatial memory acquisition and retention in rodents [201, 292]. Although female *APP/PS1* mice were not significantly different from controls in memory performance, *Slc11a2* knockdown resulted in a significant worsening of memory function in the *APP/PS1* females in the MWM memory probe trial. While male *APP/PS1* mice overall performed worse in MWM compared to WT controls, we found no significant effects due to microglial *Slc11a2* knockdown in this assay. This suggests a sex-specific disease-modifying cognitive effect of *Slc11a2* knockdown in female *APP/PS1* animals.

Previous work has shown conflicting results on sex differences in behavior and memory in the *APP/PS1* model of AD. Some report no differences in behavior between WT or *APP/PS1* males and females in some cognitive tasks [47], whereas others demonstrate that female *APP/PS1* mice are worse in MWM [48, 293] but better at IntelliCage [49] and Barnes Maze [294] than male *APP/PS1* animals. The conflicting results may in part be due to age and strain of mice tested, AD

model characteristics, cognitive task utilized, and stress level of the mice. Similar to our findings in mice of the same age, Melnikova et al. uncovered a sex-specific deficit in spatial memory only after overexpression of cyclooxygenase 2 in female, but not male, *APP/PS1* mice [295]. It may be that some of the memory-associated tasks used in Melnikova's and our studies require a later timepoint in disease in the females to detect cognitive deficits in the *APP/PS1* model. Indeed, it has been shown that male *APP/PS1* mice develop cognitive deficits earlier than female *APP/PS1* mice [296]. Both male and female *APP/PS1* mice at the time point of testing in our studies exhibited robust deficits in nest building capacity compared to WT controls, demonstrating the high sensitivity of this task in detecting early disease-related differences in overall well-being and general cognition in both sexes [297, 298]. However, due to the purported lower sensitivity of memory-associated assays such as Y-maze and MWM in detecting differences [290, 299], a later time point may have illuminated more baseline cognitive differences in female *APP/PS1* mice compared to WT controls. If this is the case, it is intriguing to consider the implications of *Slc11a2* knockdown accelerating *APP/PS1*-associated memory deficits at an earlier time point specifically in female mice.

To further probe this memory phenotype, we also used a fear conditioning assay consisting of both a contextual conditioning and cued conditioning task. *APP/PS1* females overall performed significantly worse than control WT mice in the contextual fear conditioning task, although *Slc11a2* knockdown had no additional effect in this task. In the cued fear conditioning assay however, we observed a significant deficit in learned cued fear memory in female *APP/PS1* mice with *Slc11a2* knockdown compared to controls. Others have shown that hyperactivity can impair freezing capacity in fear conditioning tasks [300, 301]. However, it is unlikely that enhanced hyperactivity accounts for the deficit in the cued fear conditioning task we observed in female

APP/PS1 knockdown mice, as female knockdown and control *APP/PS1* mice froze to the same degree in response to the tone during initial training of the fear conditioning task (both exhibited increased freezing after the third tone presentation preceding the third shock). Thus, the impairment we observed in the cued fear memory task suggests a specific memory-associated deficit in the female knockdown *APP/PS1* animals. It may be that the cued fear conditioning task utilizing the re-presentation of a cue (tone previously paired with a shock) requires the use of a separate, parallel neural processing system from the contextual fear memory task, involving inputs primarily from the amygdala, insular cortex, associated regions in the parietal and temporal lobes, sensory cortices, and thalamus [302, 303]. These complex networks likely converge with hippocampal circuits to acquire and express fear memory associated with a conditioned stimulus [304]. Interestingly, dysfunction and neurodegeneration in the amygdala [305-307] and insular cortex [308, 309] have been implicated in AD models and patient brains as an early indicator of disease. Indeed, deficits in amygdala-related signaling may also underlie many of the neuropsychiatric symptoms observed in AD patients, such as hyperactivity, agitation, and aggression [310]. The deficit we observed in cued fear memory, paired with the significant hyperactivity observed particularly in the female *APP/PS1* knockdown mice suggests that *Slc11a2* knockdown worsens AD-associated behavior mediated by both hippocampal and non-hippocampal-dependent circuits in female mice. In males, we found a significant *APP/PS1*-associated deficit in cued fear conditioning; however, there were no significant differences due to knockdown. These data thus reflect a significant sex-specific effect of *Slc11a2* knockdown on hippocampal-dependent memory function (i.e., MWM deficit), as well as cortical and amygdala-associated function (i.e., hyperactivity, fear conditioning deficits) in female, but not male, *APP/PS1* mice.

The sex differences observed in our model are of particular interest. In humans, females are significantly more likely to develop AD than males [311, 312]. Furthermore, although there is a lack of consensus on sex differences in specific cognitive tasks in different mouse models of AD, females show higher plaque burden compared to males across several AD models suggesting worsened AD phenotypes over time [293, 313, 314]. In these studies, we also report a sex difference in *APP/PS1*-associated *Slc11a2* microglial gene expression. In whole-brain isolated microglia from these mice, *Slc11a2* was found to be significantly increased in male, but not female, *APP/PS1* animals compared to WT controls. Similarly, in our previous work, we noted a sex-specific LPS-induced increase in male, but not female, microglial *Slc11a2,* suggesting a male-specific inflammatory-iron-associated transcriptional pathway in the microglia of these mice [276].

Sex differences in brain iron-handling and changes in iron-associated markers as they relate to disease development are not well understood. Studies in humans have shown that brain ferritin levels are generally higher in older men than women in several regions [259], which is thought to contribute to the risk for males developing neurodegenerative disease at earlier ages than females [315]. Additionally, gene variants involved in iron metabolism (i.e., hemochromatosis gene variant HFE H63D and transferrin gene variant TfC2) have been associated with higher brain iron levels in older men [260, 316] and these variants have been associated with higher risk of developing AD in some studies [317-319]. In females, a change in iron levels has also been linked with the development of AD dementia, although the directionality of the change and the underlying mechanisms are unclear. For example, prior iron-deficiency anemia has been significantly associated with the development of dementia in females, but not males [320]. On the other hand, studies have also shown that there is a significant rise in serum ferritin levels associated with

menopause in aging females [321] and earlier age of menopausal onset has been associated with higher risk of dementia in females as well [322]. Indeed, the rise in iron status during female mid-life in humans has been directly correlated with declining cognitive performance [323]. Although the exact associations between brain iron status, sex, and disease are still being elucidated, our work highlights another potential site of sex-specific regulation of cellular iron-handling machinery. Specifically, these data suggest a sex-specific regulation of microglial DMT1/*Slc11a2* in the context of inflammation and disease development. Corresponding with this, research has illuminated significant sex differences in microglial morphology, inflammatory markers, and activity in age and disease [225, 324]. It may be that the lack of an increase in microglial *Slc11a2* in female mice during AD development is a deleterious adaptation associated with the worsened pathological development reported in female AD mice (e.g., worsened microglial function, greater plaque burden) [314, 325, 326]). The lack of an increase in *Slc11a2* in female *APP/PS1* microglia compared to male *APP/PS1* mice may reflect enhanced cellular iron burden in the females, as the IRE-IRP system works in a compensatory manner to decrease iron import markers during high iron load. This has previously been shown in a sex-specific manner in other models of iron load-related disease and may be a detrimental adaptation [88]. Our future work aims to characterize iron load in the knockdown cells to examine whether *Slc11a2* knockdown alters iron levels and distribution per se in the brains of the female *APP/PS1* mice.

Further work will also more deeply phenotype hippocampal microglia from these mice in the RNASeq dataset. In our preliminary RT-qPCR gene expression analyses, the subtle decrease in *APP/PS1*-associated *Ftl1* in whole-brain microglia isolated from female knockdown animals is of note. It may be that *Slc11a2* knockdown alters total iron load or intracellular iron distribution in these cells, which is associated with worsened disease parameters. If this is the case, it could be

that an increase in microglial iron-related markers serves as a protective adaptation during the disease process, disallowing iron-handling by cells such as neurons and astrocytes, which are less able to withstand a high iron load [148, 149]. In fact, work has shown that a decline in ferritin^{+} microglia and subsequent increase in free iron in aged animals is associated with deleterious effects [327]. If mechanisms involved in iron import are a protective measure in disease, this may partially underlie the exacerbated AD phenotypes we observed in female mice with decreased *Slc11a2.* It is important to note that significant technical challenges limited us to gene expression analyses in these studies. While we cannot make definitive conclusions related to iron levels per se and/or protein-level changes in DMT1 and inflammatory makers, others have suggested an important role for transcription-level changes in iron-related genes [102, 328]. Other limitations and caveats of this work are discussed in Chapter V.

Lastly, it is also intriguing to consider a different time point for manipulation of microglial *Slc11a2* during the disease process. As alluded to above, initial ferritin/iron loading in microglia may be a neuroprotective measure, whereas a late transition to an iron-loaded phenotype exceeds the cell's capacity for non-toxic iron storage and leads to neurodegenerative consequences [161, 329]. Despite the remaining questions, this work highlights a sex-specific role for microglial *Slc11a2* during disease development in mice, and contributes to the ongoing debate on the beneficial or detrimental roles of microglia in AD.

CHAPTER 5

General Discussion/Conclusions/Future Directions

5.1 Conclusions and discussion

5.1.1 Summary of findings: LPS model and *APP/PS1* model of Alzheimer's disease

The studies in this dissertation determined the effects of knocking down iron import gene *Slc11a2* in microglial cells on pro-inflammatory markers, iron load markers, and behavior and cognition in two mouse models related to Alzheimer's disease. First, I characterized the significant effect of microglial *Slc11a2* knockdown on blunting LPS-induced inflammatory responses in male mice, as detailed in Chapter III. Specifically, *Slc11a2* knockdown male mice exhibited a significant improvement in acute LPS-induced sickness behavior, which was associated with a robust decrease in systemic inflammatory cytokines. However, there was no lasting effect on cognition in the knockdown animals given LPS compared to controls. It is likely that the short-term stimulus of LPS in this acute neuroinflammatory model is not robust enough to elicit significant changes in cognition at the time point tested. Conversely, in Chapter IV, we demonstrated a significant worsening of AD-associated behavioral phenotypes in middle-aged female *APP/PS1* mice with microglial *Slc11a2* knockdown. Female *APP/PS1* animals with *Slc11a2* knockdown performed significantly worse on several measures of memory capacity, including Morris water maze and a fear conditioning assay, and were significantly hyperactive in EZ maze, open field locomotor activity chambers, and Y-maze. It is intriguing to consider the difference in directionality of the *Slc11a2* knockdown-induced behavioral changes observed in both models. *Slc11a2 k*nockdown significantly improved short-term male sickness behavior in the LPS model, yet considerably exacerbated behavioral and cognitive deficits in females in the chronic model of AD (Fig. 5.1).

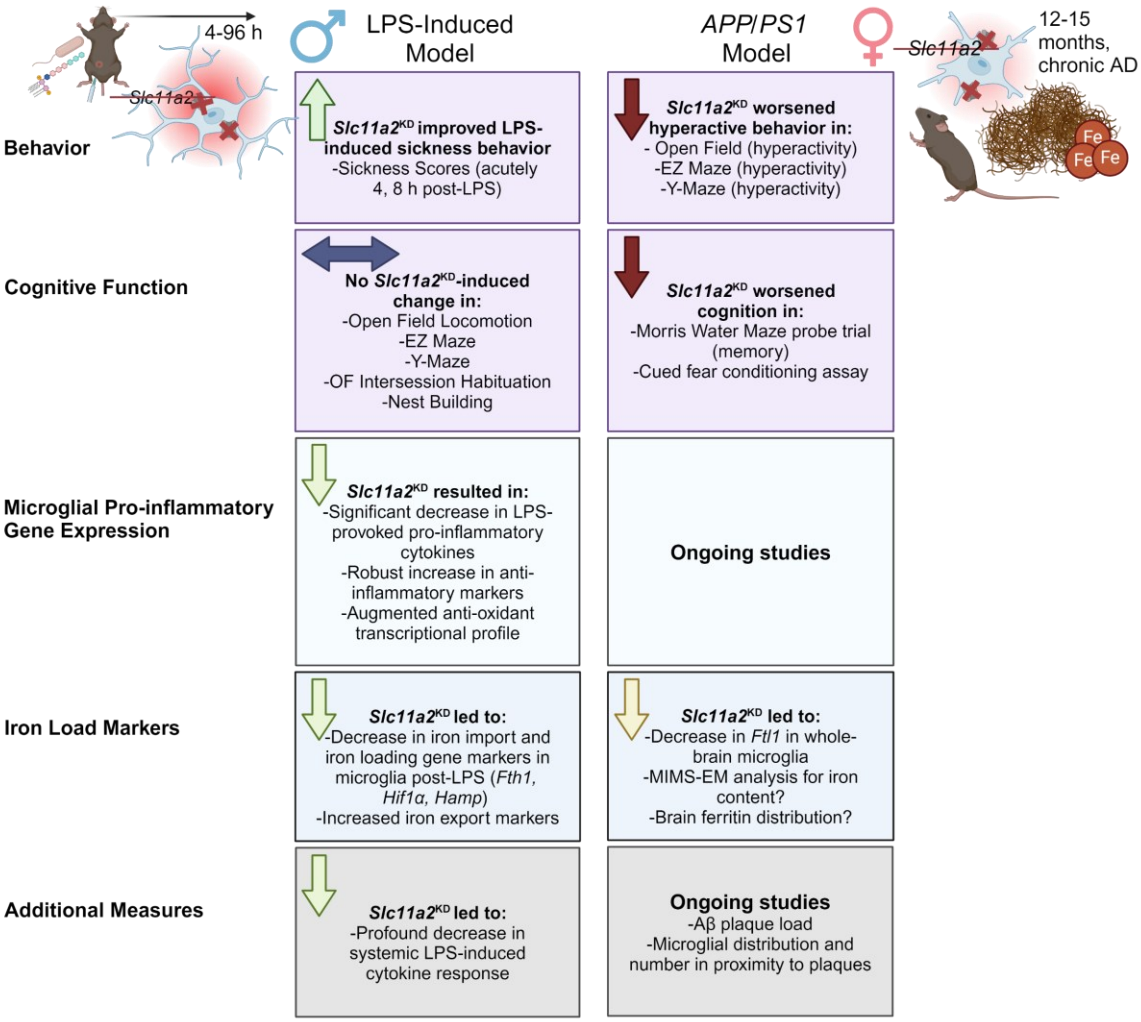

Figure 5.1. Comparison of findings in short-term LPS inflammation model and chronic AD model.
Microglial *Slc11a2* knockdown resulted in an acute improvement in sickness behavior in male mice in the short-term LPS (i.p.) inflammatory model (left side). This was associated with a significant decrease in pro-inflammatory markers and augmented anti-inflammatory, antioxidant, and growth markers in isolated microglia. Cellular iron loading and import genes were also downregulated. Systemically, knockdown led to a robust blunting of LPS-induced cytokines in male mice. *Slc11a2* knockdown in the *APP/PS1* model of AD led to a significant exacerbation of hyperactive behavior and worsened memory performance specifically in female mice (right side). This was associated with a significant decrease in *Ftl* in whole-brain microglia. Ongoing and future work will characterize effects of knockdown on microglial gene expression of inflammatory and oxidative markers, additional markers of cellular iron load, Aβ plaque deposition, and microglial reactivity near plaques.
Figure made with BioRender.com, with permission.

It may be that in the context of acute inflammation, microglial *Slc11a2* helps orchestrate a sickness-inducing pro-inflammatory behavioral response, whereas in chronic AD, where conditions of long-

lasting inflammation are present, *Slc11a2* mediates iron-associated and inflammatory responses that help preserve behavior and cognition. This will be discussed in further detail in **section 5.1.3.2.**

In addition to changes in behavior, we also assessed alterations in microglial gene expression in both models, which may underlie the behavioral and cognitive changes observed. In the acute model of systemic LPS-induced inflammation, there was a significant decrease in microglial pro-inflammatory markers in male *Slc11a2* knockdown animals, which was associated with an augmentation in an anti-inflammatory, antioxidant, and pro-growth transcriptional profile (Chapter III). In examining iron-related gene markers, microglia from male *Slc11a2* knockdown animals displayed upregulations in genes associated with iron export and homeostasis (i.e., *Slc40a1, Hfe*) and a significant decrease in LPS-induced *Fth1*. In preliminary gene expression analyses from whole-brain microglia in the *APP/PS1* females from Chapter IV, there was a significant decrease in *APP/PS1*-associated *Ftl1* expression in *Slc11a2* knockdown animals. This suggests a shared general effect of *Slc11a2* knockdown on decreasing iron storage marker ferritin in both models; however, the specific and divergent alterations in *Fth1* and *Ftl* in each model are of note. In acute and more severe inflammatory settings (e.g., LPS-induced inflammation), it may be that a rapid induction in cellular iron uptake requires pathways more actively involved in oxidizing incoming iron for safe and short-term cellular storage (i.e., an increase in *Fth* in the LPS model) [180, 330]. However, a significant upregulation in *Ftl1* in AD may reflect long-term cellular storage of iron involved in conditions of chronic inflammation and iron load [146, 164, 331]. Regardless, *Slc11a2* knockdown altered transcription of both *Fth1* in the LPS-induced inflammatory model and of *Ftl1* in the chronic *APP/PS1* model. While further work will examine other iron-related markers in the *APP/PS1* mice, it is intriguing to consider how *Slc11a2* knockdown differentially impacts iron-associated gene markers in an acute inflammatory model

versus a chronic model of disease. Additionally, future work will characterize broader gene expression changes (e.g., inflammatory and oxidative stress markers) in hippocampal-specific microglia from the female *APP/PS1* mice to assess transcriptional changes in a brain region relevant to the behavioral and cognitive changes observed in Chapter IV.

5.1.2 Sex differences in inflammation and Alzheimer's disease

The sex differences observed in both the LPS and *APP/PS1* models are especially noteworthy. In the acute model of LPS-induced inflammation, *Slc11a2* knockdown had a sex-specific effect on blunting inflammatory responses in male, but not female, mice. On the other hand, in the *APP/PS1* model, *Slc11a2* knockdown exerted significant effects on disease-associated parameters in female, but not male, mice (Fig. 5.1). Studies have shown significant sex differences in the LPS-induced response in young adult rodents, such that males typically display worsened sickness symptoms, enhanced inflammatory signaling, and more reactive microglia than females [224, 226, 266]. In fact, adult females overall demonstrate significant protection against infectious diseases compared to more-susceptible males [332, 333]. In our work, expression levels of female microglial *Slc11a2,* unlike in male microglia, remained unaltered in response to LPS, which may reflect the overall decreased sensitivity to and protection against inflammatory stimuli observed in young females. This suggests that a change in microglial *Slc11a2* during LPS-induced inflammation plays a prominent role in enhancing the male immune response to an acute inflammatory bout. Indeed, the significant effect of *Slc11a2* knockdown on blunting multiple inflammatory measures in the male animals supports this.

Interestingly, this sex difference in female protection against inflammatory and infectious disease appears to reverse in middle-age and onward, where females exhibit heightened sensitivity

to LPS compared to males [334, 335]. In chronic models of aging and neurodegenerative disease, females are also typically more affected than males, exhibiting increased inflammatory markers, more severe cognitive deficits, and more robust cellular dysfunction [225, 293]. Females are also in general significantly more likely to develop late-onset AD than males [311, 312]. Overall, previous work has shown that females experience a greater extent of chronic low-grade inflammation in late life than males, which may contribute to the greater likelihood for females of developing autoimmune diseases and age-related diseases of hyper-immune activation such as AD dementia [312, 332, 336, 337]. Thus, it is possible that the same mechanisms that protect females from infection and disease in young adulthood become sources of dysfunction and drivers of disease later in life.

Previous work suggests that sex-dependent changes, specifically in microglia during different stages of life, help drive this switch in disease susceptibility between males and females [225]. Similar to the gross differences in immune responses observed in males and females, microglia themselves display differential sensitivity to activation in males and females depending on the context. In response to an acute inflammatory stimulus, young males typically display higher microglia immunoreactivity, greater migratory capacity, and significantly greater pro-inflammatory gene expression compared to females [338-340]. My data correspond with this and additionally suggest that an upregulation in *Slc11a2* contributes to this heightened microglial inflammatory response in males. Conversely, work has shown that aged female microglia are significantly more pro-inflammatory and display more robust disease-associated phenotypes (i.e., increased expression of "DAM" genes, senescence, decreased phagocytic ability, significantly altered metabolism) compared to aged male cells [225, 341]. It may be that microglial *Slc11a2* plays a role in this sex difference in late life as well. As in the LPS model, my data in the *APP/PS1*

mice showed that female microglial *Slc11a2* remained unaltered in relation to the disease model, whereas microglial *Slc11a2* was significantly upregulated in *APP/PS1* males. While a resistance to increase microglial *Slc11a2* was associated with improved sickness behavior for females in the LPS model, it may be that the lack of a change in *Slc11a2* becomes a maladaptive microglial response in the context of age and disease. This may underlie in part why we observed significantly worse AD-associated impairments due to microglial *Slc11a2* knockdown in the *APP/PS1* middle-aged females, but not in the short-term acute LPS model. The exact mechanisms behind the female switch from a microglial protective phenotype in adulthood to an age-associated microglial type prone to disease and overactivity are still under investigation; however, hormonal changes associated with menopause in female mid-to-late life are likely a major contributor to the unique sensitivity older females display to age and disease-associated disruptions in microglial function [342-344]. Nonetheless, this work suggests that a sex difference in the regulation of microglial *Slc11a2* and associated iron-handling mechanisms plays a role in this divergent susceptibility to dysfunction for males and females during different stages of life.

5.1.3 Current understanding of microglial iron-handling in different contexts

5.1.3.1 Acute inflammation

In addition to elucidating sex-differential roles, the work in this dissertation further suggests disparate roles for microglial *Slc11a2* during acute inflammatory events in young adulthood and during chronic disease. Indeed, changes in *Slc11a2* may mirror changes in cellular iron uptake that have been known to occur in a differential manner in macrophages during acute inflammation or in microglia during chronic disease (the latter discussed in the following section **5.1.3.2**). In acute inflammatory settings, much work has been completed to understand the systemic iron-handling

response to short-lived viral or bacterial infection. As a form of nutritional immunity, peripheral macrophages rapidly import iron in conditions of pathogen invasion to limit systemic iron availability and prevent sustained pathogen growth and proliferation [182, 241, 345]. This cellular iron-related response has been shown to be critical for better prognosis and recovery, as individuals with high systemic iron load are significantly more prone to infection and disease [182, 346]. Inflammatory pathways activated in response to infection further stimulate this iron uptake [347], reinforcing the inflammatory-iron cellular pathway critical to host defense. Iron chelation in peripheral macrophages significantly inhibits cellular inflammation and cytokine production in response to LPS stimulation [182, 348] and macrophage DMT1 in particular is essential in mediating inflammatory responses necessary for survival during microbial infection [242, 349]. These data suggest that overall, DMT1 and macrophage iron-handling during acute peripheral inflammation is critically important.

Similar research on a role for cellular iron-handling during inflammation in the brain, however, has been historically lacking. Thus, my work suggests a novel role for microglial DMT1/*Slc11a2* during acute inflammation. Previous work has shown iron deposition in activated microglia during acute ischemic stroke [350] which then were shown to release these temporary iron stores to aid in tissue repair during post-stroke recovery [351, 352]. Furthermore, *in vitro* studies using inflammatory stimuli (i.e., LPS and Aβ) or pro-inflammatory cytokines involved in CNS injury (i.e., TNFα, IL-6) also demonstrate significant microglial iron retention [179, 353], similar to what is observed in peripheral macrophages during systemic infection. Indeed, *in vitro* studies of inflammatory stimulation demonstrate that microglia engage the same mechanisms as peripheral macrophages when encountering acute pro-inflammatory stimuli such as LPS or Aβ, such that they preferentially upregulate NTBI uptake via DMT1 [179, 180]. However, no work to

our knowledge had examined a role for microglial iron-handling mechanisms *in vivo* during an inflammatory bout of LPS. The data in this dissertation demonstrate a microglial upregulation in *Slc11a2* in response to acute inflammatory stimulation (LPS *in vivo* in Chapter III, Aβ in primary cells in Chapter IV). Importantly, the work in Chapter III suggests that this upregulation in DMT1/*Slc11a2* is a critical step in initiating the robust inflammatory response, at least in males. This is corroborated by *in vitro* experiments in Chapter IV, which showed that ebselen-mediated DMT1 inhibition profoundly decreases acute Aβ-induced inflammation in microglia. In fact, others have also shown that inhibition of DMT1 *in vitro* leads to a significant blunting of the microglial inflammatory response to an acute stimulus [185]. Our *in vivo* work thus lends credence to a primary role for iron uptake and DMT1/*Slc11a2* in mediating cellular responses in the context of short-term inflammation in the brain. Although our data is limited to gene expression analyses of *Slc11a2,* studies have shown that DMT1-mediated responses to acute inflammatory stress in the periphery can be largely IRE-independent [94, 354], suggesting that transcriptional mechanisms may be significantly involved in the observed effects on inflammation due to *Slc11a2* knockdown. Questions remain as to whether this anti-inflammatory effect of microglial *Slc11a2* knockdown shown in these studies would be beneficial or detrimental in the context of actual microbial infection in mice. Similar to work done in peripheral macrophages, do microglia require DMT1 to protect the brain against long-standing infection and subsequent death? It is intriguing to consider the parallels between microglial DMT1 and peripheral macrophage DMT1 during conditions of short-term inflammation.

5.1.3.2 Chronic neurodegenerative disease

In aging and during AD, microglial iron load has been more extensively studied in recent years. Iron storage markers *Fth* and *Ftl* consistently emerge as "DAM" markers of diseased and senescent

microglia in AD [133, 134, 171] and significant microglial iron load has been widely demonstrated in multiple models of neurodegenerative disease [50, 51, 146, 154, 176], which we also demonstrated (Fig. 1.7). In these settings, cellular iron load is thought to be a significant driver of disease, leading to excessive ROS production, inflammatory cytokine production, and cell death [172, 181]. In fact, a type of iron-dependent cell death called ferroptosis was described within the last two decades [162, 355]. Microglia are particularly susceptible to ferroptosis [273] and it has been recently shown that microglial iron loading and subsequent ferroptosis are central in initiating proximal neuronal cell death [161, 356]. However, the mechanisms behind microglial sensitivity to ferroptosis during age and disease are far from understood. It would be intriguing to examine a role for microglial DMT1 in mediating this ferroptotic susceptibility in neurodegenerative disease conditions. In this case, a microglial iron import system described earlier as likely situated to defend an organism during acute inflammatory settings may become detrimental in the context of excess iron load and chronic disease. Interestingly, however, my data in *Slc11a2* knockdown *APP/PS1* mice suggest that *Slc11a2* may instead be involved in a protective pathway during disease. Decreasing *Slc11a2* led to a worsening of AD-like phenotypes in females and an exacerbated hyperactive phenotype in male *APP/PS1* animals, suggesting a role for microglial *Slc11a2* in limiting cognitive deficit in this AD model. Although we hypothesized that inhibiting microglial *Slc11a2* would improve disease parameters based off an assumption that iron-loading mechanisms in microglia are generally detrimental, these results contribute to the ongoing debate related to the mechanisms by which iron exerts effects on microglial function in neurodegenerative disease [283]. For example, studies have shown that iron load increases neuroinflammation in a feed-forward loop of pro-inflammatory signaling and toxicity [166, 185, 217, 357], while others demonstrate a role for iron in dampening microglial inflammatory cytokine production and

exaggerating oxidative stress [167, 178]. Furthermore, ferritin positivity in microglia has been associated with protection against RNA oxidation and cellular dystrophy [327] and deletion of mitochondrial ferritin in an AD mouse model resulted in exacerbated disease symptoms [358]. My work suggests that microglial iron import mechanisms serve a protective response during early stages of disease, particularly in females. It is intriguing to surmise that the deleterious behavioral effects observed in female *Slc11a2* knockdown *APP/PS1* mice are due to the loss of a protective microglial iron import mechanism. This mechanism may be engaged in microglia during early stages of disease to limit availability of excess toxic, free iron in the brain parenchyma, which can significantly damage neurons that have lower capacity for iron storage [148, 149]. As *Slc11a2* was knocked down at an early stage of disease in the *APP/PS1* model in my studies, this may underlie why we observed a significant impairment in behavior and cognition in the females. Future work will assess iron content in cells from the knockdown mice to determine whether early *Slc11a2* knockdown altered cellular iron levels per se or whether the effect of *Slc11a2* knockdown on disease is independent of changes in total iron levels. In fact, it may be that *Slc11a2* knockdown changes the distribution (and not total levels) of iron in the cell, which could be detrimental or beneficial depending on the timing and context.

Additionally, this work also suggests a critical role for DMT1/*Slc11a2* in mediating inflammation, even in the absence of excess iron. The *in vitro* work in Chapter IV demonstrated that iron per se may not have a significant direct effect on Aβ-induced inflammatory cytokine expression or on DMT1/*Slc11a2* in IMG cells, and my *in vivo* work in Chapter III showed significant anti-inflammatory effects of *Slc11a2* knockdown without additional iron added. Based on these findings, it is intriguing to consider how *Slc11a2* knockdown during early disease pathology in the *APP/PS1* animals affected initial inflammatory signaling in microglia even before

excess iron accumulated. It may be that the detrimental effects of *Slc11a2* knockdown on behavior in the females are a result of a significant blunting of inflammation, which has been shown to be an important protective mechanism during initial periods of disease development [359-361]. A change in microglial DMT1/*Slc11a2* during pathological development thus may play a prominent role in mediating appropriate inflammatory responses to mitigate disease onset (purported roles summarized in Fig. 5.2). Future studies examining inflammatory markers in these cells will help elucidate whether this might be the case. Nonetheless, it is intriguing to consider the implications of these data on our understanding of microglial iron-handling mechanisms during chronic disease development.

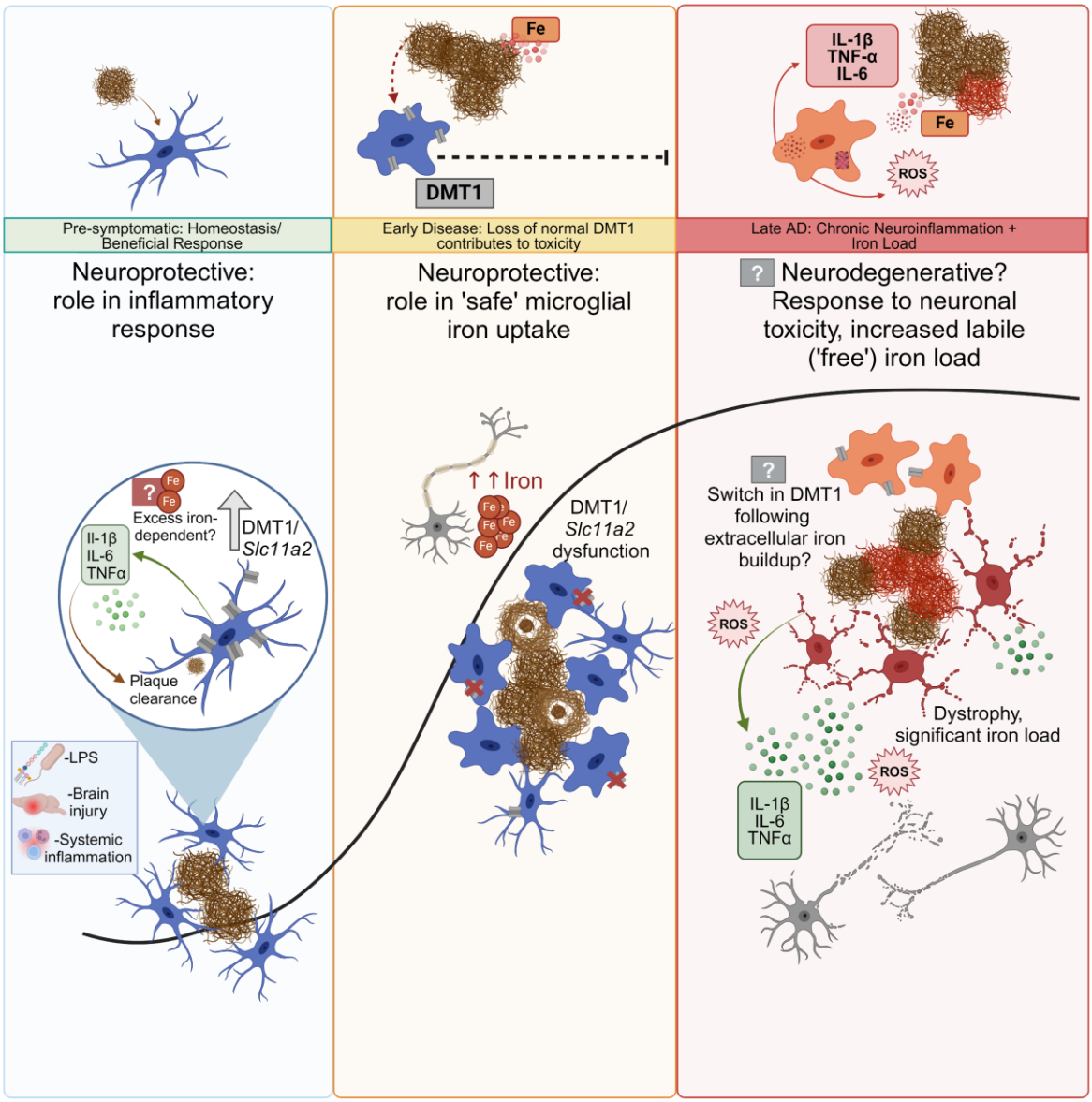

Figure 5.2. Purported role(s) for microglial DMT1 in health and disease development. During prodromal disease stages of initial Aβ plaque deposition and/or in response to the presence of AD risk factors (e.g., systemic inflammation, LPS neuroinflammation, brain injury), microglia engage acute inflammatory mechanisms to effectively remove Aβ plaques and return the tissue to homeostasis. In this setting, an upregulation in DMT1/*Slc11a2* may be a critical step to initiate early, neuroprotective inflammatory responses. As disease progresses (i.e., Aβ load increases, age-associated brain iron burden grows), microglial DMT1/*Slc11a2* may still play a protective role in mitigating the presence of free parenchymal iron, which can significantly damage neurons. Knockdown of *Slc11a2* thus results in acceleration into the next phase of disease. A role for DMT1/*Slc11a2* in late-stage disease was not explored in this work; however, *Slc11a2*/DMT1 may assume a detrimental role in importing an excessive iron load that ultimately results in microglial ROS production, inflammatory cytokine signaling, and cell death. This significantly contributes to neurodegeneration and the seemingly irreversible decline in disease at this late phase.
Figure made with BioRender.com, with permission.

5.1.4 Understanding and targeting microglial diversity in Alzheimer's disease

Although further understanding is needed as to how exactly microglial DMT1 contributes to or protects against disease, my work adds to the growing body of research demonstrating the nuanced nature of microglia in disease. Research over the past decade has highlighted the incredible diversity of microglial functions and phenotypes in the healthy and diseased brain [362-364]. The remarkable plasticity of microglia and their ability to adopt a wide range of phenotypes contributes to their capacity to play either protective or aggravating roles during disease development. This is likely why depletion of all microglia from the brain parenchyma in models of AD has resulted in disparate results – with some studies demonstrating improvement in disease [365, 366] and others demonstrating a significant worsening of disease parameters [360, 367]. These studies thus point to the need for targeted manipulation of specific microglial phenotypes and functions in disease. A subtype of microglia has been identified in aged and diseased brains, characterized primarily by markers of iron load, senescence, inflammatory signaling, and dystrophic morphology [146, 171, 284]. Indeed, it is thought that this group of microglia significantly contributes to disease severity [168], suggesting a potential cellular target for disease prevention. The work in my dissertation targeted a specific iron-related gene in microglia to determine whether this cellular function is associated with the detrimental contributions of microglial phenotypes in disease. The impairments observed due to *Slc11a2* knockdown in the *APP/PS1* females in my studies could suggest that 1) the iron loading phenotype reported in late-stage diseased microglia was initially a protective mechanism, as discussed above or 2) there is a specific time-dependency to the detrimental effect of microglial iron loading mechanisms, which become significantly deleterious towards late disease stages. Since *Slc11a2* was decreased at a prodromal stage of disease in these studies, it would be intriguing to consider a time point for DMT1/*Slc11a2* manipulation later in disease, when

pathology is more significant. Indeed, the data in Chapter III demonstrate that manipulating DMT1/*Slc11a2* significantly blunts short-term inflammation, which could serve a protective role in contexts where enhanced inflammatory signaling becomes disadvantageous (i.e., late in AD). My data thus suggest that initial changes in *Slc11a2* early in inflammatory disease are a beneficial mechanism to preserve downstream cognition. In concordance with previous work manipulating microglia in neurodegenerative disease, this work highlights the importance of considering timing, context, and functional specificity in devising treatments targeting microglia in disease.

5.1.5 Current developments in therapeutics to treat neurodegeneration

The work in my dissertation illuminates a pathway involved in disease that holds potential for therapeutic development. Unfortunately, AD remains an untreatable disease despite decades of effort by many groups around the world. For years, the only clinically-available therapeutics for AD were in the form of acetylcholinesterase inhibitors targeting cholinergic pathways; yet, these only served to mildly and temporarily improve quality of life if administered at the right time [368, 369]. Additionally, decades of clinical trials targeting Aβ deposition have consistently suggested little to no effect on cognition despite significant declines in plaque presence [370]. Following the controversial FDA approval of two recent anti-amyloid therapies, aducanumab and lecanemab, some have argued about the lack of evidence of clinically meaningful improvements in cognition in trial participants [20, 371]. Thus, much of the field has begun to examine alternative therapeutics targeting pathologies that occur in parallel with amyloid deposition. In recent years, therapeutic development of pharmaceuticals targeting neuroinflammation and brain iron metabolism have garnered substantial attention. However, studies have shown conflicting results and/or negligible effect on cognitive improvement thus far. For example, the anti-inflammatory compound

resveratrol was shown to effectively inhibit inflammation and reduce oxidative stress in treated patients [372], yet there was little effect on measures of cognition in a randomized clinical trial using the drug [373]. Furthermore, other trials targeting inflammatory pathways such as the use of the antibiotic minocycline [374] or non-steroidal anti-inflammatory drug (NSAID) ibuprofen [375] have shown lackluster results in effectively improving cognition [376]. On the other hand, studies have associated NSAID use with decreased incidence of AD [377], and two NSAIDs in particular (diclofenac and fenamate) have been suggested as potentially promising therapeutics that target microglial inflammation [378, 379]. As alluded to earlier, the efficacy of targeting inflammatory pathways during disease is likely highly dependent on time, context, and cell type specificity. My data highlight the nuanced mechanisms of microglial function during disease, suggesting that trials using systemic drugs such as minocycline or ibuprofen have likely failed in part due to the lack of specificity in target (i.e., microglia) or pathway (i.e., detrimental inflammatory pathways) engagement.

In clinical trials targeting iron-related pathways in neurodegeneration, results have also been conflicting [380]. In an initial trial in a small group of early Parkinson's disease patients, patients treated with iron chelator deferiprone exhibited a significant decrease in brain iron content associated with a slowing of motor-related indicators of disease progression [381]. However, in the follow-up multi-center clinical trial, iron chelation substantially worsened symptoms in patients with Parkinson's disease [382]. In patients with Huntington's disease, a clinical trial using iron chelator PBT2 demonstrated little effect on cognition as well [383]. In AD, rodent models suggest iron chelation as a promising avenue of treatment [121, 384, 385] and an initial phase II study in patients with early AD showed promising cognitive improvement following iron chelation treatment [386]. An ongoing clinical trial using deferiprone to treat dementia will further elucidate

the effects of iron chelation on disease progression (3D Study; ClinicalTrials.gov Identifier NCT03234686). However, it is again likely that a more precision approach to therapeutic development will be needed to effectively slow or prevent disease. Brain-wide removal of iron may result in a variety of undesired off-target effects [213] and the conflicting results observed in iron chelation trials conducted thus far are likely due to this lack of specificity in targeting a type of iron (ferrous versus ferric) and/or in targeting a certain cell type. My work exploring a specific mechanism involved in microglial iron handling aids in this ongoing search for a distinct pathway which could eventually be targeted to treat disease.

5.2 Limitations and caveats

Although my findings point to an important role for microglial *Slc11a2* in mediating short-term inflammation and contributing to behavioral deficits in the *APP/PS1* mice, there are several limitations to note. These include a lack of analysis of protein-level changes, iron levels and transport, and changes in the transport of other metals. First, much of our data is derived from gene-level analyses, which limits an understanding of protein-level changes in DMT1 in these studies. In regards to the known IRE-IRP system of DMT1 regulation, the work in this dissertation does not explicitly take into account post-transcriptional regulation of DMT1, which may alter protein levels in a manner that does not correspond to changes in gene expression per se. Indeed, technical challenges in collecting sufficient material from isolated microglia for a reliable Western blot signal of DMT1 significantly limited our ability to examine protein levels. Future work aims to troubleshoot various antibodies against DMT1 to determine if an antibody signal is strong enough despite low protein volumes from isolated cells. Nonetheless, others have pointed out non-IRE-dependent regulation of *Slc11a2* – particularly in the brain – suggesting the relevance of

changes in transcription as well [102, 328]. We also were unable to measure changes in iron transport and total iron levels in isolated cells due to significant limitations in ICP-MS sensitivity. Although this limits our interpretation of the results due to *Slc11a2* knockdown, it is intriguing to note (particularly in Chapter III), that *Slc11a2* knockdown was associated with significant changes in several other iron-related genes, such as *Fth1, Tfrc, Cd163, Hfe, Hamp,* and *Slc40a1,* implying a change in cellular iron content or distribution. Future directions aimed at measuring cellular iron levels using different techniques are discussed in the next section **5.3**. DMT1 also transports a variety of other divalent metals, suggesting there may be changes in manganese, zinc, and/or copper levels in these cells, which contribute to the observed phenotypes. It is important to note, however, that iron is the most abundant transition metal in the brain, suggesting a primary role for iron transport via DMT1.

There are also a few caveats worth mentioning about the animal models used in my studies. Both the LPS inflammatory model and the *APP/PS1* mouse line are insufficient models to recapitulate the complexity of human disease. Indeed, there is ongoing work in the field to generate a mouse model which more fully mimics AD phenotypes observed in human patients [387] (i.e., MODEL-AD consortium). The use of an Aβ-driven model confines my results to an understanding of amyloid-related pathology and does not directly consider the relationship between iron-related pathology and tau deposition and/or the additional effects of genetic risk factors (i.e., *APOE*, *TREM2* mutations). However, my findings add to our knowledge of the known associations between amyloid pathology and iron toxicity [52] and suggest that iron-targeted treatment, alongside the developed anti-amyloid therapies, could be a promising therapeutic direction to pursue. Lastly, caution must be applied to deriving conclusions from the bulk RNA analysis of microglial gene expression in Chapters III (sequencing) and IV (RT-qPCR). As discussed in

section 5.1.4, microglia are remarkably heterogenous in transcriptional profiles, phenotypes, and functions and this cellular resolution is lost in bulk samples of microglial cells. Future directions related to these limitations are discussed in the following section.

5.3 Future directions

There is a plethora of remaining questions following the results of my dissertation work. There was a significant worsening of downstream disease parameters in middle-aged female mice when *Slc11a2* was knocked down at an early stage of disease during initial plaque deposition. It is curious to consider a later time point of *Slc11a2* manipulation and whether this would have an opposing effect on disease measures (i.e., improved disease in late stages). Furthermore, a later time point of behavioral assessment is a possible future direction. In the studies reported in this dissertation, there was a significant deficit in MWM and fear conditioned memory in female *Slc11a2* knockdown animals between 12-15 months of age, but do these behavioral impairments plateau at this age or continue to worsen dramatically as the disease progresses? The mice in these studies are considered 'middle-aged,' thus, would aged mice perform even worse on the cognitive tasks? Would aging in these mice also reveal a significant cognitive deficit in *Slc11a2* knockdown males?

Future directions also include assessment of DMT1 protein levels and iron content in knockdown cells. I am currently pursuing two separate avenues for the measurement of cellular iron. A hybrid isotope imaging mass spectrometry (MIMS) electron microscopy (MIMS-EM) analysis will be utilized in isolated microglial cells to assess subcellular iron distribution [388]. Additionally, work is ongoing with the Vanderbilt Neurovisualization Core to assess ferritin deposition in microglia in whole-brain images of cleared brains from knockdown female animals. As mentioned above, I am also pursuing the use of different antibodies against DMT1 to conduct

Western blot-level analysis of transporter protein expression. Lastly, I plan to conduct RNAseq analyses on isolated hippocampal microglia from female *Slc11a2* knockdown *APP/PS1* animals to determine global changes in the transcriptome (e.g., inflammatory, oxidative, iron-related, "DAM" markers) of knockdown cells in the AD model.

Outside of these ongoing future directions, these data lend fuel for a variety of additional research directions. An overexpression model of DMT1 would be interesting to explore to determine whether microglial DMT1 can be protective in chronic disease. Related to the multiplicity of DMT1-mediated divalent metal transport, it would be intriguing to examine whether this overexpression of DMT1 results in increased import of non-iron metal ions as well (i.e., Mn^{2+}, Cu^{2+}, Co^{2+}, Zn^{2+}). These other non-Fe divalent metals have also been implicated in AD [389]; thus, it would be interesting to determine a role for DMT1 in mediating increased uptake of these ions and the effect on disease. The burgeoning study of ferroptosis also holds tremendous potential for further study [390]. The importance of microglial ferroptosis has recently been appreciated, yet a role for microglial DMT1 in mediating ferroptosis has not been explored and would be a novel and compelling future direction. Can DMT1 be targeted to prevent ferroptosis in microglia at certain stages of AD? Additionally, in this area, few studies have further examined sex differences in cellular ferroptotic susceptibility. Are there sex differences in microglial ferroptosis and could this be mediated in part by DMT1/*Slc11a2*? Considering the known profound sex differences related to AD risk, exploring sex differences in microglial function, iron regulation, and ferroptosis are critical future avenues to understand the mechanisms that drive disease.

5.4 Summary

In conclusion, my work showed that knockdown of iron import gene, *Slc11a2*, improved male-specific sickness behavior following LPS treatment and exacerbated female hyperactivity and memory deficits in the *APP/PS1* model of AD. This was associated with decreased cellular iron import and storage markers and a blunted inflammatory response in the LPS model. The disparate results between the two models are suggestive of time-, context-, and sex-dependent roles for microglial *Slc11a2 in vivo.* Overall, this work adds to our understanding of the complex mechanisms that drive AD and the intricate interplay between cellular iron-handling mechanisms and inflammation. Ultimately, this work aids in the continual search for a successful AD therapeutic to treat this debilitating neurological disease.

BIBLIOGRAPHY

1. Winn, N.C., K.M. Volk, and A.H. Hasty, *Regulation of tissue iron homeostasis: the macrophage "ferrostat".* JCI Insight, 2020. **5**(2).
2. Sfera, A., et al., *Rusty Microglia: Trainers of Innate Immunity in Alzheimer's Disease.* Front Neurol, 2018. **9**: p. 1062.
3. Yokoyama, M., et al., *Mouse Models of Alzheimer's Disease.* Front Mol Neurosci, 2022. **15**: p. 912995.
4. Ennerfelt, H.E. and J.R. Lukens, *The role of innate immunity in Alzheimer's disease.* Immunol Rev, 2020. **297**(1): p. 225-246.
5. Rajan, K.B., et al., *Population estimate of people with clinical Alzheimer's disease and mild cognitive impairment in the United States (2020-2060).* Alzheimers Dement, 2021. **17**(12): p. 1966-1975.
6. Gustavsson, A., et al., *Global estimates on the number of persons across the Alzheimer's disease continuum.* Alzheimers Dement, 2023. **19**(2): p. 658-670.
7. Association, A.s., *2023 Alzheimer's disease facts and figures.* Alzheimers Dement, 2023. **19**(4): p. 1598-1695.
8. Taylor, C.A., et al., *Deaths from Alzheimer's Disease - United States, 1999-2014.* MMWR Morb Mortal Wkly Rep, 2017. **66**(20): p. 521-526.
9. Perl, D.P., *Neuropathology of Alzheimer's disease.* Mt Sinai J Med, 2010. **77**(1): p. 32-42.
10. Ingelsson, M., et al., *Early Abeta accumulation and progressive synaptic loss, gliosis, and tangle formation in AD brain.* Neurology, 2004. **62**(6): p. 925-31.
11. Serrano-Pozo, A., et al., *Neuropathological alterations in Alzheimer disease.* Cold Spring Harb Perspect Med, 2011. **1**(1): p. a006189.
12. Selkoe, D.J. and J. Hardy, *The amyloid hypothesis of Alzheimer's disease at 25 years.* EMBO Mol Med, 2016. **8**(6): p. 595-608.
13. Kepp, K.P., et al., *The amyloid cascade hypothesis: an updated critical review.* Brain, 2023. **146**(10): p. 3969-3990.
14. Makin, S., *The amyloid hypothesis on trial.* Nature, 2018. **559**(7715): p. S4-S7.
15. Bennett, D.A., et al., *Neuropathology of older persons without cognitive impairment from two community-based studies.* Neurology, 2006. **66**(12): p. 1837-44.
16. Aizenstein, H.J., et al., *Frequent amyloid deposition without significant cognitive impairment among the elderly.* Arch Neurol, 2008. **65**(11): p. 1509-17.
17. Giannakopoulos, P., et al., *Tangle and neuron numbers, but not amyloid load, predict cognitive status in Alzheimer's disease.* Neurology, 2003. **60**(9): p. 1495-500.
18. Wolf, D.S., et al., *Progression of regional neuropathology in Alzheimer disease and normal elderly: findings from the Nun study.* Alzheimer Dis Assoc Disord, 1999. **13**(4): p. 226-31.
19. Beker, N., et al., *Association of Cognitive Function Trajectories in Centenarians With Postmortem Neuropathology, Physical Health, and Other Risk Factors for Cognitive Decline.* JAMA Netw Open, 2021. **4**(1): p. e2031654.
20. Knopman, D.S., D.T. Jones, and M.D. Greicius, *Failure to demonstrate efficacy of aducanumab: An analysis of the EMERGE and ENGAGE trials as reported by Biogen, December 2019.* Alzheimers Dement, 2021. **17**(4): p. 696-701.
21. Musiek, E.S., T. Gomez-Isla, and D.M. Holtzman, *Aducanumab for Alzheimer disease: the amyloid hypothesis moves from bench to bedside.* J Clin Invest, 2021. **131**(20).
22. Zhang, Y., et al., *Amyloid beta-based therapy for Alzheimer's disease: challenges, successes and future.* Signal Transduct Target Ther, 2023. **8**(1): p. 248.
23. Marucci, G., et al., *Efficacy of acetylcholinesterase inhibitors in Alzheimer's disease.* Neuropharmacology, 2021. **190**: p. 108352.

24. Targa Dias Anastacio, H., N. Matosin, and L. Ooi, *Neuronal hyperexcitability in Alzheimer's disease: what are the drivers behind this aberrant phenotype?* Transl Psychiatry, 2022. **12**(1): p. 257.
25. Siskova, Z., et al., *Dendritic structural degeneration is functionally linked to cellular hyperexcitability in a mouse model of Alzheimer's disease.* Neuron, 2014. **84**(5): p. 1023-33.
26. Vossel, K.A., et al., *Epileptic activity in Alzheimer's disease: causes and clinical relevance.* Lancet Neurol, 2017. **16**(4): p. 311-322.
27. Bezprozvanny, I. and M.P. Mattson, *Neuronal calcium mishandling and the pathogenesis of Alzheimer's disease.* Trends Neurosci, 2008. **31**(9): p. 454-63.
28. Wang, R. and P.H. Reddy, *Role of Glutamate and NMDA Receptors in Alzheimer's Disease.* J Alzheimers Dis, 2017. **57**(4): p. 1041-1048.
29. Nixon, R.A., A.M. Cataldo, and P.M. Mathews, *The endosomal-lysosomal system of neurons in Alzheimer's disease pathogenesis: a review.* Neurochem Res, 2000. **25**(9-10): p. 1161-72.
30. Hung, C. and F.J. Livesey, *Endolysosome and autophagy dysfunction in Alzheimer disease.* Autophagy, 2021. **17**(11): p. 3882-3883.
31. Szabo, M.P., et al., *The role of Alzheimer's disease risk genes in endolysosomal pathways.* Neurobiol Dis, 2022. **162**: p. 105576.
32. Leyns, C.E.G. and D.M. Holtzman, *Glial contributions to neurodegeneration in tauopathies.* Mol Neurodegener, 2017. **12**(1): p. 50.
33. Taddei, R.N., et al., *Changes in glial cell phenotypes precede overt neurofibrillary tangle formation, correlate with markers of cortical cell damage, and predict cognitive status of individuals at Braak III-IV stages.* Acta Neuropathol Commun, 2022. **10**(1): p. 72.
34. Gonzalez-Reyes, R.E., et al., *Involvement of Astrocytes in Alzheimer's Disease from a Neuroinflammatory and Oxidative Stress Perspective.* Front Mol Neurosci, 2017. **10**: p. 427.
35. Habib, N., et al., *Disease-associated astrocytes in Alzheimer's disease and aging.* Nat Neurosci, 2020. **23**(6): p. 701-706.
36. Lee, H.G., M.A. Wheeler, and F.J. Quintana, *Function and therapeutic value of astrocytes in neurological diseases.* Nat Rev Drug Discov, 2022. **21**(5): p. 339-358.
37. Kenigsbuch, M., et al., *A shared disease-associated oligodendrocyte signature among multiple CNS pathologies.* Nat Neurosci, 2022. **25**(7): p. 876-886.
38. Sun, N., et al., *Single-nucleus multiregion transcriptomic analysis of brain vasculature in Alzheimer's disease.* Nat Neurosci, 2023. **26**(6): p. 970-982.
39. Jankowsky, J.L. and H. Zheng, *Practical considerations for choosing a mouse model of Alzheimer's disease.* Mol Neurodegener, 2017. **12**(1): p. 89.
40. Haass, C., et al., *The Swedish mutation causes early-onset Alzheimer's disease by beta-secretase cleavage within the secretory pathway.* Nat Med, 1995. **1**(12): p. 1291-6.
41. Kelleher, R.J., 3rd and J. Shen, *Presenilin-1 mutations and Alzheimer's disease.* Proc Natl Acad Sci U S A, 2017. **114**(4): p. 629-631.
42. Jankowsky, J.L., et al., *Mutant presenilins specifically elevate the levels of the 42 residue beta-amyloid peptide in vivo: evidence for augmentation of a 42-specific gamma secretase.* Hum Mol Genet, 2004. **13**(2): p. 159-70.
43. Jankowsky, J.L., et al., *APP processing and amyloid deposition in mice haplo-insufficient for presenilin 1.* Neurobiol Aging, 2004. **25**(7): p. 885-92.
44. Borchelt, D.R., et al., *Accelerated amyloid deposition in the brains of transgenic mice coexpressing mutant presenilin 1 and amyloid precursor proteins.* Neuron, 1997. **19**(4): p. 939-45.
45. Forner, S., et al., *Systematic phenotyping and characterization of the 5xFAD mouse model of Alzheimer's disease.* Sci Data, 2021. **8**(1): p. 270.
46. AlzForum, *Research Models.* n.d.
47. Hulshof, L.A., et al., *Both male and female APPswe/PSEN1dE9 mice are impaired in spatial memory and cognitive flexibility at 9 months of age.* Neurobiol Aging, 2022. **113**: p. 28-38.

48. Gallagher, J.J., A.M. Minogue, and M.A. Lynch, *Impaired performance of female APP/PS1 mice in the Morris water maze is coupled with increased Abeta accumulation and microglial activation.* Neurodegener Dis, 2013. **11**(1): p. 33-41.
49. Mifflin, M.A., et al., *Sex differences in the IntelliCage and the Morris water maze in the APP/PS1 mouse model of amyloidosis.* Neurobiol Aging, 2021. **101**: p. 130-140.
50. McIntosh, A., et al., *Iron accumulation in microglia triggers a cascade of events that leads to altered metabolism and compromised function in APP/PS1 mice.* Brain Pathol, 2019. **29**(5): p. 606-621.
51. Holland, R., et al., *Inflammatory microglia are glycolytic and iron retentive and typify the microglia in APP/PS1 mice.* Brain Behav Immun, 2018. **68**: p. 183-196.
52. Peters, D.G., J.R. Connor, and M.D. Meadowcroft, *The relationship between iron dyshomeostasis and amyloidogenesis in Alzheimer's disease: Two sides of the same coin.* Neurobiol Dis, 2015. **81**: p. 49-65.
53. Nazem, A., et al., *Rodent models of neuroinflammation for Alzheimer's disease.* J Neuroinflammation, 2015. **12**: p. 74.
54. Zhao, J., et al., *Neuroinflammation induced by lipopolysaccharide causes cognitive impairment in mice.* Sci Rep, 2019. **9**(1): p. 5790.
55. Liu, Y., et al., *Beta-amyloid activates NLRP3 inflammasome via TLR4 in mouse microglia.* Neurosci Lett, 2020. **736**: p. 135279.
56. Sheppard, O., M.P. Coleman, and C.S. Durrant, *Lipopolysaccharide-induced neuroinflammation induces presynaptic disruption through a direct action on brain tissue involving microglia-derived interleukin 1 beta.* J Neuroinflammation, 2019. **16**(1): p. 106.
57. Jung, H., et al., *LPS induces microglial activation and GABAergic synaptic deficits in the hippocampus accompanied by prolonged cognitive impairment.* Sci Rep, 2023. **13**(1): p. 6547.
58. Kim, H.S., et al., *Gram-negative bacteria and their lipopolysaccharides in Alzheimer's disease: pathologic roles and therapeutic implications.* Transl Neurodegener, 2021. **10**(1): p. 49.
59. Batista, C.R.A., et al., *Lipopolysaccharide-Induced Neuroinflammation as a Bridge to Understand Neurodegeneration.* Int J Mol Sci, 2019. **20**(9).
60. Lane, D.J.R., S. Ayton, and A.I. Bush, *Iron and Alzheimer's Disease: An Update on Emerging Mechanisms.* J Alzheimers Dis, 2018. **64**(s1): p. S379-S395.
61. Bush, A.I., *The metal theory of Alzheimer's disease.* J Alzheimers Dis, 2013. **33 Suppl 1**: p. S277-81.
62. Kenkhuis, B., A.I. Bush, and S. Ayton, *How iron can drive neurodegeneration.* Trends Neurosci, 2023. **46**(5): p. 333-335.
63. Chifman, J., R. Laubenbacher, and S.V. Torti, *A systems biology approach to iron metabolism.* Adv Exp Med Biol, 2014. **844**: p. 201-25.
64. Zhao, Z., *Iron and oxidizing species in oxidative stress and Alzheimer's disease.* Aging Med (Milton), 2019. **2**(2): p. 82-87.
65. Fleming, R.E. and P. Ponka, *Iron overload in human disease.* N Engl J Med, 2012. **366**(4): p. 348-59.
66. Levy, J.E., et al., *Transferrin receptor is necessary for development of erythrocytes and the nervous system.* Nat Genet, 1999. **21**(4): p. 396-9.
67. Park, C.H., et al., *Hepcidin, a urinary antimicrobial peptide synthesized in the liver.* J Biol Chem, 2001. **276**(11): p. 7806-10.
68. Soares, M.P. and I. Hamza, *Macrophages and Iron Metabolism.* Immunity, 2016. **44**(3): p. 492-504.
69. Recalcati, S. and G. Cairo, *Macrophages and Iron: A Special Relationship.* Biomedicines, 2021. **9**(11).
70. Nairz, M., et al., *"Pumping iron"-how macrophages handle iron at the systemic, microenvironmental, and cellular levels.* Pflugers Arch, 2017. **469**(3-4): p. 397-418.

71. Byrnes, V., et al., *Increased duodenal DMT-1 expression and unchanged HFE mRNA levels in HFE-associated hereditary hemochromatosis and iron deficiency.* Blood Cells Mol Dis, 2002. **29**(3): p. 251-60.
72. Tong, X., H. Kawabata, and H.P. Koeffler, *Iron deficiency can upregulate expression of transferrin receptor at both the mRNA and protein level.* Br J Haematol, 2002. **116**(2): p. 458-64.
73. Pantopoulos, K., *Iron metabolism and the IRE/IRP regulatory system: an update.* Ann N Y Acad Sci, 2004. **1012**: p. 1-13.
74. Mullner, E.W., B. Neupert, and L.C. Kuhn, *A specific mRNA binding factor regulates the iron-dependent stability of cytoplasmic transferrin receptor mRNA.* Cell, 1989. **58**(2): p. 373-82.
75. Gray, N.K. and M.W. Hentze, *Iron regulatory protein prevents binding of the 43S translation pre-initiation complex to ferritin and eALAS mRNAs.* EMBO J, 1994. **13**(16): p. 3882-91.
76. Brissot, P., et al., *Non-transferrin bound iron: a key role in iron overload and iron toxicity.* Biochim Biophys Acta, 2012. **1820**(3): p. 403-10.
77. Czachorowski, M., et al., *Transmembrane topology of the mammalian Slc11a2 iron transporter.* Biochemistry, 2009. **48**(35): p. 8422-34.
78. Gunshin, H., et al., *Cloning and characterization of a mammalian proton-coupled metal-ion transporter.* Nature, 1997. **388**(6641): p. 482-8.
79. Shawki, A., et al., *H(+)-coupled divalent metal-ion transporter-1: functional properties, physiological roles and therapeutics.* Curr Top Membr, 2012. **70**: p. 169-214.
80. Illing, A.C., et al., *Substrate profile and metal-ion selectivity of human divalent metal-ion transporter-1.* J Biol Chem, 2012. **287**(36): p. 30485-96.
81. Shawki, A., et al., *Intestinal DMT1 is critical for iron absorption in the mouse but is not required for the absorption of copper or manganese.* Am J Physiol Gastrointest Liver Physiol, 2015. **309**(8): p. G635-47.
82. Fleming, M.D., et al., *Microcytic anaemia mice have a mutation in Nramp2, a candidate iron transporter gene.* Nat Genet, 1997. **16**(4): p. 383-6.
83. Su, M.A., et al., *The G185R mutation disrupts function of the iron transporter Nramp2.* Blood, 1998. **92**(6): p. 2157-63.
84. Tolone, C., et al., *The DMT1 IVS4+44C>A polymorphism and the risk of iron deficiency anemia in children with celiac disease.* PLoS One, 2017. **12**(10): p. e0185822.
85. Priwitzerova, M., et al., *Functional consequences of the human DMT1 (SLC11A2) mutation on protein expression and iron uptake.* Blood, 2005. **106**(12): p. 3985-7.
86. Bell, S., et al., *A genome-wide meta-analysis yields 46 new loci associating with biomarkers of iron homeostasis.* Commun Biol, 2021. **4**(1): p. 156.
87. Jing, X., et al., *Iron Overload Is Associated With Accelerated Progression of Osteoarthritis: The Role of DMT1 Mediated Iron Homeostasis.* Front Cell Dev Biol, 2020. **8**: p. 594509.
88. Brewer, C.J., R.I. Wood, and J.C. Wood, *mRNA regulation of cardiac iron transporters and ferritin subunits in a mouse model of iron overload.* Exp Hematol, 2014. **42**(12): p. 1059-67.
89. Rhee, J.W., et al., *Modeling Secondary Iron Overload Cardiomyopathy with Human Induced Pluripotent Stem Cell-Derived Cardiomyocytes.* Cell Rep, 2020. **32**(2): p. 107886.
90. Pietrangelo, A., *Hereditary hemochromatosis: pathogenesis, diagnosis, and treatment.* Gastroenterology, 2010. **139**(2): p. 393-408, 408 e1-2.
91. Fan, Y., et al., *Site-specific intestinal DMT1 silencing to mitigate iron absorption using pH-sensitive multi-compartmental nanoparticulate oral delivery system.* Nanomedicine, 2019. **22**: p. 102091.
92. Gunshin, H., et al., *Slc11a2 is required for intestinal iron absorption and erythropoiesis but dispensable in placenta and liver.* J Clin Invest, 2005. **115**(5): p. 1258-66.
93. Wu, W., et al., *Divalent metal-ion transporter 1 is decreased in intestinal epithelial cells and contributes to the anemia in inflammatory bowel disease.* Sci Rep, 2015. **5**: p. 16344.
94. Tybl, E., et al., *Control of Systemic Iron Homeostasis by the 3′ Iron-Responsive Element of Divalent Metal Transporter 1 in Mice.* Hemasphere, 2020. **4**(5): p. e459.

95. Carlson, E.S., et al., *Iron is essential for neuron development and memory function in mouse hippocampus.* J Nutr, 2009. **139**(4): p. 672-9.
96. Cheli, V.T., et al., *The Divalent Metal Transporter 1 (DMT1) Is Required for Iron Uptake and Normal Development of Oligodendrocyte Progenitor Cells.* J Neurosci, 2018. **38**(43): p. 9142-9159.
97. Erikson, K.M. and M. Aschner, *Increased manganese uptake by primary astrocyte cultures with altered iron status is mediated primarily by divalent metal transporter.* Neurotoxicology, 2006. **27**(1): p. 125-30.
98. Zhang, Y., et al., *An RNA-sequencing transcriptome and splicing database of glia, neurons, and vascular cells of the cerebral cortex.* J Neurosci, 2014. **34**(36): p. 11929-47.
99. Ingrassia, R., B. Garavaglia, and M. Memo, *DMT1 Expression and Iron Levels at the Crossroads Between Aging and Neurodegeneration.* Front Neurosci, 2019. **13**: p. 575.
100. Salazar, J., et al., *Divalent metal transporter 1 (DMT1) contributes to neurodegeneration in animal models of Parkinson's disease.* Proc Natl Acad Sci U S A, 2008. **105**(47): p. 18578-83.
101. Zheng, W., et al., *Divalent metal transporter 1 is involved in amyloid precursor protein processing and Abeta generation.* FASEB J, 2009. **23**(12): p. 4207-17.
102. Ingrassia, R., et al., *1B/(-)IRE DMT1 expression during brain ischemia contributes to cell death mediated by NF-kappaB/RelA acetylation at Lys310.* PLoS One, 2012. **7**(5): p. e38019.
103. Du, L., et al., *Increased Iron Deposition on Brain Quantitative Susceptibility Mapping Correlates with Decreased Cognitive Function in Alzheimer's Disease.* ACS Chem Neurosci, 2018. **9**(7): p. 1849-1857.
104. Connor, J.R., et al., *Regional distribution of iron and iron-regulatory proteins in the brain in aging and Alzheimer's disease.* J Neurosci Res, 1992. **31**(2): p. 327-35.
105. Leskovjan, A.C., et al., *Increased brain iron coincides with early plaque formation in a mouse model of Alzheimer's disease.* Neuroimage, 2011. **55**(1): p. 32-8.
106. Meadowcroft, M.D., et al., *MRI and histological analysis of beta-amyloid plaques in both human Alzheimer's disease and APP/PS1 transgenic mice.* J Magn Reson Imaging, 2009. **29**(5): p. 997-1007.
107. Everett, J., et al., *Nanoscale synchrotron X-ray speciation of iron and calcium compounds in amyloid plaque cores from Alzheimer's disease subjects.* Nanoscale, 2018. **10**(25): p. 11782-11796.
108. Liu, B., et al., *Iron promotes the toxicity of amyloid beta peptide by impeding its ordered aggregation.* J Biol Chem, 2011. **286**(6): p. 4248-56.
109. Rottkamp, C.A., et al., *Redox-active iron mediates amyloid-beta toxicity.* Free Radic Biol Med, 2001. **30**(4): p. 447-50.
110. Becerril-Ortega, J., et al., *Iron overload accelerates neuronal amyloid-beta production and cognitive impairment in transgenic mice model of Alzheimer's disease.* Neurobiol Aging, 2014. **35**(10): p. 2288-301.
111. Ward, R.J., et al., *The role of iron in brain ageing and neurodegenerative disorders.* Lancet Neurol, 2014. **13**(10): p. 1045-60.
112. Hogarth, P., *Neurodegeneration with brain iron accumulation: diagnosis and management.* J Mov Disord, 2015. **8**(1): p. 1-13.
113. Zhou, Z.D. and E.K. Tan, *Iron regulatory protein (IRP)-iron responsive element (IRE) signaling pathway in human neurodegenerative diseases.* Mol Neurodegener, 2017. **12**(1): p. 75.
114. Cho, H.H., et al., *Selective translational control of the Alzheimer amyloid precursor protein transcript by iron regulatory protein-1.* J Biol Chem, 2010. **285**(41): p. 31217-32.
115. Telling, N.D., et al., *Iron Biochemistry is Correlated with Amyloid Plaque Morphology in an Established Mouse Model of Alzheimer's Disease.* Cell Chem Biol, 2017. **24**(10): p. 1205-1215 e3.
116. Ayton, S., et al., *Ferritin levels in the cerebrospinal fluid predict Alzheimer's disease outcomes and are regulated by APOE.* Nat Commun, 2015. **6**: p. 6760.

117. Ayton, S., et al., *Brain iron is associated with accelerated cognitive decline in people with Alzheimer pathology.* Mol Psychiatry, 2020. **25**(11): p. 2932-2941.
118. Ayton, S., et al., *Regional brain iron associated with deterioration in Alzheimer's disease: A large cohort study and theoretical significance.* Alzheimers Dement, 2021. **17**(7): p. 1244-1256.
119. Smith, M.A., et al., *Increased iron and free radical generation in preclinical Alzheimer disease and mild cognitive impairment.* J Alzheimers Dis, 2010. **19**(1): p. 363-72.
120. Ghadery, C., et al., *R2* mapping for brain iron: associations with cognition in normal aging.* Neurobiol Aging, 2015. **36**(2): p. 925-32.
121. Xiao, Y., et al., *Iron Chelation Remits Memory Deficits Caused by the High-Fat Diet in a Mouse Model of Alzheimer's Disease.* J Alzheimers Dis, 2022. **86**(4): p. 1959-1971.
122. Lee, J.Y., et al., *The lipophilic metal chelator DP-109 reduces amyloid pathology in brains of human beta-amyloid precursor protein transgenic mice.* Neurobiol Aging, 2004. **25**(10): p. 1315-21.
123. Li, Q. and B.A. Barres, *Microglia and macrophages in brain homeostasis and disease.* Nat Rev Immunol, 2018. **18**(4): p. 225-242.
124. Salter, M.W. and B. Stevens, *Microglia emerge as central players in brain disease.* Nat Med, 2017. **23**(9): p. 1018-1027.
125. Morrison, V., et al., *Jedi-1/MEGF12-mediated phagocytosis controls the pro-neurogenic properties of microglia in the ventricular-subventricular zone.* Cell Rep, 2023. **42**(11): p. 113423.
126. Colonna, M. and O. Butovsky, *Microglia Function in the Central Nervous System During Health and Neurodegeneration.* Annu Rev Immunol, 2017. **35**: p. 441-468.
127. Hansen, D.V., J.E. Hanson, and M. Sheng, *Microglia in Alzheimer's disease.* J Cell Biol, 2018. **217**(2): p. 459-472.
128. Hemonnot, A.L., et al., *Microglia in Alzheimer Disease: Well-Known Targets and New Opportunities.* Front Aging Neurosci, 2019. **11**: p. 233.
129. Hickman, S., et al., *Microglia in neurodegeneration.* Nat Neurosci, 2018. **21**(10): p. 1359-1369.
130. Heneka, M.T., et al., *Neuroinflammation in Alzheimer's disease.* Lancet Neurol, 2015. **14**(4): p. 388-405.
131. Liddelow, S.A., et al., *Neurotoxic reactive astrocytes are induced by activated microglia.* Nature, 2017. **541**(7638): p. 481-487.
132. Park, J.S., et al., *Blocking microglial activation of reactive astrocytes is neuroprotective in models of Alzheimer's disease.* Acta Neuropathol Commun, 2021. **9**(1): p. 78.
133. Keren-Shaul, H., et al., *A Unique Microglia Type Associated with Restricting Development of Alzheimer's Disease.* Cell, 2017. **169**(7): p. 1276-1290 e17.
134. Mathys, H., et al., *Single-cell transcriptomic analysis of Alzheimer's disease.* Nature, 2019. **570**(7761): p. 332-337.
135. Sobue, A., et al., *Microglial gene signature reveals loss of homeostatic microglia associated with neurodegeneration of Alzheimer's disease.* Acta Neuropathol Commun, 2021. **9**(1): p. 1.
136. Lee, C.Y.D., et al., *Elevated TREM2 Gene Dosage Reprograms Microglia Responsivity and Ameliorates Pathological Phenotypes in Alzheimer's Disease Models.* Neuron, 2018. **97**(5): p. 1032-1048 e5.
137. Krasemann, S., et al., *The TREM2-APOE Pathway Drives the Transcriptional Phenotype of Dysfunctional Microglia in Neurodegenerative Diseases.* Immunity, 2017. **47**(3): p. 566-581 e9.
138. Grubman, A., et al., *Transcriptional signature in microglia associated with Abeta plaque phagocytosis.* Nat Commun, 2021. **12**(1): p. 3015.
139. Chen, W.T., et al., *Spatial Transcriptomics and In Situ Sequencing to Study Alzheimer's Disease.* Cell, 2020. **182**(4): p. 976-991 e19.
140. Jung, E.S., et al., *Amyloid-beta activates NLRP3 inflammasomes by affecting microglial immunometabolism through the Syk-AMPK pathway.* Aging Cell, 2022. **21**(5): p. e13623.
141. Wang, Y., et al., *TREM2 lipid sensing sustains the microglial response in an Alzheimer's disease model.* Cell, 2015. **160**(6): p. 1061-71.

142. Ulrich, J.D., et al., *Altered microglial response to Abeta plaques in APPPS1-21 mice heterozygous for TREM2.* Mol Neurodegener, 2014. **9**: p. 20.
143. Cai, Y., et al., *Microglia in the Neuroinflammatory Pathogenesis of Alzheimer's Disease and Related Therapeutic Targets.* Front Immunol, 2022. **13**: p. 856376.
144. Baik, S.H., et al., *Microglia contributes to plaque growth by cell death due to uptake of amyloid beta in the brain of Alzheimer's disease mouse model.* Glia, 2016. **64**(12): p. 2274-2290.
145. Mathys, H., et al., *Temporal Tracking of Microglia Activation in Neurodegeneration at Single-Cell Resolution.* Cell Rep, 2017. **21**(2): p. 366-380.
146. Kenkhuis, B., et al., *Iron loading is a prominent feature of activated microglia in Alzheimer's disease patients.* Acta Neuropathol Commun, 2021. **9**(1): p. 27.
147. Reinert, A., et al., *Iron concentrations in neurons and glial cells with estimates on ferritin concentrations.* BMC Neurosci, 2019. **20**(1): p. 25.
148. Healy, S., et al., *Significant glial alterations in response to iron loading in a novel organotypic hippocampal slice culture model.* Sci Rep, 2016. **6**: p. 36410.
149. Bishop, G.M., et al., *Accumulation of non-transferrin-bound iron by neurons, astrocytes, and microglia.* Neurotox Res, 2011. **19**(3): p. 443-51.
150. Wang, H.F., et al., *Effect of glial cells on remyelination after spinal cord injury.* Neural Regen Res, 2017. **12**(10): p. 1724-1732.
151. Zhang, W., et al., *Role and mechanism of microglial activation in iron-induced selective and progressive dopaminergic neurodegeneration.* Mol Neurobiol, 2014. **49**(3): p. 1153-65.
152. Zhang, X., et al., *Cellular iron status influences the functional relationship between microglia and oligodendrocytes.* Glia, 2006. **54**(8): p. 795-804.
153. Nnah, I.C. and M. Wessling-Resnick, *Brain Iron Homeostasis: A Focus on Microglial Iron.* Pharmaceuticals (Basel), 2018. **11**(4).
154. Zeineh, M.M., et al., *Activated iron-containing microglia in the human hippocampus identified by magnetic resonance imaging in Alzheimer disease.* Neurobiol Aging, 2015. **36**(9): p. 2483-500.
155. van Duijn, S., et al., *Cortical Iron Reflects Severity of Alzheimer's Disease.* J Alzheimers Dis, 2017. **60**(4): p. 1533-1545.
156. Thomsen, M.S., et al., *Neurodegeneration with inflammation is accompanied by accumulation of iron and ferritin in microglia and neurons.* Neurobiol Dis, 2015. **81**: p. 108-18.
157. Guo, J.J., et al., *Intranasal administration of alpha-synuclein preformed fibrils triggers microglial iron deposition in the substantia nigra of Macaca fascicularis.* Cell Death Dis, 2021. **12**(1): p. 81.
158. Jeong, S.Y., et al., *Dysregulation of iron homeostasis in the CNS contributes to disease progression in a mouse model of amyotrophic lateral sclerosis.* J Neurosci, 2009. **29**(3): p. 610-9.
159. Gillen, K.M., et al., *Significance and In Vivo Detection of Iron-Laden Microglia in White Matter Multiple Sclerosis Lesions.* Front Immunol, 2018. **9**: p. 255.
160. Rathnasamy, G., E.A. Ling, and C. Kaur, *Consequences of iron accumulation in microglia and its implications in neuropathological conditions.* CNS Neurol Disord Drug Targets, 2013. **12**(6): p. 785-98.
161. Ryan, S.K., et al., *Microglia ferroptosis is regulated by SEC24B and contributes to neurodegeneration.* Nat Neurosci, 2023. **26**(1): p. 12-26.
162. Dixon, S.J. and B.R. Stockwell, *The role of iron and reactive oxygen species in cell death.* Nat Chem Biol, 2014. **10**(1): p. 9-17.
163. Masaldan, S., et al., *Iron accumulation in senescent cells is coupled with impaired ferritinophagy and inhibition of ferroptosis.* Redox Biol, 2018. **14**: p. 100-115.
164. Lopes, K.O., D.L. Sparks, and W.J. Streit, *Microglial dystrophy in the aged and Alzheimer's disease brain is associated with ferritin immunoreactivity.* Glia, 2008. **56**(10): p. 1048-60.
165. Lau, V., L. Ramer, and M.E. Tremblay, *An aging, pathology burden, and glial senescence build-up hypothesis for late onset Alzheimer's disease.* Nat Commun, 2023. **14**(1): p. 1670.
166. Angelova, D.M. and D.R. Brown, *Model Senescent Microglia Induce Disease Related Changes in alpha-Synuclein Expression and Activity.* Biomolecules, 2018. **8**(3).

167. Yauger, Y.J., et al., *Iron accentuated reactive oxygen species release by NADPH oxidase in activated microglia contributes to oxidative stress in vitro.* J Neuroinflammation, 2019. **16**(1): p. 41.
168. Angelova, D.M. and D.R. Brown, *Microglia and the aging brain: are senescent microglia the key to neurodegeneration?* J Neurochem, 2019. **151**(6): p. 676-688.
169. Jin, M., et al., *Type-I-interferon signaling drives microglial dysfunction and senescence in human iPSC models of Down syndrome and Alzheimer's disease.* Cell Stem Cell, 2022. **29**(7): p. 1135-1153 e8.
170. Olah, M., et al., *Single cell RNA sequencing of human microglia uncovers a subset associated with Alzheimer's disease.* Nat Commun, 2020. **11**(1): p. 6129.
171. Prater, K.E., et al., *Human microglia show unique transcriptional changes in Alzheimer's disease.* Nat Aging, 2023. **3**(7): p. 894-907.
172. Urrutia, P.J., D.A. Borquez, and M.T. Nunez, *Inflaming the Brain with Iron.* Antioxidants (Basel), 2021. **10**(1).
173. Nnah, I.C., C.H. Lee, and M. Wessling-Resnick, *Iron potentiates microglial interleukin-1beta secretion induced by amyloid-beta.* J Neurochem, 2019.
174. Zhou, Y., et al., *Iron overloaded polarizes macrophage to proinflammation phenotype through ROS/acetyl-p53 pathway.* Cancer Med, 2018. **7**(8): p. 4012-4022.
175. Mehta, V., et al., *Iron is a sensitive biomarker for inflammation in multiple sclerosis lesions.* PLoS One, 2013. **8**(3): p. e57573.
176. Donley, D.W., et al., *Iron activates microglia and directly stimulates indoleamine-2,3-dioxygenase activity in the N171-82Q mouse model of Huntington's disease.* PLoS One, 2021. **16**(5): p. e0250606.
177. Nakamura, K., et al., *Activation of the NLRP3 inflammasome by cellular labile iron.* Exp Hematol, 2016. **44**(2): p. 116-24.
178. Kenkhuis, B., et al., *Iron accumulation induces oxidative stress, while depressing inflammatory polarization in human iPSC-derived microglia.* Stem Cell Reports, 2022. **17**(6): p. 1351-1365.
179. Urrutia, P., et al., *Inflammation alters the expression of DMT1, FPN1 and hepcidin, and it causes iron accumulation in central nervous system cells.* J Neurochem, 2013. **126**(4): p. 541-9.
180. McCarthy, R.C., et al., *Inflammation-induced iron transport and metabolism by brain microglia.* J Biol Chem, 2018. **293**(20): p. 7853-7863.
181. Long, H.Z., et al., *The Role of Microglia in Alzheimer's Disease From the Perspective of Immune Inflammation and Iron Metabolism.* Front Aging Neurosci, 2022. **14**: p. 888989.
182. Wessling-Resnick, M., *Iron homeostasis and the inflammatory response.* Annu Rev Nutr, 2010. **30**: p. 105-22.
183. Kroner, A., et al., *TNF and increased intracellular iron alter macrophage polarization to a detrimental M1 phenotype in the injured spinal cord.* Neuron, 2014. **83**(5): p. 1098-116.
184. Belaidi, A.A. and A.I. Bush, *Iron neurochemistry in Alzheimer's disease and Parkinson's disease: targets for therapeutics.* J Neurochem, 2016. **139 Suppl 1**: p. 179-197.
185. Nnah, I.C., C.H. Lee, and M. Wessling-Resnick, *Iron potentiates microglial interleukin-1beta secretion induced by amyloid-beta.* J Neurochem, 2020. **154**(2): p. 177-189.
186. Yona, S., et al., *Fate mapping reveals origins and dynamics of monocytes and tissue macrophages under homeostasis.* Immunity, 2013. **38**(1): p. 79-91.
187. Willis, E.F. and J. Vukovic, *Protocol for brain-wide or region-specific microglia depletion and repopulation in adult mice.* STAR Protoc, 2020. **1**(3): p. 100211.
188. Sahasrabuddhe, V. and H.S. Ghosh, *Cx3Cr1-Cre induction leads to microglial activation and IFN-1 signaling caused by DNA damage in early postnatal brain.* Cell Rep, 2022. **38**(3): p. 110252.
189. Parkhurst, C.N., et al., *Microglia promote learning-dependent synapse formation through brain-derived neurotrophic factor.* Cell, 2013. **155**(7): p. 1596-609.

190. Valdearcos, M., et al., *Microglial Inflammatory Signaling Orchestrates the Hypothalamic Immune Response to Dietary Excess and Mediates Obesity Susceptibility.* Cell Metab, 2017. **26**(1): p. 185-197 e3.
191. Murray, S.A., et al., *Beyond knockouts: cre resources for conditional mutagenesis.* Mamm Genome, 2012. **23**(9-10): p. 587-99.
192. Hoogland, I.C., et al., *Systemic inflammation and microglial activation: systematic review of animal experiments.* J Neuroinflammation, 2015. **12**: p. 114.
193. Kang, S.S., et al., *Behavioral and transcriptomic analysis of Trem2-null mice: not all knockout mice are created equal.* Hum Mol Genet, 2018. **27**(2): p. 211-223.
194. House, L.M., 2nd, et al., *Tissue inflammation and nitric oxide-mediated alterations in cardiovascular function are major determinants of endotoxin-induced insulin resistance.* Cardiovasc Diabetol, 2015. **14**: p. 56.
195. Raduolovic, K., et al., *Injections of Lipopolysaccharide into Mice to Mimic Entrance of Microbial-derived Products After Intestinal Barrier Breach.* J Vis Exp, 2018(135).
196. Consoli, D.C., et al., *A Cecal Slurry Mouse Model of Sepsis Leads to Acute Consumption of Vitamin C in the Brain.* Nutrients, 2020. **12**(4).
197. Meegan, J.E., et al., *Cell-free hemoglobin increases inflammation, lung apoptosis, and microvascular permeability in murine polymicrobial sepsis.* PLoS One, 2020. **15**(2): p. e0228727.
198. Deacon, R.M., *Assessing nest building in mice.* Nat Protoc, 2006. **1**(3): p. 1117-9.
199. Consoli, D.C., et al., *Altered EEG, disrupted hippocampal long-term potentiation and neurobehavioral deficits implicate a delirium-like state in a mouse model of sepsis.* Brain Behav Immun, 2023. **107**: p. 165-178.
200. Bolivar, V.J., *Intrasession and intersession habituation in mice: from inbred strain variability to linkage analysis.* Neurobiol Learn Mem, 2009. **92**(2): p. 206-14.
201. Nunez, J., *Morris Water Maze Experiment.* J Vis Exp, 2008(19).
202. Park, Y.G., et al., *Protection of tissue physicochemical properties using polyfunctional crosslinkers.* Nat Biotechnol, 2018.
203. Grabert, K. and B.W. McColl, *Isolation and Phenotyping of Adult Mouse Microglial Cells.* Methods Mol Biol, 2018. **1784**: p. 77-86.
204. Lee, J.K. and M.G. Tansey, *Microglia isolation from adult mouse brain.* Methods Mol Biol, 2013. **1041**: p. 17-23.
205. Bordt, E.A., et al., *Isolation of Microglia from Mouse or Human Tissue.* STAR Protoc, 2020. **1**(1).
206. Livak, K.J. and T.D. Schmittgen, *Analysis of relative gene expression data using real-time quantitative PCR and the 2(-Delta Delta C(T)) Method.* Methods, 2001. **25**(4): p. 402-8.
207. Love, M.I., W. Huber, and S. Anders, *Moderated estimation of fold change and dispersion for RNA-seq data with DESeq2.* Genome Biol, 2014. **15**(12): p. 550.
208. Zhu, A., J.G. Ibrahim, and M.I. Love, *Heavy-tailed prior distributions for sequence count data: removing the noise and preserving large differences.* Bioinformatics, 2019. **35**(12): p. 2084-2092.
209. Benjamini, Y., et al., *Controlling the false discovery rate in behavior genetics research.* Behav Brain Res, 2001. **125**(1-2): p. 279-84.
210. Benjamini, Y.a.H., Y., *Controlling the False Discovery Rate: A Practical and Powerful Approach to Multiple Testing.* Journal of the Royal Statistical Society. Series B (Methodological), 1995. **57**(1): p. 289-300.
211. McCarthy, R.C., et al., *Characterization of a novel adult murine immortalized microglial cell line and its activation by amyloid-beta.* J Neuroinflammation, 2016. **13**: p. 21.
212. Connor, J.R., et al., *A histochemical study of iron, transferrin, and ferritin in Alzheimer's diseased brains.* J Neurosci Res, 1992. **31**(1): p. 75-83.
213. Liu, J.L., et al., *Iron and Alzheimer's Disease: From Pathogenesis to Therapeutic Implications.* Front Neurosci, 2018. **12**: p. 632.

214. Raven, E.P., et al., *Increased iron levels and decreased tissue integrity in hippocampus of Alzheimer's disease detected in vivo with magnetic resonance imaging.* J Alzheimers Dis, 2013. **37**(1): p. 127-36.
215. Calsolaro, V. and P. Edison, *Neuroinflammation in Alzheimer's disease: Current evidence and future directions.* Alzheimers Dement, 2016. **12**(6): p. 719-32.
216. Kinney, J.W., et al., *Inflammation as a central mechanism in Alzheimer's disease.* Alzheimers Dement (N Y), 2018. **4**: p. 575-590.
217. Hoeft, K., et al., *Iron Loading Exaggerates the Inflammatory Response to the Toll-like Receptor 4 Ligand Lipopolysaccharide by Altering Mitochondrial Homeostasis.* Anesthesiology, 2017. **127**(1): p. 121-135.
218. Semmler, A., et al., *Sepsis causes neuroinflammation and concomitant decrease of cerebral metabolism.* J Neuroinflammation, 2008. **5**: p. 38.
219. Tejera, D., et al., *Systemic inflammation impairs microglial Abeta clearance through NLRP3 inflammasome.* EMBO J, 2019. **38**(17): p. e101064.
220. Widmann, C.N. and M.T. Heneka, *Long-term cerebral consequences of sepsis.* Lancet Neurol, 2014. **13**(6): p. 630-6.
221. Semmler, A., et al., *Persistent cognitive impairment, hippocampal atrophy and EEG changes in sepsis survivors.* J Neurol Neurosurg Psychiatry, 2013. **84**(1): p. 62-9.
222. Qin, L., et al., *Systemic LPS causes chronic neuroinflammation and progressive neurodegeneration.* Glia, 2007. **55**(5): p. 453-62.
223. Biesmans, S., et al., *Systemic immune activation leads to neuroinflammation and sickness behavior in mice.* Mediators Inflamm, 2013. **2013**: p. 271359.
224. Cai, K.C., et al., *Age and sex differences in immune response following LPS treatment in mice.* Brain Behav Immun, 2016. **58**: p. 327-337.
225. Lynch, M.A., *Exploring Sex-Related Differences in Microglia May Be a Game-Changer in Precision Medicine.* Front Aging Neurosci, 2022. **14**: p. 868448.
226. Loram, L.C., et al., *Sex and estradiol influence glial pro-inflammatory responses to lipopolysaccharide in rats.* Psychoneuroendocrinology, 2012. **37**(10): p. 1688-99.
227. Valero, J., et al., *Long-term effects of an acute and systemic administration of LPS on adult neurogenesis and spatial memory.* Front Neurosci, 2014. **8**: p. 83.
228. Bossu, P., et al., *A single intraperitoneal injection of endotoxin in rats induces long-lasting modifications in behavior and brain protein levels of TNF-alpha and IL-18.* J Neuroinflammation, 2012. **9**: p. 101.
229. Meneses, G., et al., *Recovery from an acute systemic and central LPS-inflammation challenge is affected by mouse sex and genetic background.* PLoS One, 2018. **13**(8): p. e0201375.
230. Gahima, I., Twizeyimana, E., LuckGonzales, E., Remonde, C.G., Jeon, S.J.., and Shin, C.Y., *Strain, Age, and Gender Differences in Response to Lipopolysaccharide (LPS) Animal Model of Sepsis in Mice.* Yakhak Hoeji, 2021. **65**(1): p. 17-22.
231. Kozak, W., C.A. Conn, and M.J. Kluger, *Lipopolysaccharide induces fever and depresses locomotor activity in unrestrained mice.* Am J Physiol, 1994. **266**(1 Pt 2): p. R125-35.
232. Peek, V., et al., *LPS Primes Brain Responsiveness to High Mobility Group Box-1 Protein.* Pharmaceuticals (Basel), 2021. **14**(6).
233. Alexander, A.F., et al., *Single-cell secretion analysis reveals a dual role for IL-10 in restraining and resolving the TLR4-induced inflammatory response.* Cell Rep, 2021. **36**(12): p. 109728.
234. Chucair-Elliott, A.J., et al., *Tamoxifen induction of Cre recombinase does not cause long-lasting or sexually divergent responses in the CNS epigenome or transcriptome: implications for the design of aging studies.* Geroscience, 2019. **41**(5): p. 691-708.
235. Hoogland, I.C.M., et al., *Microglial Activation After Systemic Stimulation With Lipopolysaccharide and Escherichia coli.* Front Cell Neurosci, 2018. **12**: p. 110.
236. Yen, J.J. and Yu, II, *The role of ApoE-mediated microglial lipid metabolism in brain aging and disease.* Immunometabolism (Cobham), 2023. **5**(1): p. e00018.

237. Sanjay, M. Park, and H.J. Lee, *Roles of Fatty Acids in Microglial Polarization: Evidence from In Vitro and In Vivo Studies on Neurodegenerative Diseases.* Int J Mol Sci, 2022. **23**(13).
238. Philippidis, P., et al., *Hemoglobin scavenger receptor CD163 mediates interleukin-10 release and heme oxygenase-1 synthesis: antiinflammatory monocyte-macrophage responses in vitro, in resolving skin blisters in vivo, and after cardiopulmonary bypass surgery.* Circ Res, 2004. **94**(1): p. 119-26.
239. Alvarado-Vazquez, P.A., et al., *Macrophage-specific nanotechnology-driven CD163 overexpression in human macrophages results in an M2 phenotype under inflammatory conditions.* Immunobiology, 2017. **222**(8-9): p. 900-912.
240. Gallagher, J.J., et al., *Modest amyloid deposition is associated with iron dysregulation, microglial activation, and oxidative stress.* J Alzheimers Dis, 2012. **28**(1): p. 147-61.
241. Weiss, G., *Macrophage vesicles starve bacteria of iron.* Nat Metab, 2023. **5**(1): p. 10-12.
242. Grander, M., et al., *DMT1 Protects Macrophages from Salmonella Infection by Controlling Cellular Iron Turnover and Lipocalin 2 Expression.* Int J Mol Sci, 2022. **23**(12).
243. Zhao, Z., et al., *A novel role of NLRP3-generated IL-1beta in the acute-chronic transition of peripheral lipopolysaccharide-elicited neuroinflammation: implications for sepsis-associated neurodegeneration.* J Neuroinflammation, 2020. **17**(1): p. 64.
244. Zhang, F., et al., *Central Nervous System Inflammation Induced by Lipopolysaccharide Up-Regulates Hepatic Hepcidin Expression by Activating the IL-6/JAK2/STAT3 Pathway in Mice.* Front Nutr, 2021. **8**: p. 649640.
245. Silverman, H.A., et al., *Brain region-specific alterations in the gene expression of cytokines, immune cell markers and cholinergic system components during peripheral endotoxin-induced inflammation.* Mol Med, 2015. **20**(1): p. 601-11.
246. Simats, A. and A. Liesz, *Systemic inflammation after stroke: implications for post-stroke comorbidities.* EMBO Mol Med, 2022. **14**(9): p. e16269.
247. Pandur, E., et al., *Fractalkine Induces Hepcidin Expression of BV-2 Microglia and Causes Iron Accumulation in SH-SY5Y Cells.* Cell Mol Neurobiol, 2019. **39**(7): p. 985-1001.
248. Nemeth, E. and T. Ganz, *The role of hepcidin in iron metabolism.* Acta Haematol, 2009. **122**(2-3): p. 78-86.
249. Vela, D., *Hepcidin, an emerging and important player in brain iron homeostasis.* J Transl Med, 2018. **16**(1): p. 25.
250. Lazzaro, M., et al., *Ceruloplasmin potentiates nitric oxide synthase activity and cytokine secretion in activated microglia.* J Neuroinflammation, 2014. **11**: p. 164.
251. Bok, S., et al., *Hypoxia-inducible factor-1alpha regulates microglial functions affecting neuronal survival in the acute phase of ischemic stroke in mice.* Oncotarget, 2017. **8**(67): p. 111508-111521.
252. Friedman, B.A., et al., *Diverse Brain Myeloid Expression Profiles Reveal Distinct Microglial Activation States and Aspects of Alzheimer's Disease Not Evident in Mouse Models.* Cell Rep, 2018. **22**(3): p. 832-847.
253. Simpson, D.S.A. and P.L. Oliver, *ROS Generation in Microglia: Understanding Oxidative Stress and Inflammation in Neurodegenerative Disease.* Antioxidants (Basel), 2020. **9**(8).
254. Dantzer, R., *Cytokine, sickness behavior, and depression.* Neurol Clin, 2006. **24**(3): p. 441-60.
255. Liu, Y., et al., *Galantamine improves cognition, hippocampal inflammation, and synaptic plasticity impairments induced by lipopolysaccharide in mice.* J Neuroinflammation, 2018. **15**(1): p. 112.
256. Zhang, X.Y., et al., *Deferoxamine attenuates lipopolysaccharide-induced neuroinflammation and memory impairment in mice.* J Neuroinflammation, 2015. **12**: p. 20.
257. Schuurs, A.H. and H.A. Verheul, *Effects of gender and sex steroids on the immune response.* J Steroid Biochem, 1990. **35**(2): p. 157-72.
258. Erickson, M.A., et al., *Genetics and sex influence peripheral and central innate immune responses and blood-brain barrier integrity.* PLoS One, 2018. **13**(10): p. e0205769.

259. Bartzokis, G., et al., *Brain ferritin iron may influence age- and gender-related risks of neurodegeneration.* Neurobiol Aging, 2007. **28**(3): p. 414-23.
260. Bartzokis, G., et al., *Gender and iron genes may modify associations between brain iron and memory in healthy aging.* Neuropsychopharmacology, 2011. **36**(7): p. 1375-84.
261. Duck, K.A., et al., *A role for sex and a common HFE gene variant in brain iron uptake.* J Cereb Blood Flow Metab, 2018. **38**(3): p. 540-548.
262. Marriott, I. and Y.M. Huet-Hudson, *Sexual dimorphism in innate immune responses to infectious organisms.* Immunol Res, 2006. **34**(3): p. 177-92.
263. Everhardt Queen, A., et al., *Differential Expression of Inflammatory Cytokines and Stress Genes in Male and Female Mice in Response to a Lipopolysaccharide Challenge.* PLoS One, 2016. **11**(4): p. e0152289.
264. Vegeto, E., et al., *Estrogen prevents the lipopolysaccharide-induced inflammatory response in microglia.* J Neurosci, 2001. **21**(6): p. 1809-18.
265. Zhang, L., et al., *Estrogen receptor subtype mediated anti-inflammation and vasorelaxation via genomic and nongenomic actions in septic mice.* Front Endocrinol (Lausanne), 2023. **14**: p. 1152634.
266. Rossetti, A.C., et al., *Differential Neuroinflammatory Response in Male and Female Mice: A Role for BDNF.* Front Mol Neurosci, 2019. **12**: p. 166.
267. Sato, T., et al., *Aging is associated with increased brain iron through cortex-derived hepcidin expression.* Elife, 2022. **11**.
268. Ficiara, E., I. Stura, and C. Guiot, *Iron Deposition in Brain: Does Aging Matter?* Int J Mol Sci, 2022. **23**(17).
269. Qin, Y., et al., *Investigation on positive correlation of increased brain iron deposition with cognitive impairment in Alzheimer disease by using quantitative MR R2' mapping.* J Huazhong Univ Sci Technolog Med Sci, 2011. **31**(4): p. 578.
270. Spotorno, N., et al., *Relationship between cortical iron and tau aggregation in Alzheimer's disease.* Brain, 2020. **143**(5): p. 1341-1349.
271. Smith, M.A., et al., *Iron accumulation in Alzheimer disease is a source of redox-generated free radicals.* Proc Natl Acad Sci U S A, 1997. **94**(18): p. 9866-8.
272. Jomova, K., et al., *Metals, oxidative stress and neurodegenerative disorders.* Mol Cell Biochem, 2010. **345**(1-2): p. 91-104.
273. Jiao, L., et al., *Iron metabolism mediates microglia susceptibility in ferroptosis.* Front Cell Neurosci, 2022. **16**: p. 995084.
274. Adeniyi, P.A., et al., *Ferroptosis of microglia in aging human white matter injury.* Ann Neurol, 2023.
275. Ndayisaba, A., C. Kaindlstorfer, and G.K. Wenning, *Iron in Neurodegeneration - Cause or Consequence?* Front Neurosci, 2019. **13**: p. 180.
276. Volk Robertson, K., et al., *Microglial-specific knockdown of iron import gene, Slc11a2, blunts LPS-induced neuroinflammatory responses in a sex-specific manner.* Brain Behav Immun, 2023. **116**: p. 370-384.
277. Mims, M.P. and J.T. Prchal, *Divalent metal transporter 1.* Hematology, 2005. **10**(4): p. 339-45.
278. Wetli, H.A., P.D. Buckett, and M. Wessling-Resnick, *Small-molecule screening identifies the selanazal drug ebselen as a potent inhibitor of DMT1-mediated iron uptake.* Chem Biol, 2006. **13**(9): p. 965-72.
279. Luo, W., et al., *Acquiring new memories in neocortex of hippocampal-lesioned mice.* Nat Commun, 2022. **13**(1): p. 1601.
280. Bird, C.M. and N. Burgess, *The hippocampus and memory: insights from spatial processing.* Nat Rev Neurosci, 2008. **9**(3): p. 182-94.
281. Nguyen, A.T., et al., *APOE and TREM2 regulate amyloid-responsive microglia in Alzheimer's disease.* Acta Neuropathol, 2020. **140**(4): p. 477-493.

282. Kwiatek-Majkusiak, J., et al., *Relationships between typical histopathological hallmarks and the ferritin in the hippocampus from patients with Alzheimer's disease.* Acta Neurobiol Exp (Wars), 2015. **75**(4): p. 391-8.
283. Levi, S., et al., *Iron imbalance in neurodegeneration.* Mol Psychiatry, 2024.
284. Simmons, D.A., et al., *Ferritin accumulation in dystrophic microglia is an early event in the development of Huntington's disease.* Glia, 2007. **55**(10): p. 1074-84.
285. Niraula, A., J.F. Sheridan, and J.P. Godbout, *Microglia Priming with Aging and Stress.* Neuropsychopharmacology, 2017. **42**(1): p. 318-333.
286. Norden, D.M. and J.P. Godbout, *Review: microglia of the aged brain: primed to be activated and resistant to regulation.* Neuropathol Appl Neurobiol, 2013. **39**(1): p. 19-34.
287. Wang, T., et al., *Locomotor Hyperactivity in the Early-Stage Alzheimer's Disease-like Pathology of APP/PS1 Mice: Associated with Impaired Polarization of Astrocyte Aquaporin 4.* Aging Dis, 2022. **13**(5): p. 1504-1522.
288. Tag, S.H., et al., *Neuropathological and behavioral features of an APP/PS1/MAPT (6xTg) transgenic model of Alzheimer's disease.* Mol Brain, 2022. **15**(1): p. 51.
289. Jul, P., et al., *Hyperactivity with Agitative-Like Behavior in a Mouse Tauopathy Model.* J Alzheimers Dis, 2016. **49**(3): p. 783-95.
290. Oblak, A.L., et al., *Comprehensive Evaluation of the 5XFAD Mouse Model for Preclinical Testing Applications: A MODEL-AD Study.* Front Aging Neurosci, 2021. **13**: p. 713726.
291. Fernandez, M., et al., *Behavioural symptoms in patients with Alzheimer's disease and their association with cognitive impairment.* BMC Neurol, 2010. **10**: p. 87.
292. Brandeis, R., Y. Brandys, and S. Yehuda, *The use of the Morris Water Maze in the study of memory and learning.* Int J Neurosci, 1989. **48**(1-2): p. 29-69.
293. Li, X., et al., *Sex differences between APPswePS1dE9 mice in A-beta accumulation and pancreatic islet function during the development of Alzheimer's disease.* Lab Anim, 2016. **50**(4): p. 275-85.
294. O'Leary, T.P. and R.E. Brown, *Visuo-spatial learning and memory deficits on the Barnes maze in the 16-month-old APPswe/PS1dE9 mouse model of Alzheimer's disease.* Behav Brain Res, 2009. **201**(1): p. 120-7.
295. Melnikova, T., et al., *Cycloxygenase-2 activity promotes cognitive deficits but not increased amyloid burden in a model of Alzheimer's disease in a sex-dimorphic pattern.* Neuroscience, 2006. **141**(3): p. 1149-62.
296. Kommaddi, R.P., et al., *Sex difference in evolution of cognitive decline: studies on mouse model and the Dominantly Inherited Alzheimer Network cohort.* Transl Psychiatry, 2023. **13**(1): p. 123.
297. Yuan, D., et al., *Nest-building activity as a reproducible and long-term stroke deficit test in a mouse model of stroke.* Brain Behav, 2018. **8**(6): p. e00993.
298. Neely, C.L.C., et al., *Nest Building Behavior as an Early Indicator of Behavioral Deficits in Mice.* J Vis Exp, 2019(152).
299. Stewart, S., F. Cacucci, and C. Lever, *Which memory task for my mouse? A systematic review of spatial memory performance in the Tg2576 Alzheimer's mouse model.* J Alzheimers Dis, 2011. **26**(1): p. 105-26.
300. Miyakawa, T., et al., *Hyperactivity and intact hippocampus-dependent learning in mice lacking the M1 muscarinic acetylcholine receptor.* J Neurosci, 2001. **21**(14): p. 5239-50.
301. Kennard, J.A. and D.S. Woodruff-Pak, *Age sensitivity of behavioral tests and brain substrates of normal aging in mice.* Front Aging Neurosci, 2011. **3**: p. 9.
302. Maren, S., K.L. Phan, and I. Liberzon, *The contextual brain: implications for fear conditioning, extinction and psychopathology.* Nat Rev Neurosci, 2013. **14**(6): p. 417-28.
303. Knafo, S., et al., *Morphological alterations to neurons of the amygdala and impaired fear conditioning in a transgenic mouse model of Alzheimer's disease.* J Pathol, 2009. **219**(1): p. 41-51.

304. Tovote, P., J.P. Fadok, and A. Luthi, *Neuronal circuits for fear and anxiety.* Nat Rev Neurosci, 2015. **16**(6): p. 317-31.
305. Poulin, S.P., et al., *Amygdala atrophy is prominent in early Alzheimer's disease and relates to symptom severity.* Psychiatry Res, 2011. **194**(1): p. 7-13.
306. Prieto Del Val, L., J.L. Cantero, and M. Atienza, *Atrophy of amygdala and abnormal memory-related alpha oscillations over posterior cingulate predict conversion to Alzheimer's disease.* Sci Rep, 2016. **6**: p. 31859.
307. Lin, T.W., et al., *Neurodegeneration in Amygdala Precedes Hippocampus in the APPswe/ PS1dE9 Mouse Model of Alzheimer's Disease.* Curr Alzheimer Res, 2015. **12**(10): p. 951-63.
308. Kitamura, J., et al., *The Insular Cortex, Alzheimer Disease Pathology, and Their Effects on Blood Pressure Variability.* Alzheimer Dis Assoc Disord, 2020. **34**(3): p. 282-291.
309. Bonthius, D.J., A. Solodkin, and G.W. Van Hoesen, *Pathology of the insular cortex in Alzheimer disease depends on cortical architecture.* J Neuropathol Exp Neurol, 2005. **64**(10): p. 910-22.
310. Rosenberg, P.B., M.A. Nowrangi, and C.G. Lyketsos, *Neuropsychiatric symptoms in Alzheimer's disease: What might be associated brain circuits?* Mol Aspects Med, 2015. **43-44**: p. 25-37.
311. Beam, C.R., et al., *Differences Between Women and Men in Incidence Rates of Dementia and Alzheimer's Disease.* J Alzheimers Dis, 2018. **64**(4): p. 1077-1083.
312. Podcasy, J.L. and C.N. Epperson, *Considering sex and gender in Alzheimer disease and other dementias.* Dialogues Clin Neurosci, 2016. **18**(4): p. 437-446.
313. Wang, J., et al., *Gender differences in the amount and deposition of amyloidbeta in APPswe and PS1 double transgenic mice.* Neurobiol Dis, 2003. **14**(3): p. 318-27.
314. Yang, J.T., et al., *Sex Differences in Neuropathology and Cognitive Behavior in APP/PS1/tau Triple-Transgenic Mouse Model of Alzheimer's Disease.* Neurosci Bull, 2018. **34**(5): p. 736-746.
315. Bartzokis, G., et al., *Brain ferritin iron as a risk factor for age at onset in neurodegenerative diseases.* Ann N Y Acad Sci, 2004. **1012**: p. 224-36.
316. Bartzokis, G., et al., *Prevalent iron metabolism gene variants associated with increased brain ferritin iron in healthy older men.* J Alzheimers Dis, 2010. **20**(1): p. 333-41.
317. Lehmann, D.J., et al., *Transferrin and HFE genes interact in Alzheimer's disease risk: the Epistasis Project.* Neurobiol Aging, 2012. **33**(1): p. 202 e1-13.
318. Sampietro, M., et al., *The hemochromatosis gene affects the age of onset of sporadic Alzheimer's disease.* Neurobiol Aging, 2001. **22**(4): p. 563-8.
319. Connor, J.R. and S.Y. Lee, *HFE mutations and Alzheimer's disease.* J Alzheimers Dis, 2006. **10**(2-3): p. 267-76.
320. Chung, S.D., et al., *Dementia is associated with iron-deficiency anemia in females: a population-based study.* J Neurol Sci, 2014. **346**(1-2): p. 90-3.
321. Whitfield, J.B., et al., *Relative importance of female-specific and non-female-specific effects on variation in iron stores between women.* Br J Haematol, 2003. **120**(5): p. 860-6.
322. Coppus, A.M., et al., *Early age at menopause is associated with increased risk of dementia and mortality in women with Down syndrome.* J Alzheimers Dis, 2010. **19**(2): p. 545-50.
323. Andreeva, V.A., et al., *Midlife iron status is inversely associated with subsequent cognitive performance, particularly in perimenopausal women.* J Nutr, 2013. **143**(12): p. 1974-81.
324. Guillot-Sestier, M.V., et al., *Microglial metabolism is a pivotal factor in sexual dimorphism in Alzheimer's disease.* Commun Biol, 2021. **4**(1): p. 711.
325. Carroll, J.C., et al., *Sex differences in beta-amyloid accumulation in 3xTg-AD mice: role of neonatal sex steroid hormone exposure.* Brain Res, 2010. **1366**: p. 233-45.
326. Ocanas, S.R., et al., *Microglial senescence contributes to female-biased neuroinflammation in the aging mouse hippocampus: implications for Alzheimer's disease.* bioRxiv, 2023.
327. Rodriguez-Callejas, J.D., et al., *Loss of ferritin-positive microglia relates to increased iron, RNA oxidation, and dystrophic microglia in the brains of aged male marmosets.* Am J Primatol, 2019. **81**(2): p. e22956.

328. Huang, E., et al., *Upregulation of iron regulatory proteins and divalent metal transporter-1 isoforms in the rat hippocampus after kainate induced neuronal injury.* Exp Brain Res, 2006. **170**(3): p. 376-86.
329. Swanson, M.E.V., et al., *Microglial CD68 and L-ferritin upregulation in response to phosphorylated-TDP-43 pathology in the amyotrophic lateral sclerosis brain.* Acta Neuropathol Commun, 2023. **11**(1): p. 69.
330. Mesquita, G., et al., *H-Ferritin is essential for macrophages' capacity to store or detoxify exogenously added iron.* Sci Rep, 2020. **10**(1): p. 3061.
331. Kaneko, Y., et al., *Ferritin immunohistochemistry as a marker for microglia.* Acta Neuropathol, 1989. **79**(2): p. 129-36.
332. Klein, S.L. and K.L. Flanagan, *Sex differences in immune responses.* Nat Rev Immunol, 2016. **16**(10): p. 626-38.
333. Fischer, J., et al., *Sex differences in immune responses to infectious diseases.* Infection, 2015. **43**(4): p. 399-403.
334. Dockman, R.L., et al., *Sex differences in behavior, response to LPS, and glucose homeostasis in middle-aged mice.* Behav Brain Res, 2022. **418**: p. 113628.
335. Murtaj, V., et al., *Age and Sex Influence the Neuro-inflammatory Response to a Peripheral Acute LPS Challenge.* Front Aging Neurosci, 2019. **11**: p. 299.
336. Hanamsagar, R. and S.D. Bilbo, *Sex differences in neurodevelopmental and neurodegenerative disorders: Focus on microglial function and neuroinflammation during development.* J Steroid Biochem Mol Biol, 2016. **160**: p. 127-33.
337. Gold, S.M., et al., *Sex differences in autoimmune disorders of the central nervous system.* Semin Immunopathol, 2019. **41**(2): p. 177-188.
338. Han, J., et al., *Uncovering sex differences of rodent microglia.* J Neuroinflammation, 2021. **18**(1): p. 74.
339. Lively, S., et al., *Sex- and Development-Dependent Responses of Rat Microglia to Pro- and Anti-inflammatory Stimulation.* Front Cell Neurosci, 2018. **12**: p. 433.
340. Villapol, S., et al., *Early Sex Differences in the Immune-Inflammatory Responses to Neonatal Ischemic Stroke.* Int J Mol Sci, 2019. **20**(15).
341. Cleland, N.R.W., et al., *Altered metabolism and DAM-signatures in female brains and microglia with aging.* Brain Res, 2024: p. 148772.
342. Mishra, A. and R.D. Brinton, *Inflammation: Bridging Age, Menopause and APOEepsilon4 Genotype to Alzheimer's Disease.* Front Aging Neurosci, 2018. **10**: p. 312.
343. McCarthy, M. and A.P. Raval, *The peri-menopause in a woman's life: a systemic inflammatory phase that enables later neurodegenerative disease.* J Neuroinflammation, 2020. **17**(1): p. 317.
344. Xiong, J., et al., *FSH blockade improves cognition in mice with Alzheimer's disease.* Nature, 2022. **603**(7901): p. 470-476.
345. Ganz, T. and E. Nemeth, *Iron homeostasis in host defence and inflammation.* Nat Rev Immunol, 2015. **15**(8): p. 500-10.
346. Moalem, S., E.D. Weinberg, and M.E. Percy, *Hemochromatosis and the enigma of misplaced iron: implications for infectious disease and survival.* Biometals, 2004. **17**(2): p. 135-9.
347. Weiss, G., *Iron metabolism in the anemia of chronic disease.* Biochim Biophys Acta, 2009. **1790**(7): p. 682-93.
348. Tsukamoto, H., *Iron regulation of hepatic macrophage TNFalpha expression.* Free Radic Biol Med, 2002. **32**(4): p. 309-13.
349. Ullah, I. and M. Lang, *Key players in the regulation of iron homeostasis at the host-pathogen interface.* Front Immunol, 2023. **14**: p. 1279826.
350. Zrzavy, T., et al., *Dominant role of microglial and macrophage innate immune responses in human ischemic infarcts.* Brain Pathol, 2018. **28**(6): p. 791-805.
351. Shin, J.A., et al., *Iron released from reactive microglia by noggin improves myelin repair in the ischemic brain.* Neuropharmacology, 2018. **133**: p. 202-215.

352. Xu, S.Y., et al., *Role of Ferroptosis in Glial Cells after Ischemic Stroke.* Front Biosci (Landmark Ed), 2023. **28**(9): p. 208.
353. Rathore, K.I., A. Redensek, and S. David, *Iron homeostasis in astrocytes and microglia is differentially regulated by TNF-alpha and TGF-beta1.* Glia, 2012. **60**(5): p. 738-50.
354. Qatato, M., et al., *IRE-dependent Regulation of Intestinal Dmt1 Prevails During Chronic Dietary Iron Deficiency but is Dispensable in Conditions of Acute Erythropoietic Stress.* Hemasphere, 2022. **6**(3): p. e693.
355. Dixon, S.J., et al., *Ferroptosis: an iron-dependent form of nonapoptotic cell death.* Cell, 2012. **149**(5): p. 1060-72.
356. Liddell, J.R., et al., *Microglial ferroptotic stress causes non-cell autonomous neuronal death.* Mol Neurodegener, 2024. **19**(1): p. 14.
357. Zhou, S., et al., *Interleukin-6 regulates iron-related proteins through c-Jun N-terminal kinase activation in BV2 microglial cell lines.* PLoS One, 2017. **12**(7): p. e0180464.
358. Wang, P., et al., *Mitochondrial Ferritin Deletion Exacerbates beta-Amyloid-Induced Neurotoxicity in Mice.* Oxid Med Cell Longev, 2017. **2017**: p. 1020357.
359. Liao, B., et al., *Transformation from a neuroprotective to a neurotoxic microglial phenotype in a mouse model of ALS.* Exp Neurol, 2012. **237**(1): p. 147-52.
360. Kiani Shabestari, S., et al., *Absence of microglia promotes diverse pathologies and early lethality in Alzheimer's disease mice.* Cell Rep, 2022. **39**(11): p. 110961.
361. Spangenberg, E.E. and K.N. Green, *Inflammation in Alzheimer's disease: Lessons learned from microglia-depletion models.* Brain Behav Immun, 2017. **61**: p. 1-11.
362. Boche, D. and M.N. Gordon, *Diversity of transcriptomic microglial phenotypes in aging and Alzheimer's disease.* Alzheimers Dement, 2022. **18**(2): p. 360-376.
363. Wei, Y. and X. Li, *Different phenotypes of microglia in animal models of Alzheimer disease.* Immun Ageing, 2022. **19**(1): p. 44.
364. Paolicelli, R.C., et al., *Microglia states and nomenclature: A field at its crossroads.* Neuron, 2022. **110**(21): p. 3458-3483.
365. Spangenberg, E., et al., *Sustained microglial depletion with CSF1R inhibitor impairs parenchymal plaque development in an Alzheimer's disease model.* Nat Commun, 2019. **10**(1): p. 3758.
366. Rice, R.A., et al., *Elimination of Microglia Improves Functional Outcomes Following Extensive Neuronal Loss in the Hippocampus.* J Neurosci, 2015. **35**(27): p. 9977-89.
367. Zhao, R., et al., *Microglia limit the expansion of beta-amyloid plaques in a mouse model of Alzheimer's disease.* Mol Neurodegener, 2017. **12**(1): p. 47.
368. Conti Filho, C.E., et al., *Advances in Alzheimer's disease's pharmacological treatment.* Front Pharmacol, 2023. **14**: p. 1101452.
369. Raina, P., et al., *Effectiveness of cholinesterase inhibitors and memantine for treating dementia: evidence review for a clinical practice guideline.* Ann Intern Med, 2008. **148**(5): p. 379-97.
370. Mullard, A., *Anti-amyloid failures stack up as Alzheimer antibody flops.* Nat Rev Drug Discov, 2019.
371. Osborne, O.M., et al., *Anti-amyloid: An antibody to cure Alzheimer's or an attitude.* iScience, 2023. **26**(8): p. 107461.
372. Moussa, C., et al., *Resveratrol regulates neuro-inflammation and induces adaptive immunity in Alzheimer's disease.* J Neuroinflammation, 2017. **14**(1): p. 1.
373. Turner, R.S., et al., *A randomized, double-blind, placebo-controlled trial of resveratrol for Alzheimer disease.* Neurology, 2015. **85**(16): p. 1383-91.
374. Howard, R., et al., *Minocycline at 2 Different Dosages vs Placebo for Patients With Mild Alzheimer Disease: A Randomized Clinical Trial.* JAMA Neurol, 2020. **77**(2): p. 164-174.
375. Pasqualetti, P., et al., *A randomized controlled study on effects of ibuprofen on cognitive progression of Alzheimer's disease.* Aging Clin Exp Res, 2009. **21**(2): p. 102-10.

376. Rivers-Auty, J., et al., *Anti-inflammatories in Alzheimer's disease-potential therapy or spurious correlate?* Brain Commun, 2020. **2**(2): p. fcaa109.
377. Zhang, C., et al., *NSAID Exposure and Risk of Alzheimer's Disease: An Updated Meta-Analysis From Cohort Studies.* Front Aging Neurosci, 2018. **10**: p. 83.
378. Stuve, O., et al., *Diclofenac reduces the risk of Alzheimer's disease: a pilot analysis of NSAIDs in two US veteran populations.* Ther Adv Neurol Disord, 2020. **13**: p. 1756286420935676.
379. Stopschinski, B.E., et al., *Microglia as a cellular target of diclofenac therapy in Alzheimer's disease.* Ther Adv Neurol Disord, 2023. **16**: p. 17562864231156674.
380. Nunez, M.T. and P. Chana-Cuevas, *New Perspectives in Iron Chelation Therapy for the Treatment of Neurodegenerative Diseases.* Pharmaceuticals (Basel), 2018. **11**(4).
381. Devos, D., et al., *Targeting chelatable iron as a therapeutic modality in Parkinson's disease.* Antioxid Redox Signal, 2014. **21**(2): p. 195-210.
382. Devos, D., et al., *Trial of Deferiprone in Parkinson's Disease.* N Engl J Med, 2022. **387**(22): p. 2045-2055.
383. Huntington Study Group Reach, H.D.I., *Safety, tolerability, and efficacy of PBT2 in Huntington's disease: a phase 2, randomised, double-blind, placebo-controlled trial.* Lancet Neurol, 2015. **14**(1): p. 39-47.
384. Salkovic-Petrisic, M., et al., *Multi-target iron-chelators improve memory loss in a rat model of sporadic Alzheimer's disease.* Life Sci, 2015. **136**: p. 108-19.
385. Fine, J.M., et al., *Intranasal deferoxamine improves performance in radial arm water maze, stabilizes HIF-1alpha, and phosphorylates GSK3beta in P301L tau transgenic mice.* Exp Brain Res, 2012. **219**(3): p. 381-90.
386. Lannfelt, L., et al., *Safety, efficacy, and biomarker findings of PBT2 in targeting Abeta as a modifying therapy for Alzheimer's disease: a phase IIa, double-blind, randomised, placebo-controlled trial.* Lancet Neurol, 2008. **7**(9): p. 779-86.
387. King, A., *The search for better animal models of Alzheimer's disease.* Nature, 2018. **559**(7715): p. S13-S15.
388. Arrojo, E.D.R., et al., *Age Mosaicism across Multiple Scales in Adult Tissues.* Cell Metab, 2019. **30**(2): p. 343-351 e3.
389. Liu, F., et al., *Effect of metal ions on Alzheimer's disease.* Brain Behav, 2022. **12**(3): p. e2527.
390. Feng, S., et al., *The mechanism of ferroptosis and its related diseases.* Mol Biomed, 2023. **4**(1): p. 33.

APPENDIX

Funding sources: The work in this dissertation was funded by NIH grant DK121520-02S1, a Pilot and Feasibility Award from the Vanderbilt Diabetes and Research Training Center (DK020593) and a Pilot and Feasibility Award from the Vanderbilt Memory and Alzheimer's Center (P20-AG068082). Alyssa Hasty is supported by a Career Scientist Award from the Veterans Affairs (IK6 BX005649). I was supported by the Molecular Endocrinology Training Program (T32 DK007563-31), the Interdisciplinary Alzheimer's Disease Training Program (T32-AG058524) and an individual Ruth L. Kirschstein National Research Service Award (1F31AG081025). Work done in Vanderbilt research cores was supported by the Vanderbilt Kennedy Center P50 HD103537 (Murine Neurobehavior Core Lab, MNL), NIH grant DK020593 (Vanderbilt Analytical Services Core), Clinical and Translational Science Award Grant 5UL1 RR024975-03, Vanderbilt Ingram Cancer Center Grant P30 CA68485, Vanderbilt Vision Center Grant P30 EY08126, and NIH/National Center for Research Resources Grant G20 RR030956 (Vanderbilt Technologies for Advanced Genomics, VANTAGE).